Det Norske Videnskaps-Akademi i Oslo

Geophysica Norvegica

GEOFYSISKE PUBLIKASJONER

VOL. 30 NO. 2 1973

UNIVERSITETSFORLAGET

Geophysica Norvegica

is a journal of geophysics, issued under the auspices of the Norwegian Academy of Science and Letters in Oslo

PUBLISHER

Universitetsforlaget: P. O. Box 307, Blindern, Oslo 3, Norway.
P. O. Box 142, Boston, Mass. 02113, U.S.A.

SUBSCRIPTION

Geophysica Norvegica (Geofysiske Publikasjoner) is published at irregular intervals. Order from the Publisher, Universitetsforlaget.

Geophysica Norvegica (Geofysiske Publikasjoner) is a series of scientific publications issued by the Norwegian Academy of Science and Letters in Oslo. The Geophysical Commission appoints an editor and editorial committee.
Manuscripts for publication in Geophysica Norvegica should be carefully prepared (see Instructions to Author on p. 3 of the cover) and sent to the editor. The next step is the manuscript's submission to the Academy by a competent member, who is responsible for ensuring that the paper meets a sufficiently high scientific standard. (Members of the Academy are allowed to submit their own papers.) The final decision as to whether the paper should be published is taken by the editor.
Geophysica Norvegica is mainly intended as a journal for Norwegian authors, but papers from other authors may be accepted provided that the work has been carried out at a Norwegian institution or its content has a special relevance to Norway.

Diurnal Variations of Atmospheric Constituents in an Oxygen–Hydrogen–Nitrogen–Carbon Atmospheric Model, and the Role of Minor Neutral Constituents in the Chemistry of the Lower Ionosphere

IVAR S. A. ISAKSEN
Institute of Geophysics, University of Oslo

Isaksen, I. S. A. Diurnal Variations of Atmospheric Constituents in an Oxygen-Hydrogen-Nitrogen-Carbon Atmospheric Model, and the Role of Minor Neutral Constituents in the Chemistry of the Lower Ionosphere. *Geophysica Norvegica*, Vol. 30, No. 2, 1973.

Diurnal variations of neutral as well as ionic components have been calculated in the height region 10–110 km. Ionic species depend strongly on the diurnal variations of atmospheric constituents such as atomic oxygen, ozone, nitrogen oxide, and hydroxyl, and on height distribution of long-lived neutral species like water vapour and carbon dioxide. Neutral and ionic species depend strongly on atmospheric parameters such as temperature and eddy diffusion coefficient profiles. Hydronium water clusters are the main positive ions below 80 km, and NO_3^-, CO_3^-, and CO_3^- and their water clusters are the main negative ions.

I. S. A. Isaksen, Institute of Geophysics, University of Oslo, Blindern, Oslo 3, Norway

INTRODUCTION

Model calculations of atmospheric constituents have turned out to be a very helpful tool for understanding minor atmospheric species. In the two decades after the important work of Bates & Nicolet (1950) on the oxygen-hydrogen atmosphere, a large number of papers concerning the distribution of minor constituents in the upper atmosphere have been presented.

A more realistic model is obtained when turbulent diffusion on long-lived oxygen and hydrogen species, such as atomic oxygen and water vapour, is introduced (Hesstvedt 1968). Atomic oxygen is transported downward in the 90 km region, which gives increased number densities of $O(^3P)$ compared with a pure photochemical model. This leads to a secondary maximum in the ozoneprofile between about 85 km and 90 km, which is in good agreement with observations of $O_2(^1\Delta g)$ (Evans et al. 1968, Wood 1969). $O_2(^1\Delta g)$ is known to be produced by photolysis of ozone at $\lambda < 3110$ Å.

The production and distribution of nitrogen oxides have gained increased attention the last few years. They are produced in the upper atmosphere (Strobel et al. 1970, Barth et al. 1970, Nicolet 1970). By considering X-ray ionization and neutral-ionic interactions, height profiles in good agreement with observations of Meira (1970) are obtained above about 85 km (Isaksen 1971).

There is also an odd-nitrogen production of great stratospheric interest through the reaction between excited-state atomic oxygen, $O(^1D)$ and nitrous oxide, N_2O (Nicolet 1970a). This production is strong enough to give NO_x profiles of importance for the ozone layer (Crutzen 1971).

E. Hesstvedt submitted this paper to the Norwegian Academy of Science and Letters in Oslo, 16th March, 1973.

In the lower stratosphere, hydroxyl seems to be a key component. It is produced by the reaction of $O(^1D)$ with water vapour (Hampson 1965), and it reacts fast enough with CO and CH_4 to effect the mixing ratio of these two components in the stratosphere. The fast drop in CO mixing ratio above the tropopause (Seiler & Warneck 1972), and the slower decrease in CH_4 mixing ratio (Bainbridge & Heidt 1966), is a result of the reaction with hydroxyl. Further, when the fast reaction with NO_2 (Morley & Smith 1972) forming HNO_3 is considered, it effectively controls the nitrogen oxides present in the stratosphere.

D-region ion chemistry is characterized by a great number of ion species. Stable clusters of positive ions are formed, and negative-ion components are present with number densities comparable to electrons.

Positive ions were first detected by mass spectrometric measurements (Narcisi & Bailey 1966). Since then, both positive and negative ions have been measured (Krankowsky et al. 1971, Narcisi et al. 1972, Johannesen & Krankowsky 1972). The cluster ions $H_3O^+.(H_2O)_n$, with $n = 1, 2, 3, 4$, are the dominating positive ions in the *D*-region. Below, higher hydrates are expected to dominate.

Reactions leading to the terminal ions from the initial ions N_2^+, O_2^+, and NO^+ have been given by several authors (Kebarle et al. 1967, Good et al. 1970a, Fehsenfeld et al. 1971a). Due to the high density in the D-region and below, three-body reactions involving a minor constituent like H_2O are fast enough to make cluster ions dominate. Rate constants of the order of 10^{-27} are typical for these reactions.

It is, however, still left to explain what reaction is responsible for the fast convection from the NO^+ ion, the main initial ion in the *D*-region, to the $H_3O^+.(H_2O)_n$ ions, the mainly observed ions. Several reactions have been suggested to be fast enough, but so far there are no measurements to verify these suggestions (Ferguson 1971).

Negative ions are primarily produced in a three-body reaction as O_2^-, with some contribution from the reaction of electrons with O_3. In reaction with neutral species, the ions O_4^-, CO_3^-, CO_4^-, NO_2^-, and NO_3^- are formed (Bortner & Kummler 1968). Observations performed by Narcisi et al. (1972), and Johannesen & Krankowsky (1972), show that the main ions present in the D-region are NO_3^-, CO_3^-, and their hydrates. Only a few rate constants for three-body reactions forming negative clusters are so far reported (Park & Phelps 1971, Kebarle et al. 1972), which give rate constants similar to those for three-body reactions with positive ions. It is reasonable to expect that all negative ions in the D-region form clusters in the same way as has been measured for positive ions (Ferguson 1971).

It is convenient to divide the calculations of the species into two parts. Species with long lifetimes like H_2O, H_2, H_2O, CO, CH_4, and in the upper part $O(^3P)$, H, and NO, which have negligible diurnal variations, are also calculated in a steady-state model. Average daytime values of species with short lifetimes are used in these calculations. These average values are then used as initial conditions in a time-dependent model of the short-lived species. All ion species have short chemical lifetimes and are not directly influenced by diffusion. It has been necessary to calculate the ion species simultaneously with the neutral species, since they depend very strongly on species like $O(^3P)$, O_3, $O_2(^1\Delta g)$, NO, and perhaps OH, all of which have a pronounced diurnal variation.

The following neutral species are considered: $O(^3P)$, $O(^1D)$, O_2, $O_2(^1\Delta_g)$, $N(^4S)$, $N(^2D)$, NO, N_2O, NO_2, NO_3, N_2O_5, N_2, HNO_3, CO, CO_2, H, H_2, H_2O, H_2O_2, OH, HO_2, and the following ionic species: N_2^+, O_2^+, NO^+, H_3O^+, O_4^+, $O_2^+.(H_3O)$, $H_3O^+.(H_2O)$, $H_3O^+.(H_2O)_2$, $H_3O^+.(H_2O)_3$, $NO^+.(H_2O)$, $NO^+.(H_2O)_2$, $NO^+.(H_2O)_3$, O^-, O_2^-, O_3^-, O_4^-, CO_3^-, CO_4^-, NO_2^-, NO_3^-, $O_2^-.(H_2O)_n$, $CO_3^-.(H_2O)_n$, $CO_4^-.(H_2O)_n$, $NO_3^-.(H_2O)_n$, e, $NO^+.CO_2$, $NO^+.N_2$, $H_3O^+.(H_2O)_4$, $H_3O^+.(H_2O)_5$, $H_3O^+.(H_2O)_6$, $H_3O^+.(H_2O)_7$.

2. PHOTODISSOCIATION AND PHOTOIONIZATION

Dissociation of atmospheric constituents takes place mainly in the ultraviolet and extreme ultraviolet ($\lambda < 3110$ Å). Some constituents (O_3, NO_2,

HNO_3) have important dissociation for longer wavelengths also. Molecular dissociation is a reaction of the type

$$X \cdot Y + h\nu \rightarrow X + Y$$

where X and Y are molecules or atoms in the ground state or in an excited state.

The photon fluxes, F, are absorbed by atmospheric constituents, mainly O_2 and O_3, and in practice it is permissible to disregard the absorption by other components. This absorption is highly wavelength-dependent. The dissociation rate constant for the component i, expressed in s^{-1} per molecule, is therefore calculated in a spectral interval $\Delta\lambda$, and summed for all values of λ:

$$J_i = \sum_{\lambda} F_{O\lambda} \cdot \sigma'_{\lambda i} \cdot \exp\left(-\sigma_{O_2\lambda} \cdot \sum_{z} O_{2z} \cdot ds - \sigma_{O_3\lambda} \cdot \sum_{z} O_{3z} ds\right) \cdot \Delta\lambda \qquad (2.1)$$

$F_{0\lambda}$ is the photon flux in the spectral interval $\Delta\lambda$ outside the earth's atmosphere, $\sigma'_{\lambda i}$ is the dissociation cross-section in the same spectral interval of the component i, σ_λ is the absorption cross-section of the main atmospheric absorbers; and $\sum_z O_{2z} \cdot ds$ and $\sum_z O_{3z} \cdot ds$ are the column density of O_2 and O_3 above the height z in the direction of the sun.

In the computations presented below, variations in the solar elevation during the day are considered. For zenith distances $Z < 75°$, the flat-earth approximation is used:

$$ds = \sec Z \cdot dz \qquad (2.2)$$

For $Z > 75°$, equation (2.2) is a poor assumption, and a new expression has been used to account for the curvature of the earth. The term sec Z is replaced by the Chapman function Ch (Z,x). The Chapman function depends on the scale-height of the component, which means that we have to use different expressions for O_2 and O_3. Values tabulated by Wilkes (1954) are used in the calculations for $75° < Z < 90°$. For $Z > 90°$ the method used is illustrated below.

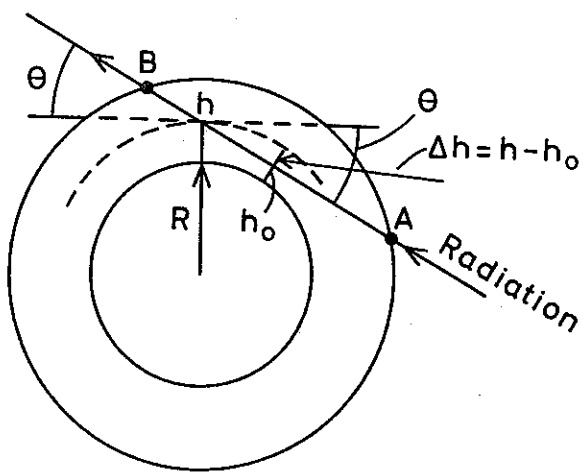

A to B is the total passage of the sun's radiation through the atmosphere at height h_0 with zenith distance $Z = 90°$. The vertical column density at h_0 is given by

$$\sum_{h_0} n_{iz} \cdot ds = \sum_{h_0} n_{iz} \cdot dz \qquad (2.3)$$

where n_{iz} is the number density of the component i. (O_2 or O_3).

For the column density at $Z = 90°$ we use

$$\sum_{h_0} n_{iz} \cdot ds = 2 \cdot \mathrm{Ch}(90°,x) \sum_{h_0} n_{iz} \cdot dz \qquad (2.4)$$

The column density from A to the height h with depression angle θ is then expressed by

$$\sum_{h} n_{iz} \cdot ds = 2 \cdot \mathrm{Ch}(90°,x) \cdot \sum_{h_0} n_{iz} \cdot dz - \mathrm{Ch}(90° - \theta, x) \cdot \sum_{h} n_{iz} \cdot dz \qquad (2.5)$$

The lowest height above the earth, h_0, is given (Hunten 1954) by

$$h_0 = h - \frac{R\theta^2}{2}. \qquad (2.6)$$

To simplify the expression, an exponential variation of the component is expected from h to h_0

$$n_{ih_0} = n_{ih} \cdot \exp\left(\frac{\Delta h}{H}\right) \qquad (2.7)$$

where Δh from (2.6) is $\frac{R\theta^2}{2}$, and H is the scale height. Putting this into equation 2.5, we get

$$\sum_{h} n_{iz} \cdot ds = \left[2 \cdot \mathrm{Ch}(90°,x) \cdot \exp\left(\frac{\Delta h}{H}\right)\right] - \mathrm{Ch}\ (90° - \theta, x) \cdot \sum_{n} n_{iz} \cdot dz \qquad (2.8)$$

Solar fluxes are taken from Ackerman (1971). Dissociation and absorption cross-sections are taken from the following authors: Jones & Woulf (1937), Inn & Tannaka (1953), Watanabe (1958), Leighton (1961), Ditchburn & Young (1962),

Schumb et al. (1955), Huffman (1968), Ackerman (1971), and Kockarts (1971).

Calculated values of the dissociation rates of O_2, O_3, H_2O, H_2O_2, NO_2, N_2O_5, HNO_3, CH_4, CO_2, and N_2O for the average daytime conditions at 45° summer are given in Fig. 2.1.

Ionization by solar photons is the main ion source above 70 km in the undisturbed atmosphere. This ionization takes place in the wavelength interval 2 Å–1350 A.

In the extreme ultraviolet, the ionization rates are calculated in a similar manner as the dissociation rates, with O_2 and N_2 as the only important absorbers:

$$J_i = \sum_\lambda F_0 \cdot \sigma''_\lambda \cdot \exp\left(-\sigma_{O_2\lambda} \cdot \sum_h O_2 \cdot ds - \sigma_{N_2\lambda} \cdot \sum_h N_2 \cdot ds\right) \cdot \Delta\lambda \qquad (2.9)$$

where σ'' is the ionization cross-section. The X-ray ionization has been calculated from

$$J_i = \sum_\lambda \frac{\lambda_0}{\lambda} \cdot F_{0\lambda} \cdot \sigma''_\lambda \cdot \exp\left(-\sigma_{O_2\lambda} \cdot \sum_h O_2\, ds - \sigma_{N_2\lambda} \cdot \sum_h N_2 ds\right) \cdot \Delta\lambda \qquad (2.10)$$

λ_0 represents the wavelength for the average energy to form one ion pair $\lambda_0 \approx 350$ A.

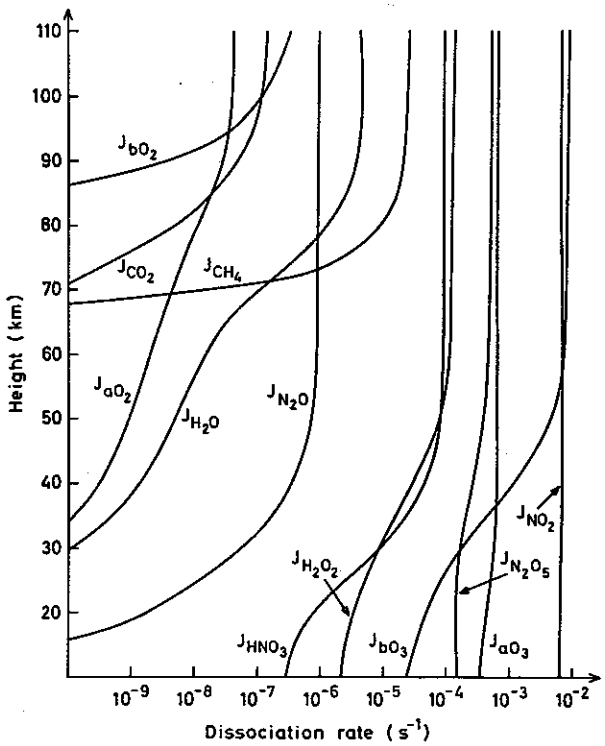

Fig. 2.1. Dissociation rates.

In the actual region the following species are ionized by the extreme ultraviolet radiation:

O_2 by Ly-β radiation at 1025.7 A, $O_2(^1\Delta g)$ for $\lambda < 1118$ A. and NO for $\lambda < 1350$ A. The main contribution to the NO ionization comes from Ly-α radiation at 1215.7 A (Table 2.1). Nighttime values of the scattered Ly-α and Ly-β radiation are set to 1.0% and 0.4% of their daytime values (Keneshea 1968).

The importance of $O_2(^1\Delta g)$ ionization is to be sought in the existence of several 'windows' in the absorption by ground state O_2 for $\lambda < 1118$ A, which allows for a considerable ionization of $O_2(^1\Delta g)$ around 80 km. When the absorption of CO_2 is introduced, as proposed by Huffman et al. (1971), the importance of $O_2(^1\Delta g)$ in the *D*-region chemistry is strongly reduced; CO_2 absorption is therefore included in the calculations. The energetic X-rays ionize the main atmospheric constituents N_2 and O_2. Values of the photon fluxes, and the ionization and absorption cross-section at different wavelengths, are given in Table 2.1. The X-ray fluxes vary strongly over a solar cycle with the enhancement at the shorter wavelengths being most marked during solar maximum conditions (Craig 1965). These calculations are carried out for solar minimum conditions (column F).

Ionization rates of $O_2(^1\Delta g)$ in the wave-length-interval $1027 < \lambda < 1118$ are taken from Clark & Wayne (1970), while the absorption by ground state O_2 is from Watanabe (1958).

In the lower ionosphere, ionization is mainly due to galactic cosmic rays. Down to about 35 km this ionization is proportional to the air density. An ionization rate of $q_{GCR} = 2 \times 10^{-17}$.

	F	σ''	σ
2	1.0+00	1.0–21	1.0–21
4	2.0+02	6.7–21	6.7–21
6	1.2×04	2.1–20	2.1–20
8	1.0+05	4.8–20	4.8–20
X-ray			
15	4.0+05	7.0–20	7.0–20
33.7	1.0+07	1.3–19	1.3–19
50	1.5+08	2.8–19	2.8–19
60	2.2+08	6.0–19	6.0–19
Ly-β 1025.7	4.4×10^9	9.8–19	1.5–19
Ly-α 1215.7	$1.5 \times 10^{+11}$	2.8–18	1.0–20

Table 2.1.

$|M|$ has been used, with $|M|$ as the particle concentration of air. Below 35 km, ionization rates are taken from George (1970).

The flux of GCR is, in contrast to solar photon fluxes, constant during the day, which gives constant ionization rates at each level during the day.

The ion pair production is obtained by multiplying ionization rates obtained in (2.9) and (2.10) with the number densities of the ionized species.

$$P = \sum_i n_i \cdot J_i \qquad (2.11)$$

The strong diurnal variation of the ion-pair production is clearly demonstrated in Fig. 2.2,

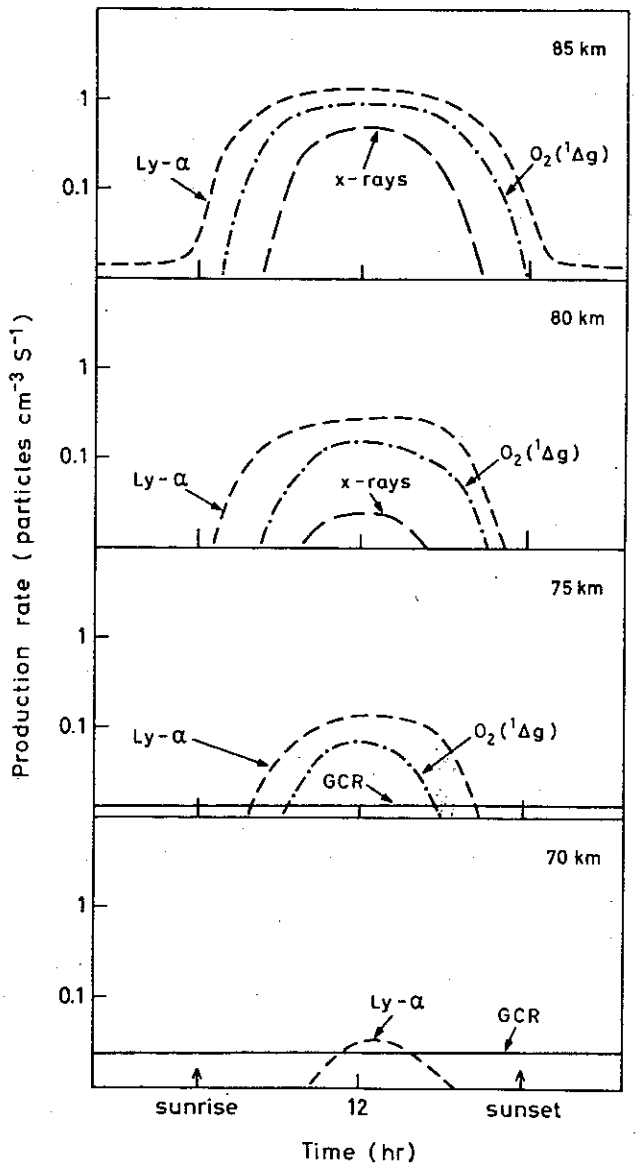

Fig. 2.2. *D*-region ionization rates.

where the productions at heights of 85 km, 80 km, 75 km, and 70 km are shown during the day. Ly-α ionization of NO is the main daytime source above 70 km with $O_2(^1\Delta g)$ as an important source in most of the region. X-ray ionization is comparable to the other daytime sources at 85 km, but it decreases below 85 km, where it has negligible effect on the total ionization. At night Ly-α ionization dominates at 85 km, but at 80 km and below, galactic cosmic ray ionization is the main night-time source. Below 70 km galactic cosmic rays are the main ion source during the whole day.

3. THE STEADY-STATE MODEL.

In the calculations it is convenient to divide the species into two parts, those with long lifetimes (hours or more), and those with short lifetimes. In calculating the number densities of the long-lived species, transport processes play a significant role in their distribution. This is specially pronounced for species where the distribution is much different from total mixing, for example for atomic oxygen and water vapour (Hesstvedt 1968).

It has been suggested that horizontal transport is of secondary importance (Hesstvedt 1971), since horizontal variations in mixing ratios are very small. We shall therefore consider vertical eddy diffusion as the only important transport process. This leaves us with a simplified model, extended upward from 10 km, which is below the tropopause at about 13 km (45° summer), to the turbopause, here placed at 110 km. Above 110 km, molecular diffusion is expected to dominate. All components except N_2 and O_2 are calculated. Ozone is calculated down to 30 km. In the lower stratosphere (below 25 km) horizontal transport is known to dominate over vertical processes (Hesstvedt 1972); a vertical column model will therefore be a poor assumption at such low levels. This will, however, not raise any problems since ozone number densities are well known form measurements (Hering & Borden 1964). A measured ozone profile, representing summer conditions at 45°, will therefore be applied. The following species are expected to be influenced by

transport; atomic oxygen and atomic hydrogen between 75 km and 110 km, and water vapour, molecular hydrogen, carbon monoxide, carbon dioxide, methane, nitrous oxide, and odd nitrogen, mostly in the form of nitric oxide and nitrogen dioxide in the whole region. Above 80 km, eddy transport is also included in the calculation of atomic nitrogen, though it has a very small effect.

The time-dependent equation of a component x is given by the differential equation

$$\frac{d}{dt}|x| = -\frac{d}{dz}\left(K_z \cdot |M| \cdot \frac{d}{dz}\left(\frac{|x|}{|M|}\right)\right) + P_x - Q_x \cdot |x| \qquad (3.1)$$

K_z is the vertical eddy diffusion coefficient, and P_x and $Q_x \cdot |x|$ the photochemical production and loss terms. This equation is solved numerically by introducing finite-centred differences, leading to the equation

$$\frac{d}{dt}|x|_i = A_i \cdot |x|_{i-1} - B_i \cdot |x|_i - Q_i \cdot |x|_i + C_i|x|_{i+1} + P_i \qquad (3.2)$$

where i refers to the central level, $i-1$ the level above (since the calculations are started ta the upper boundary), and $i+1$ refers to the level below the central level.

$$A_i = \frac{K_{z_{i-1/2}} \cdot |M|_{i-1/2}}{|M|_{i-1} \cdot (\Delta Z)^2},$$

$$B_i = \frac{K_{z_{i-1/2}} \cdot |M|_{i-1/2} + K_{z_{i+1/2}} \cdot |M|_{i+1/2}}{[M]_i \cdot (\Delta Z)^2}$$

and

$$C_i = \frac{K_{z_{i+1/2}} \cdot |M|_{i+1/2}}{|M|_{i+1} \cdot (\Delta_z)^2}$$

the indices $i-\frac{1}{2}$ and $i+\frac{1}{2}$ give the geometrical mean value for the level above and below the central level i. The vertical diffusion coefficient is taken from Gudiksen et al. (1968), up to 27 km, and an exponential variation, similar to what is proposed by Lindzen (1971), is used above 30 km. A component is influenced by eddy diffusion when the diffusion lifetime $\tau_{diff} = \frac{H^2}{K_z}$ (Kellogg 1964) is comparable to or less than the photochemical lifetime $\tau = \frac{1}{Q}$ (Hesstvedt 1965). H is the scale height of the mixed atmosphere.

Since the diurnal variations observed in the components result from the diurnal cycle of the solar radiation, components with photochemical lifetimes of more than one day will have small diurnal variations, and the equation can be simplified by setting

$$\frac{d}{dt}|x| \approx 0 \qquad (3.3)$$

We are left with an equation where the number densities at one height depend on the number densities at the level above and the level below,

$$A_i \cdot |x|_{i-1} - (B_i + Q_i) \cdot |x|_i + C_i \cdot |x|_{i+1} = -P \qquad (3.4)$$

This equation is solved by a direct implicit method (see for instance Richtmyer 1957) for the gridpoints between the upper boundary ($i = 1$), and the lower boundary ($i = M$).

We can define the following set of simultaneous first-order equations:

$$\begin{aligned}
x_1 &= K_1 \\
A_2 \cdot x_1 - B_2 \cdot x_2 + C_2 \cdot x_3 &= K_2 \\
A_3 \cdot x_2 - B_3 \cdot x_3 + C_3 \cdot x_o &= K_3 \\
&- \\
&- \\
&- \\
A_{m-1} \cdot x_{m-2} - B_{m-1} \cdot x_{m-1} + C_{m-1} \cdot x_m &= K_{m-1} \\
x_m &= K_m
\end{aligned} \qquad (3.5)$$

where the boundary values $x_1 = K_1$ and $x_m = K_m$ are known values, and the K_i's are the photochemical production term: $-P_i$.

This three-term linear system is solved by reducing it to a two-term linear system, by combining two and two levels successively, starting at the upper boundary with the known value $x_1 = K_1$. The first step is:

$$\begin{aligned}
&\text{a)}\ x_1 = K_1 \\
&\text{b)}\ A_2 \cdot x_1 - B_2 \cdot x_2 + C_2 \cdot x_3 = K_2
\end{aligned} \qquad (3.6)$$

multiplying the last of these equations by $\left(-\frac{1}{A_2}\right)$,

and adding, gives the new equation:

c) $B_2/A_2 \cdot x_2 - C_2/A_2 \cdot x_3 = K_1 - K_2/A_2$

It is convenient to set $B_{x_2} = B_2/A_2$, $C_{x_2} = C_2/A_2$ and $K_{x_2} = K_2/A_2$ and add them to the equation for $i = 3$

$$\begin{aligned} &\text{a)}\ B_{x_2} \cdot x_2 - C_{x_2} \cdot x_3 &&= K_{x_2} \\ &\text{b)}\ A_3 \cdot x_2 - B_3 \cdot x_3 + C_3 \cdot x_4 &&= K_3 \end{aligned} \qquad (3.7)$$

multiplying the last equation with $(-B_{x_2}/A_3)$ and adding the two equations, we get the new equation:

$$\text{c)}\ \left(\frac{B_3 \cdot B_{x_2}}{A_3} - C_{x_2}\right) \cdot x_3 - \frac{C_3 \cdot B_{x_2}}{A_3} \cdot x_4 = K_{x_2} - \frac{K_3 \cdot B_{x_2}}{A_3}$$

If we set

$$B_{x_3} = \frac{B_3 \cdot B_{x_2}}{A_3} - C_{x_2}, \quad C_{x_3} = \frac{C_3 \cdot B_{x_2}}{A_3}$$

and

$$K_{x_3} = K_{x_2} - \frac{K_3 \cdot B_{x_2}}{A_3}$$

we get the equation:

$$B_{x_3} \cdot x_3 - C_{x_3} \cdot x_4 = K_{x_3} \qquad (3.8)$$

This process can be repeated for all i-values up to $i = M-1$, giving the equation:

$$B_{x_i} \cdot x_i - C_{x_i} \cdot x_{i+1} = K_{x_i} \qquad (3.9)$$

where

$$B_{x_i} = \frac{B_i \cdot B_{x_{i-1}}}{A_i} - C_{x_{i-1}}, \quad C_{x_i} = \frac{C_i \cdot B_{x_{i-1}}}{A_i}$$

and

$$K_{x_i} = K_{x_{i-1}} - \frac{K_i \cdot B_{x_{i-1}}}{A_i}$$

From equation (3.9) the number densities of x_i are given by

$$x_i = \frac{K_{x_i} + C_{x_i} \cdot x_{i+1}}{B_{x_i}} \qquad (3.10)$$

When the constants B_{x_i}, C_{x_i}, and K_{x_i} are determined for all levels $i = 2,3,\ldots,M-1$, x_i is determined by starting from the lower boundary with the known value $x_{i+1} = K_m$, all number densities of x_i up to $i = 2$ are determined through reaction (3.10).

Species with short lifetimes are in this steady-state model treated similarly to the species with long lifetimes by setting $\frac{d}{dt}|x| \approx 0$. Average daytime values are thus obtained for these species.

Odd-oxygen components, which are present in the atmosphere, either in the form of atomic oxygen in the ground state, $O(^3P)$, in the excited state, $O(^1D)$, or in the form of ozone, are initially produced by dissociation of O_2. Two oxygen atoms are formed for each O_2 dissociation:

$$\text{a)}\ O_2 + h\nu \rightarrow O(^3P) + O(^3P) \qquad \lambda < 2424\ \text{Å}$$

There are several reactions which are important for the odd-oxygen destruction. The three-body reaction:

$$O(^3P) + O(^3P) + M \rightarrow O_2 + M \qquad k_1 = 3.3 \times 10^{-33} \left(\frac{300}{T}\right) \qquad (1)$$

is only fast enough to affect the odd oxygen above about 95 km. Below, the following binary reactions have to be considered:

$$O(^3P) + O_3 \rightarrow O_2 + O_2 \qquad k = 2 \times 10^{-11}\, e^{-\frac{2395}{T}} \qquad (2)$$

$$O(^3P) + OH \rightarrow H + O_2 \quad k = 2.5 \times 10^{-11} \qquad (3)$$

$$O(^3P) + HO_2 \rightarrow OH + O_2 \quad k = 7 \times 10^{-11} \qquad (4)$$

$$O(^3P) + NO_2 \rightarrow O_2 + NO \quad k = 9.1 \times 10^{-12} \qquad (5)$$

Photochemical production and loss are given by the above reactions:

$$\begin{aligned} P &= 2 \cdot J_{O_2} \cdot |O_2| \\ Q &= 2 \cdot (k_2 \cdot |O_3| + k_3 \cdot |OH| + k_4 \cdot |HO_2| \\ &\quad + k_5 \cdot |NO_2|) \end{aligned} \qquad (3.11)$$

where the sum of the odd-oxygen species $(O + O_3)$ are determined rather than the dominating component (Hesstvedt 1970).

The loss term should be a second-order term in odd oxygen since the species O_3, OH, and HO_2 have short lifetimes and are in chemical equilibrium with O. Using it in the form as in (3.1) we get a first-order equation, and odd oxygen can be determined from (3.4).

The calculated $O(^3P)$ profile is shown in Fig. 3.1 for the height region where diurnal variations are negligible, above about 86 km. Dashed line

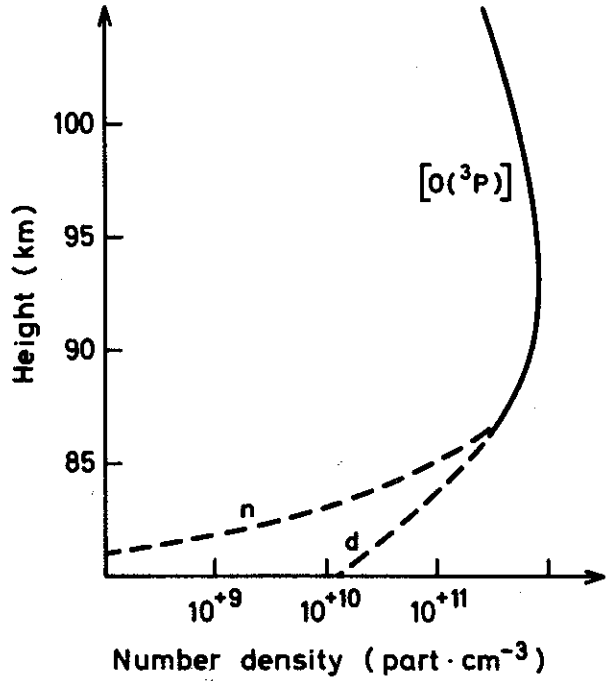

Fig. 3.1. Number densities of $O(^3P)$. Dashed lines when diurnal variations occur (*d* daytime values, *n* night-time values).

indicates heights where diurnal variations occur.

In the hydrogen cycle, water vapour, molecular hydrogen, and methane are species with lifetimes of days or more, and they are therefore determined by assuming steady-state conditions. The same assumptions have also been made for atomic hydrogen above about 82 km, where chemical lifetime is several days or more. When the long-lived hydrogen species are broken down by photochemical processes, odd-hydrogen species like OH, HO_2, and H are formed.

Water vapour is broken down by dissociation

$$H_2O + h\nu \rightarrow OH + H \quad 2420\ A \qquad (e)$$

Below about 60 km the solar radiation is absorbed strongly in the Schuman-Runge bands of O_2 (Kockarts 1971), which is at the wavelength where the water vapour dissociation takes place. Reaction (*e*) is therefore of less importance in the lower mesosphere and in the stratosphere. At these heights water vapour is broken down by reaction:

$$H_2O + O(^1D) \rightarrow OH + OH \quad k = 3 \times 10^{-10} \qquad (6)$$

Molecular hydrogen is similarly broken down by excited atomic oxygen:

$$H_2 + O(^1D) \rightarrow OH + H \quad k = 3 \times 10^{-10} \qquad (7)$$

In the lower stratosphere methane is broken down rapidly by the reaction with hydroxyl:

$$CH_4 + OH \rightarrow CH_3 + H_2O$$
$$k = 5.5 \times 10^{-12} \cdot e^{-\frac{1886}{T}} \qquad (8)$$

which is a source of water vapour. Methane is further broken down by reaction with $O(^1D)$.

$$CH_4 + O(^1D) \rightarrow CH_3 + OH \quad k = 3 \times 10^{-10} \qquad (9)$$

Above about 70 km, dissociation will take place:

$$CH_4 + h\nu \rightarrow CH_3 + H \quad \lambda 1650\ A. \qquad (p)$$

This is, however, a negligible reaction, since, as we will show, CH_4 is broken down at lower heights.

The further decomposition of CH_3 is of interest in the hydrogen cycle. Formaldehyde will be formed as a result of the following reactions:

$$CH_3 + O_2 + M \rightarrow CH_3O_2 + M$$
$$k = 1.3 \times 10^{31} \qquad (10)$$

$$CH_3 + O(^3P) \rightarrow CH_2O + H \quad k = 3 \times 10^{-13} \qquad (11)$$

$$CH_3O_2 + NO \rightarrow CH_3O + NO_2$$
$$k = 2.7 \times 10^{-12} \cdot e^{-\frac{500}{T}} \qquad (12)$$

$$CH_3O_2 + CH_3O_2 \rightarrow CH_3O + CH_3O + O_2$$
$$k = 2.6 \times 10^{-13} \qquad (13)$$

$$CH_3O + O_2 \rightarrow CH_2O + HO_2$$
$$k = 10^{-12} \cdot e^{-\frac{3300}{T}} \qquad (14)$$

Formaldehyde is broken down to give either H_2O, H_2, or odd hydrogen through the following reactions:

$$CH_2O + OH \rightarrow CHO + H_2O$$
$$k = 1.4 \times 10^{-11} \qquad (15)$$

$$CH_2O + h\nu \rightarrow CO + H_2 \quad J = 1.1 \times 10^{-4} \qquad (r)$$

$$CH_2O + h\nu \rightarrow CHO + H \quad J = 3.3 \times 10^{-5} \qquad (s)$$

$$CHO + O_2 \rightarrow CO + HO_2 \quad k = 10^{-13} \qquad (16)$$

The balance between the molecular and odd form of hydrogen is maintained when the following reaction of odd-hydrogen loss is considered:

$$OH + HO_2 \rightarrow H_2O + O_2 \quad k_{10} = 2 \times 10^{-10} \quad (17)$$

$$OH + OH \rightarrow H_2O + O(^3P)$$
$$k = 1.4 \times 10^{-11} \cdot e^{-\frac{500}{T}} \quad (18)$$

$$H + HO_2 \rightarrow H_2O + O(^3P)$$
$$k = 1.5 \times 10^{-12} \cdot T^{1/2} \cdot e^{-\frac{2000}{T}} \quad (19)$$

$$H + HO_2 \rightarrow H_2 + O_2$$
$$k = 5 \times 10^{-12} \cdot T^{1/2} \cdot e^{-\frac{1000}{T}} \quad (20)$$

$$H + H + M \rightarrow H_2 + M \quad k = 1.0 \times 10^{-32} \quad (21)$$

$$H_2O_2 + OH \rightarrow H_2O + HO_2$$
$$k = 4 \times 10^{-13} \cdot T^{1/2} \cdot e^{-\frac{600}{T}} \quad (22)$$

$$HNO_3 + OH \rightarrow H_2O + NO_3$$
$$k = 1 \times 10^{-13} \quad (23)$$

We can see from the above reactions that there are no reactions giving CH_4 in the upper atmosphere. Methane, which is produced at the earth's surface, is transported into the stratosphere and broken down by chemical reactions.

The internal distribution between the odd-oxygen species has to be determined in order to estimate the production of water vapour and molecular hydrogen. Several very fast reactions are considered:

$$OH + O(^3P) \rightarrow H + O_2 \quad k = 2.5 \times 10^{-11} \quad (3)$$

$$HO_2 + O(^3P) \rightarrow OH + O_2 \quad k = 7.0 \times 10^{-11} \quad (4)$$

$$H + O_2 + M \rightarrow HO_2 + M \quad k = 3.2 \times 10^{-32} \quad (24)$$

$$H + O_3 \rightarrow OH + O_2 \quad k = 2.6 \times 10^{-11} \quad (25)$$

$$HO_2 + NO \rightarrow OH + NO_2$$
$$k = 5 \times 10^{-11} \cdot e^{-\frac{1600}{T}} \quad (26)$$

$$OH + CO \rightarrow H + CO_2$$
$$k = 2.1 \times 10^{-13} \cdot e^{-\frac{115}{T}} \quad (27)$$

$$OH + O_3 \rightarrow HO_2 + O_2 \quad k \leq 1 \times 10^{-16} \quad (28)$$

$$OH + CH_4 \rightarrow H_2O + CH_3$$
$$k = 5.5 \times 10^{-12} \cdot e^{-\frac{1886}{T}} \quad (8)$$

The destruction of OH by CH_4 (reaction (8)), which produces CH_3, is also a source of HO_2, since CH_3, through reactions (14) and (16), forms HO_2. Through the above reactions the odd-hydrogen species are in chemical equilibrium, and it is found to be convenient to express HO_2 and H as functions of OH since hydroxyl is the dominating component in most of the height region below 90 km.

$$E_H = \frac{k_3 \cdot |O(^3P)| + k_{27} \cdot |CO|}{k_{24} \cdot |O_2| \cdot |M| + k_{25} \cdot |O_3|}$$
$$|H| = E_H \cdot |OH| \quad (3.13)$$

$$E_{HO_2} = \frac{E_H \cdot k_{24} \cdot |O_2| \cdot |M| + k_{28} \cdot |O_3| + k_8 \cdot |CH_4|}{k_4 \cdot |O(^3P)| + k_{26}|NO|}$$
$$|HO_2| = E_{HO_2} \cdot |OH| \quad (3.14)$$

Production of odd hydrogen is given by

$$P_{Hodd} = J_{H_2O} \cdot |H_2O| + k_6 \cdot |O(^1D)| \cdot |H_2O| + k_7 \cdot |H_2| \cdot |O(^1D)| + k_9 \cdot |O^1D)| \cdot |CH_4| + |k_9 \cdot |O(^1D)| + k_8 \cdot |OH| \cdot |CH_4| \times \frac{J_{ACH_2O}}{J_{ACH_2O} + J_{BCH_2O} + k_{15} \cdot OH} \quad (3.15)$$

The last term in this equation gives the production of odd hydrogen by reaction (*s*).

Loss of odd hydrogen is given by the following equation, when HO_2 and H are given by equations (3.13) and (3.14).

$$Q_{Hodd} = k_{17} \cdot E_{HO_2} + k_{18} + k_{19} \cdot E_H \cdot E_{HO_2} + k_{20} \cdot E_H \cdot E_{HO_2} + k_{21} \cdot E_H \cdot E_H \cdot |M| \quad (3.16)$$

Reactions (22) and (23) are neglected in the calculations. They are found to be minor loss reactions at all heights.

From equations (3.15) and (3.16) hydroxyl concentrations are given by

$$|OH| = \frac{2}{\sqrt{P_{Hodd}/Q_{Hodd}}}, \quad (3.17)$$

and HO_2 and H given by their equilibrium expression (3.13) and (3.14).

When the odd-hydrogen species are determined, molecular species can be calculated. Production and loss terms of water vapour are given by the equations:

$$P_{H_2O} = k_{17} \cdot |OH| \cdot |HO_2| + k_{18} \cdot |OH| \cdot |OH| + k_8 \cdot |CH_4| \cdot |OH| + |CH_4| \times [k_8 \cdot |OH| + k_9 \cdot |O(^1D|]$$

$$\times \frac{k_{15} \cdot |OH|}{J_{ACH_2O} + J_{BCH_2O} + k_{15} \cdot |OH|} \quad (3.18)$$

$$Q_{H_2O} = k_6 \cdot |O(^1D)| + J_{H_2O} \quad (3.19)$$

H_2 production and loss terms are given by

$$P_{H_2} = k_{20} \cdot |H| \cdot |HO_2| + k_{21} \cdot |H| \cdot |H| \cdot |M| + |CH_4| \cdot [k_8 \cdot |OH| + k_9 \cdot |O(^1D)|] \cdot \frac{J_{BCH_2O}}{J_{ACH_2O} + J_{BCH_2O} + k_8 \cdot |OH|} \quad (3.20)$$

$$Q_{H_2} = k_7 \cdot |O(^1D)| \quad (3.21)$$

There is no production of methane above the tropopause; its loss is given by the equation:

$$Q_{CH_4} = k_9 \cdot |O(^1D)| + k_8 \cdot |OH| \quad (3.22)$$

H_2O, H_2 and CH_4 is determined by reaction (3.10), with $\delta_{H_2O} = 3.5 \times 10^{-6}$, $\delta_{H_2} = 5 \times 10^{-7}$ and $\delta_{CH_4} = 1.5 \times 10^{-6}$ as lower boundary values of mixing ratios.

Above 80 km atomic hydrogen is calculated from the equation (3.10) with reaction (*e*) as photochemical production term, and reactions (19), (20), and (21) as photochemical loss terms.

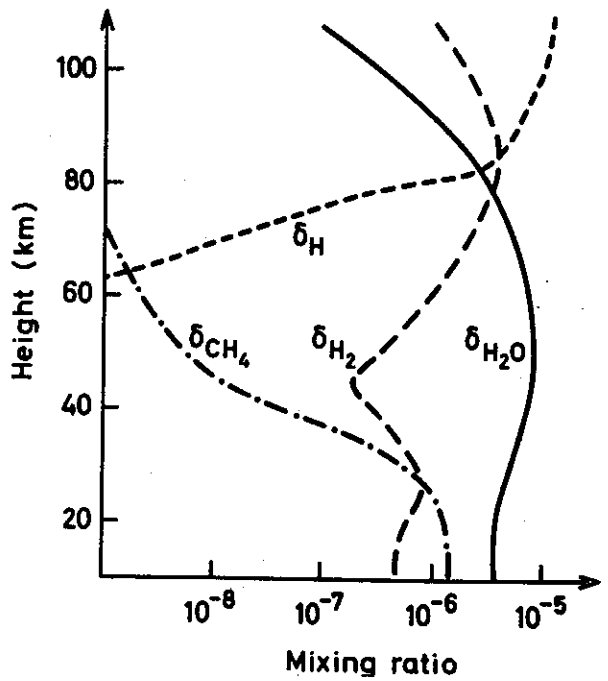

Fig. 3.2. Mixing ratios of water vapour (δ_{H_2O}), methan (δ_{CH_4}), atomic hydrogen (δ_H), and molecular hydrogen (δ_{H_2}).

Calculated values of the mixing ratios of the main hydrogen components H_2O, H_2, CH_4, and H are given in Fig. 3.2. CH_4 is effectively broken down by OH, with some contribution from the reaction with $O(^1D)$. Since there are no reactions forming methane above the tropopause, it is effectively reduced by hydroxyl above about 30 km. At 50 km, the mixing ratio is down by more than one order of magnitude.

In the case of H_2O and H_2 we have to consider both production and loss terms. Water vapour and molecular hydrogen are equally broken down by reactions (7) and (6) in the stratosphere. Water vapour is, however, reformed by the fast reaction (17), the dominating loss reaction of odd hydrogen, while there are no effective reactions converting odd hydrogen into molecular hydrogen. The only reaction producing H_2 in the stratosphere is reaction (*r*), converting CH_4 to H_2. In the upper atmosphere the mixing ratio of the total hydrogen content in molecular form β is constant and is given by

$$\beta = (\delta_{H_2O} + \delta_{H_2} + 2 \cdot \delta_{CH_4} + \tfrac{1}{2} \cdot \delta_H) \quad (3.22)$$

In the stratosphere δ_H is of no interest. A decrease in the CH_4 mixing ratio therefore will lead to an increase in the mixing ratio of either H_2O or H_2. In the lower stratosphere most of the CH_4 loss leads to an increase of H_2O, and the rest to an increase in H_2. Molecular hydrogen increases up to about 27 km, approximately 50% above its tropopause value. Above 27 km it decreases, due to reaction (7), and reaches its minimum value around 45 km with $\delta_H \approx 2 \times 10^{-7}$. Water vapour increases in the whole stratosphere, and around 45–50 km more than 95% of the total hydrogen is in the form of water vapour. In the mesosphere, molecular hydrogen increases with height and becomes a major odd-hydrogen component, a result of reaction (20), which effectively produces H_2, and above about 80 km δ_{H_2} exceeds δ_{H_2O}. Above this height the conversion from odd to molecular hydrogen is very slow, with the result that H becomes the major hydrogen component above 82 km. It should be mentioned that the result of the calculations strongly depends on the eddy transport. This is especially true for the stratosphere, where eddy diffusion coefficients

are small. Changes in H_2O would lead to marked changes in the CH_4 and H_2 profiles.

Carbon monoxide and carbon dioxide are also included in these calculations. CO_2 is one of the dominant species in the chemistry of cluster ions, while CO is involved in the chemistry of the neutral atmosphere, and controls OH in the lower stratosphere through reaction (27). Mixing ratio of CO has been measured in the troposphere (Seiler & Warneck 1972), and is constant with height, with a value of $\delta_{CO} = 1.5 \times 10^{-7}$. This has been used as boundary value at the tropopause. CO_2 mixing ratio is given the value $\delta_{CO_2} = 3.4 \times 10^{-4}$ in the lower atmosphere, while this number has been used as the total number density of $CO + CO_2$ in the upper region.

The following reactions are included in the CO and CO_2 calculations:

$$CO_2 + h\nu \rightarrow CO + O(^3P) \quad \lambda < 1800\ \text{A} \qquad (q)$$

$$CH_2O + h\nu \rightarrow CO + H_2 \qquad J_{BCH_2O} = 1.4 \times 10^{-4} \qquad (r)$$

$$HCO + O_2 \rightarrow CO + HO_2 \quad k = 10^{-13} \qquad (16)$$

$$CO + O(^3P) + M \rightarrow CO_2 + M \qquad k = 2.2 \times 10^{-36} \qquad (29)$$

$$CO + OH \rightarrow CO_2 + H \qquad k = 2.1 \times 10^{-13} \cdot e^{-\frac{115}{T}} \qquad (27)$$

The dissociation of CO_2 is limited to the atmosphere above 70 km. Below this height the conversion from CO_2 to CO is negligible. Methane destruction is therefore the only source of carbon monoxide in the stratosphere. From the above reactions it is seen that for each CH_4 molecule broken down, one carbon monoxide molecule is formed. The production and loss terms of CO and CO_2 are therefore given by

$$P_{CO} = (k_9 \cdot |O(^1D)| + k_8 \cdot |OH|) \cdot |CH_4| + J_{CO_2} \cdot |CO_2| \qquad (2.33)$$

$$Q_{CO} = k_{29} \cdot |O| \cdot |M| + k_{27} \cdot |OH| \qquad (2.34)$$

$$P_{CO_2} = k_{29} \cdot |O| \cdot |M| \cdot |CO| + k_{27}|OH| \cdot |CO| \qquad (3.25)$$

$$Q_{CO_2} = J_{CO_2} \qquad (3.26)$$

The height profiles of CO and CO_2 are then given by equation (3.10) with the above equations as photochemical production and loss terms. The result of these calculations is given as mixing ratios in Fig. 3.3.

A few km above the tropopause, the CO mixing ratio drops rapidly with height, until it reaches its minimum value around 50 km. Mixing ratio is here down by more than two orders of magnitude. In the mesosphere the δ_{CO} increases rapidly with height. This is a result of the dissociation of CO_2. At the upper boundary, 110 km, approximately one third of the atmospheric carbon is in the form of CO. CO_2 has a constant mixing ratio with height up to about 95 km. Above that height it decreases slowly, and at 110 km it is still twice as abundant as CO. If we add together all the production of CO above the tropopause by reaction (16), we find this source above the tropopause to be responsible for only 10% of the CO present in the atmosphere. It is reasonable to expect that the CO is produced more effectively in the troposphere, where the rate constant of reaction (8) is fast, due to higher temperatures and higher

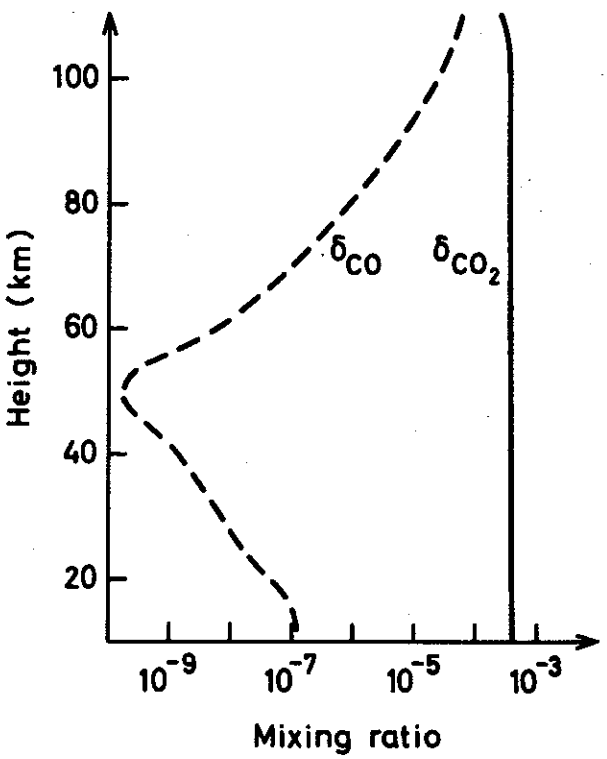

Fig. 3.3. Mixing ratios of carbon dioxide (δ_{CO_2}) and carbon monoxide (δ_{CO}).

OH densities, as shown by Wofsy, McConnell & McElroy (1972).

One constituent of special interest is nitrous oxide. It is known to be present in the troposphere, with constant mixing ratio with height $\delta_{N_2O} = 2.5 \times 10^{-7}$ (Schütz et al. 1970). Its production is believed to be at the earth's surface, from where it is transported upwards into the stratosphere. In the stratosphere it is broken down by chemical reactions:

$$N_2O + h\nu \rightarrow N_2 + O(^1D) \quad \lambda < 3370\ \text{A} \qquad (o)$$

$$N_2O + h\nu \rightarrow NO + N \qquad (o^1)$$

$$N_2O + O(^1D) \rightarrow N_2 + O_2 \quad k = 9 \times 10^{-11} \qquad (30)$$

$$N_2O + O(^1D) \rightarrow NO + NO \quad k = 9 \times 10^{-11} \qquad (31)$$

The two reactions of interest for nitrogen oxides are the reactions (O^1) and (31). Recent measurements have shown that we can exclude reaction (O^1), since the end product from dissociations is almost entirely N_2 and $O(^1D)$ (Preston & Barr 1971). The only reaction producing odd nitrogen is therefore reaction (31). There is no effective production of N_2O in the stratosphere. Production and loss of nitrous oxide are therefore given by the terms:

$$P_{N_2O} = 0$$

$$Q_{N_2O} = J_{N_2O} + k_{30} \cdot |O^1D)| + k_{31} \cdot |O(^1D)| \qquad (3.1)$$

The major loss is by solar dissociation, which increases rapidly with height (Fig. 2.1).

The height profiles of N_2O mixing ratio is given in Fig. 3.4. Up to 25 km δ_{N_2O} decreases slowly, while it falls off rapidly above 25 km. At 30 km the N_2O mixing ratio decreases by two orders of magnitude, and it is found that above this height, N_2O plays a negligible role in the chemistry of nitrogen oxides.

All calculations in the steady-state model were carried out with an average daytime value of 14.8 hours (45° summer).

Steady state conditions were obtained by repeating the calculations until there were no variations in the values from one iteration to the next. 20 repetitions turned out to be sufficient.

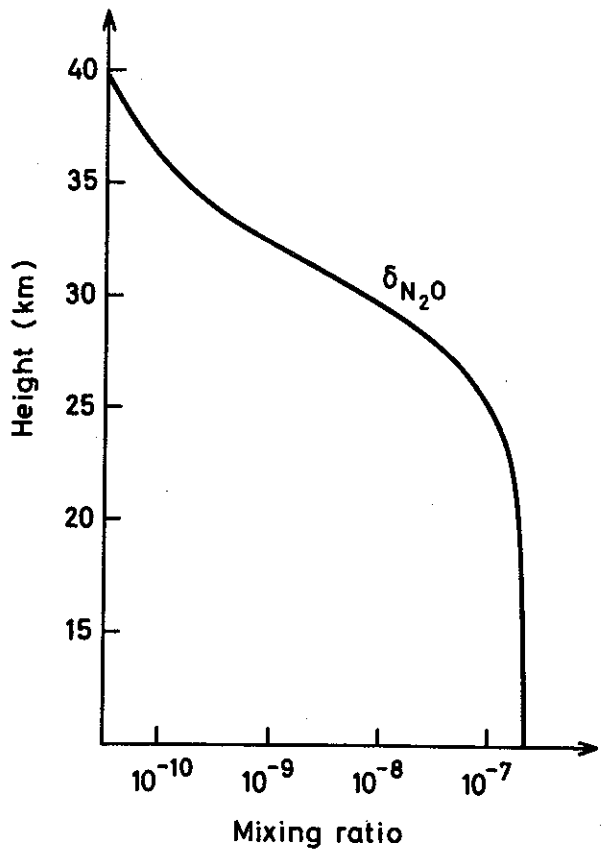

Fig. 3.4. Mixing ratio of nitrous oxide (δ_{N_2O}).

4. DIURNAL VARIATIONS OF ODD OXYGEN AND ODD HYDROGEN SPECIES

Species with short chemical lifetimes are not influenced directly by eddy transport. The time-dependent differential equation can therefore be set up with chemical production and loss terms only.

When variations of odd species are calculated, a second order term has to be included in the equation:

$$\frac{dx}{dt} = P_x - Q_x \cdot x - R_x \cdot x^2 \qquad (4.1)$$

Integration over a time step Δt gives the x-value at the time $t + \Delta t$:

$$x_{t+t} = (x_{e1} - x_{e2}) \frac{\frac{x_t - x_{e1}}{x_t - x_{e2}} \cdot e^{-(-\sqrt{Q_x^2 + 4R_x P_x} \cdot \Delta t)}}{1 - \frac{x_t - x_{e1}}{x_t - x_{e2}} \cdot e^{(-\sqrt{Q_x^2 + 4R_x P_x} \cdot \Delta t)}} \qquad (4.2)$$

x_{e1} and x_{e2} are the roots of the equation for

equilibrium conditions $\left(\frac{dx}{dt} = 0\right)$:

$$x_{e1} = \frac{-Q_x + \sqrt{Q_x^2 + 4P_xR_x}}{2 \cdot R_x},$$

$$\times\ x_{e2} = \frac{-Q_x - \sqrt{Q_x^2 + 4P_xR_x}}{2 \cdot R_x} \qquad (4.3)$$

The calculations are carried out with a time step of $\Delta t = 60$ s. Variations of the odd species are usually much slower than variations of each of the species (Hesstvedt 1970), often with lifetimes of several hours or more. It is therefore convenient to replace eq. (4.3), when the term $(Q_x \cdot x + R_x \cdot x) \cdot \Delta t$ in eq. (4.1) is less than 0.1, with:

$$x_{t+\Delta t} = x_t + (P_x - Q_x \cdot x_t - R_x \cdot x_t^2) \cdot \Delta t \qquad (4.4)$$

In this case equation (4.4) gives the variation with sufficient accuracy. In the region 70 km to 40 km, equation (4.4) is applied to the diurnal variations of odd-oxygen species and down to the tropopause for odd-hydrogen species. The variation of each odd component is calculated from the differential equation:

$$\frac{dx}{dt} = P_x - Q_x \cdot x \qquad (4.5)$$

Integrated over a time step t, we get the value of x at the time $\Delta t + t$:

$$x_{t+\Delta t} = x_e + (x_t - x_e) \cdot e^{-Q_x \cdot \Delta t} \qquad (4.6)$$

where x_e is the equilibrium value of (4.5) for $\frac{dx}{dt} = 0$.

In the transition zone 86–70 km, both photochemical and eddy diffusion are included in the calculations of H and $O(^3P)$. The same equation (4.5) is used, but the following expressions from equation (3.7) are used for the production and loss terms:

$$Q = Q_i + B_i,$$
$$P = A \cdot x_{i-1} + C \cdot x_{i+1} + P_i \qquad (4.7)$$

with (3.11) and (3.12) as production and loss terms of odd oxygen, and (3.15) and (3.16) as production and loss terms of odd hydrogen.

Odd-oxygen species are $O(^3P)$, $O(^1D)$, and O_3. Atomic oxygen in the excited-state ^1D is always in chemical equilibrium with lifetimes $\tau < 1$ second, since it is rapidly quenched by the main atmospheric constituents O_2 and N_2 to give ground-state atomic oxygen:

$$O(^1D) + M \rightarrow O(^3P) + M \quad k = 6 \times 10^{-11} \qquad (32)$$

Production of $O(^1D)$ is at the short wavelength side of the dissociation of O_2 and O_3.

$$O_2 + h\nu \rightarrow O(^1D) + O(^3P) \quad \lambda < 1750\ \text{A} \qquad (b)$$

$$O_3 + h\nu \rightarrow O(^1D) + O_2(^1\Delta_g) \quad \lambda < 3100\ \text{A} \qquad (d)$$

The equilibrium value is therefore given by:

$$|O(^1D)| = (J_b \cdot |O_2| + J_d \cdot |O_3|)/(k_{32} \cdot |M|) \qquad (4.8)$$

Atomic oxygen in its ground state is the most abundant odd-oxygen component in the upper region during the day; at night, and below about 60 km, ozone is the dominant odd-oxygen compound.

Equilibrium between $O(^3P)$ and O_3 is established through the reactions

$$O + O_2 + M \rightarrow O_3 + M$$

$$k_2 = 1.1 \times 10^{-34} \cdot e^{+\frac{500}{T}} \qquad (33)$$

$$O_3 + h\nu \rightarrow O_2 + O \quad J_{3O_3} \qquad (c,d)$$

In the lower stratosphere, where O_3 is determined by transport processes, atomic oxygen has an additional source through the dissociation of nitrogen dioxide:

$$NO_2 + h\nu \rightarrow NO + O(^3P) \quad \lambda < 3975\ \text{A} \qquad (i)$$

When $O(^3P)$ dominates, O_3 is calculated from (4.6) with reactions (c,d) and (33) as loss and production terms;

$$O_3 = \frac{k_{33} \cdot |O_2| \cdot |M|}{J_{O_3}} \cdot |O(^3P)| \qquad (4.9)$$

and atomic oxygen is given by odd oxygen:

$$|O(^3P)| = |O_{odd}| - |O_3| \qquad (4.10)$$

When O_3, on the other hand, is the main odd component, $O(^3P)$ is calculated from (4.6) with reactions (c,d) and (i) as production term, and reaction (33) as loss term:

$$O(^3P) = \frac{J_{O_3} \cdot |O_3| + J_{NO_2} \cdot |NO_2|}{k_{33} \cdot |O_2| \cdot |M|} \qquad (4.11)$$

In this case ozone is determined from the odd oxygen

$$|O_3| = |O_{odd}| - |O(^3P)| \qquad (4.12)$$

It is also of great importance to calculate the excited-state molecular oxygen, $O_2(^1\Delta g)$, which is a main participant in *D*-region chemistry. The presence of $O_2(^1\Delta g)$ in the upper atmosphere is well established by observations of infra-red atmospheric bands (Evans et al. 1968, Wood et al. 1969, Evans et al. 1972). The main source of $O_2(^1\Delta g)$ is dissociation of O_3 during the day:

$$O_3 + h\nu \rightarrow O_2(^1\Delta_g) + O(^1D) \quad \lambda < 3110\ \text{A} \qquad (d)$$

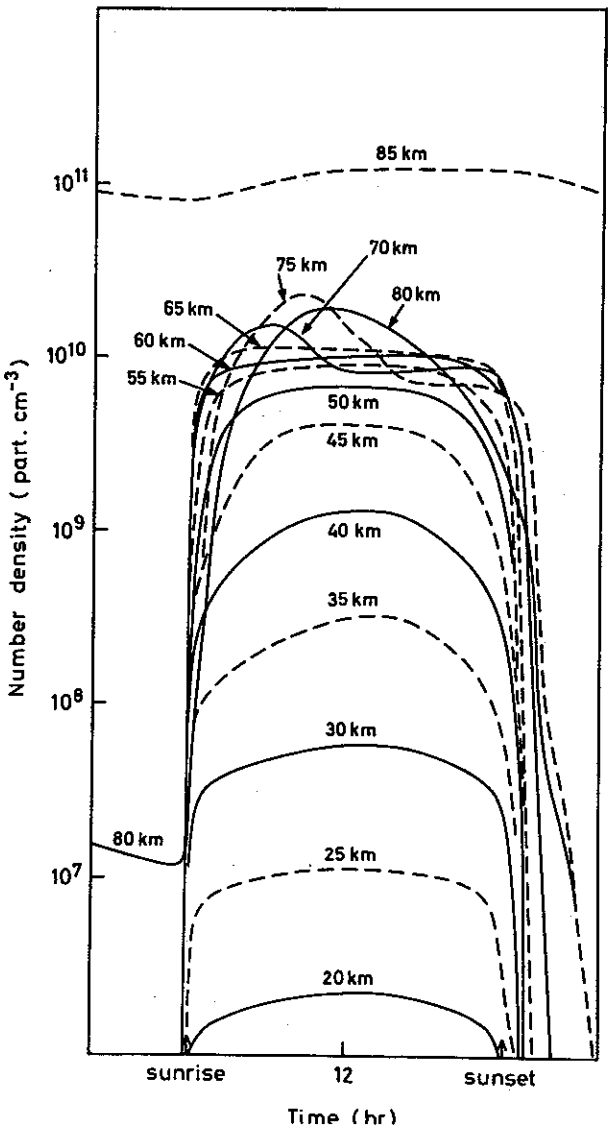

Fig. 4.1. Diurnal variations of $O(^3P)$, number densities.

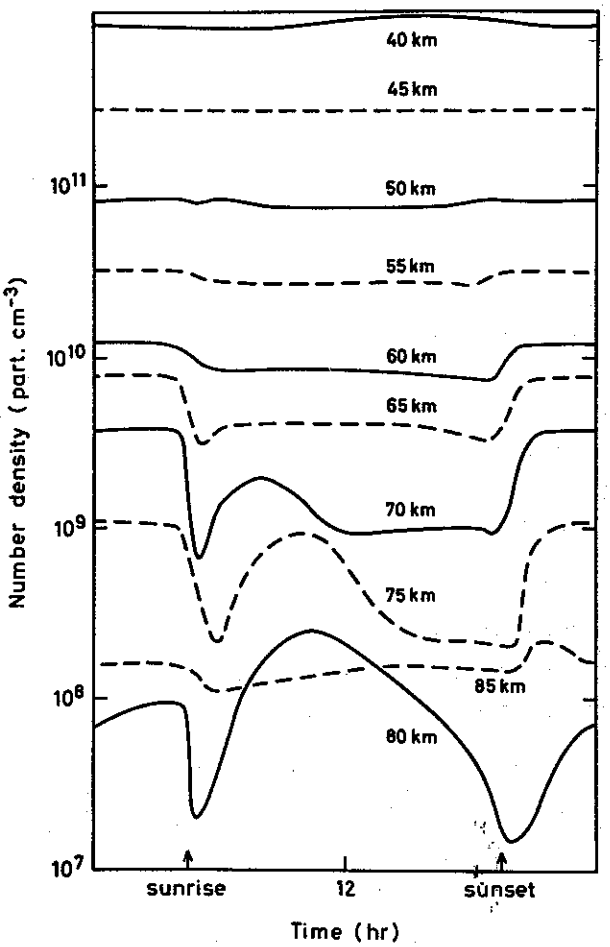

Fig. 4.2. Diurnal variations of ozone, number densities.

The night-time production is not very well known. One reaction that has been put forward, is the three-body reaction:

$$O(^3P) + O(^3P) + M \rightarrow O_2(^1\Delta_g) + M$$

$$k = 3.3 \times 10^{-33} \cdot \frac{300}{T} \qquad (1b)$$

This source is uncertain, since the end product of O_2 could well be in other excited states (Bates 1960). We would, therefore, expect one of four reactions to give $O_2(^1\Delta g)$. Another reaction that has been put forward is the reaction of atomic oxygen with perhydroxyd (Wood 1972)

$$O(^3P) + HO_2 \rightarrow OH + O_2(^1\Delta_g)$$

$$k = 7 \times 10^{-12}, \qquad (4b)$$

to explain observed night-time profiles. Reaction (4*b*) is therefore included as a night-time source. The night-time layer is explained if 10% of reaction (4) produces excited-state O_2.

There are two main loss processes of $O_2(^1\Delta_g)$. One is the radiactive deactivation:

$$O_2(^1\Delta_g) \rightarrow O_2(^3\Sigma_g^-) + h\nu \quad k = 2.8 \times 10^{-4} \quad (34)$$

and the other is the collisional deactivation by reaction (Wayne 1972):

$$O_2(^1\Delta_g) + M \rightarrow O_2(^3\Sigma_g^-) + M \quad k = 4.4 \times 10^{-19} \quad (35)$$

Below 80 km the air density is so high that reaction (35) is the main loss of $O_2(^1\Delta_g)$.

A third reaction that has aroused some interest is the reaction with ozone (Wayne 1972):

$$O_2(^1\Delta_g) + O_3 \rightarrow O_2(^3\Sigma_g^-) + O_3 \quad k = 10^{-15} \quad (36)$$

The rate constant is, however, too slow to give the reaction any atmospheric importance.

Calculations of $O_2(^1\Delta_g)$ are made in the same way as for $O(^3P)$ and for O_3 from equation (4.6) in the whole height region.

The number densities of $O(^3P)$, O_3, and $O_2(^1\Delta_g)$ are given in Figs. 4.1, 4.2, and 4.3 for the three components respectively.

Above 84 km there are small diurnal variations in $O(^3P)$, while below 82 km it decreases rapidly during the night. During the day, atomic oxygen varies slowly with height with average daytime values of 10^{10} particles cm^{-3} down to about 50 km.

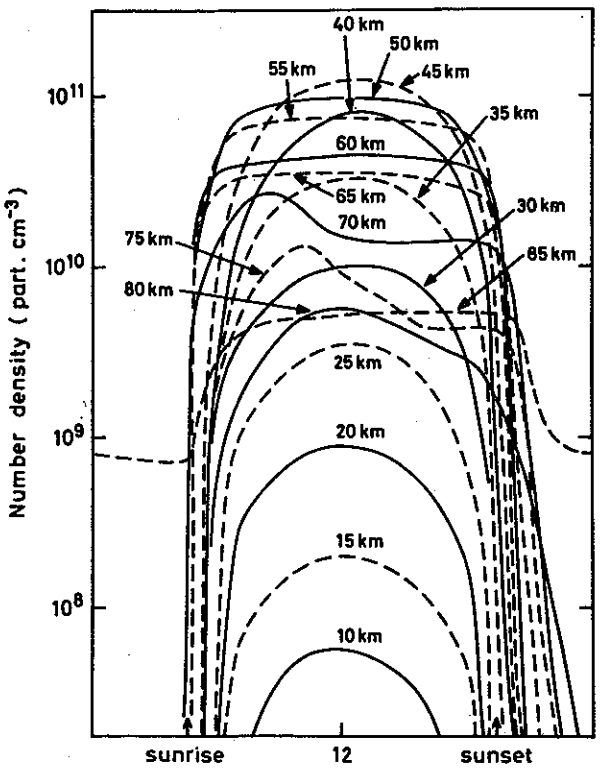

Fig. 4.3. Diurnal variations of $O_2(^1\Delta_g)$, number densities.

It is, however, interesting to note the very pronounced variation during the day of the odd-oxygen species in the height region 70 km to 80 km. In this region, oxygen loss is through reactions with OH and HO_2:

$$O(^3P) + OH \rightarrow H + O_2 \quad k = 2.5 \times 10^{-11} \quad (3)$$

$$O(^3P) + HO_2 \rightarrow OH + O_2 \quad k = 7 \times 10^{-11} \quad (4)$$

Odd hydrogen is built up slowly after sunrise. When OH and HO_2 number densities become sufficiently high, reactions (3) and (4) effectively reduce atomic oxygen. Around 50 km, where odd-hydrogen production is slower than below, maximum $O(^3P)$ occurs shortly before noon, while at 70 km maximum concentrations are reached about 2 hours after sunrise. This asymmetric variation around noon is most pronounced at 75 km, with decrease in $O(^3P)$ of more than a factor of 3 from 2 hours before noon to 2 hours after noon.

Ozone is in photochemical equilibrium with $O(^3P)$ during the day, and therefore has a variation over the day, similar to atomic oxygen. The height profile of ozone shows minimum values around 80 km, with a marked increase downward from 80 km. Below about 60 km, ozone densities exceed atomic oxygen densities. At night, ozone varies much less than atomic oxygen. Above 75 km, conversion from $O(^3P)$ through reaction (33) is not very effective. Odd oxygen is therefore effectively reduced after sunset, before ozone is formed. At 75 km and below, this conversion is much faster, and ozone densities therefore increase at sunset, and then remain constant for the rest of the night. Above 45 km, night-time values exceed the daytime values, and this increase is more pronounced at higher altitudes. The increase is 50% at 60 km, and is a factor of 3 at 70 km. This is in agreement with observations (Hilsenrath 1972). Below 45 km, diurnal variations in O_3 are negligible. Ozone is expected to be influenced by transport processes in the lower stratosphere, and horizontal processes must be considered (Hesstvedt 1972). We have, therefore, found it necessary

to adopt an observed profile of O_3 below 35 km (Hering & Borden 1964).

$O_2(^1\Delta_g)$ has a similar variation to $O(^3P)$ during the day, since it is produced by ozone photolysis. In the upper height region, $O_2(^1\Delta_g)$ deactivation has a marked time delay after sunset. At lower heights, it is deactivated almost instantly. This is a result of the strong decrease in lifetimes from the upper to the lower heights. At 80 km the lifetime $\tau_O\,(^1\Delta_g) = 1$ hour, while at 30 km $\tau_{O_2}(^1\Delta_g) =$ 10 sec.

The height profile of $O_2(^1\Delta_g)$ shows minimum densities around 80 km, similar to what was found for O_3, with number densities about 5×10 particles cm^{-3}. Below 80 km there is an increase in number densities down to 45 km, when maximum noontime values of $10^{11} cm^{-3}$ are obtained. Below 45 km it decreases downward.

Odd-hydrogen species (H, OH, and HO_2) are involved in the destruction of odd oxygen. In the mesosphere and upper stratosphere, reactions of $O(^3P)$ with odd-hydrogen species represent the major loss; in the lower stratosphere these reactions have small effects compared to reactions with odd nitrogen. In this region, however, odd-hydrogen reactions determine the balance between the main nitrogen components NO, NO_2 and HNO_3.

It is therefore necessary to calculate odd-hydrogen species in the whole height region, as well as odd-oxygen and odd-nitrogen species. The reactions which determine the production and loss of the odd-oxygen species are the same as those used in the steady-state calculations.

In the mesosphere and upper stratosphere, atomic oxygen dominates the distribution of odd hydrogen in daytime by reactions (3) and (4). At night and in the lower stratosphere, reactions with ozone, nitrogen oxides, methane, and carbon monoxide have to be considered. Hydroxyl is broken down by reaction (28) with ozone, by reaction (27) with carbon monoxide, by reaction (15) with formaldehyde, by reaction (8) with methane, and by reaction (26) with nitrogen dioxide. All these reactions are sources of HO_2. Reaction (27) produces atomic hydrogen. Atomic hydrogen is, however, rapidly converted to HO_2 through reaction (24), and is therefore present in the lower stratosphere with negligible number densities. We would not expect all HNO_3 formed to be a loss of OH; the dissociation of HNO_3 leads to two products (Johnston & Graham 1972). At the short wavelength side, HO_2 is formed by reaction (1), and at the long wavelength side OH is reformed, reaction (k). All other HNO_3 destruction is assumed to be a loss of OH. The process of converting HO_2 to OH is through the reaction with nitric oxide (26).

Down to about 65 km during the day, atomic hydrogen is the most abundant odd-hydrogen component. Hydroxyl and perhydroxyd is calculated from equation (4.6), with photochemical production and loss terms given by:

$$P_{OH} = k_4 \cdot |O(^3P)| \cdot |HO_2| + k_{25} \cdot |O_3| \cdot |H| + k_{26} \cdot |NO| \cdot |HO_2| + J_{AHNO_3} \cdot |HNO_3| \quad (4.13)$$

$$Q_{OH} = k_3 \cdot |O(^3P)| + k_{27} \cdot |CO| + k_8 \cdot |CH_4| + k_{15} \cdot |CH_2O| + k_{23} \cdot |HNO_3| + k_{41} \cdot |NO_2| \cdot |M| \quad (4.14)$$

$$P_{HO_2} = k_{24} \cdot |O_2| \cdot |M| \cdot |H| + k_8 \cdot |CH_4| \cdot |OH| + k_{15} \cdot |CH_2O| \cdot |OH| + J_{BHNO_3} \cdot |HNO_3| \quad (4.15)$$

$$Q_{HO_2} = k_4 \cdot |O(^3P)| + k_{26} \cdot |NO| \quad (4.16)$$

Atomic hydrogen is determined from the expression:

$$|H| = |H_{odd}| - |OH| - |HO_2| \quad (4.17)$$

Down to 30 km, HO_2 is broken down rapidly during the day by reaction (4). OH is, therefore, the dominating odd-hydrogen component, and under these conditions H and HO_2 are given by eq. (4.6). Production and loss terms are the same as above for HO_2, while H has the terms:

$$P_H = k_3 \cdot |OH| \cdot |O(^3P)| + k_{27} \cdot |CO| \cdot |OH| \quad (4.18)$$

$$Q_H = k_{24} \cdot |O_2| \cdot |M| + k_{25} \cdot |O_3| \quad (4.19)$$

Finally, in the lower stratosphere, where HO_2 is the main odd-hydrogen component, OH and H are calculated from eq. (4.6), with production and loss terms as given above. Hydrogen dioxide is given by:

$$HO_2 = |H_{odd}| - |OH| - |H| \quad (4.20)$$

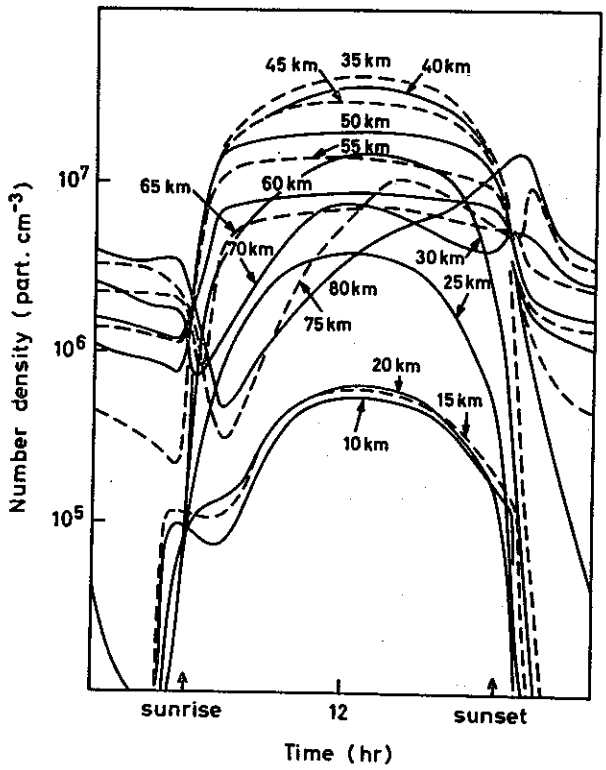

Fig. 4.4. Diurnal variations of hydroxyl, number densities.

In addition to the odd species, the diurnal variations of hydrogen peroxide are calculated. H_2O_2 is produced by reaction:

$$HO_2 + HO_2 \rightarrow H_2O_2 + O_2$$
$$k = 5 \times 10^{-11} \cdot e^{-\frac{800}{T}} \quad (37)$$

and is broken down by photodissociation:

$$H_2O_2 + h\nu \rightarrow OH + OH$$
$$J_{H_2O_2}\ \lambda < 5650\ \text{Å}, \quad (f)$$

and by the reactions with $O(^3P)$ and OH:

$$H_2O_2 + O(^3P) \rightarrow HO_2 + OH \quad k = 10^{-15} \quad (38)$$

$$H_2O_2 + OH \rightarrow H_2O + HO_2$$
$$k = 4 \times 10^{-13} \cdot T^{1/2} \cdot e^{-\frac{600}{T}} \quad (22)$$

The last reaction forms water vapour in contrast to reactions (f) and (38), which convert H_2O_2 back to odd hydrogen. The formation of hydrogen peroxide through reaction (37) is therefore not a real loss of odd hydrogen; the loss is by the fractional part going through reaction (22), which is, as already mentioned, less important than reactions (b) and (38). Dissociation rates of reaction (f) are taken from Fig. 2.1.

Diurnal variations of OH and HO_2 are given in Fig. (4.4) and (4.5). OH and HO_2 are the dominating odd-hydrogen components below 65 km during the day, and below 82 km at night.

Down to 70 km the odd-hydrogen species are built up slowly during the sunlight period, reaching maximum number densities a long time after noon. This is a result of their long lifetimes $\tau_{odd} \approx 5$ hours to 1 day.

In the lower region, odd-hydrogen components are built up much faster, with lifetimes $\tau_{odd\ H} \approx$ 1–2 hours.

Down to about 30 km, OH and HO_2 are controlled by atomic oxygen, reactions (3) and (4), and are approximately equally abundant during the day. During the night, with no production processes and lifetimes of hours, there is a decrease in number density in at least one of the components towards the end of the night.

Above 45 km, loss of OH is slow, and it becomes the main night-time component between 82 km and 45 km. Below 45 km the destruction of OH is fast enough to remove OH effectively during the night. In addition, the conversion from

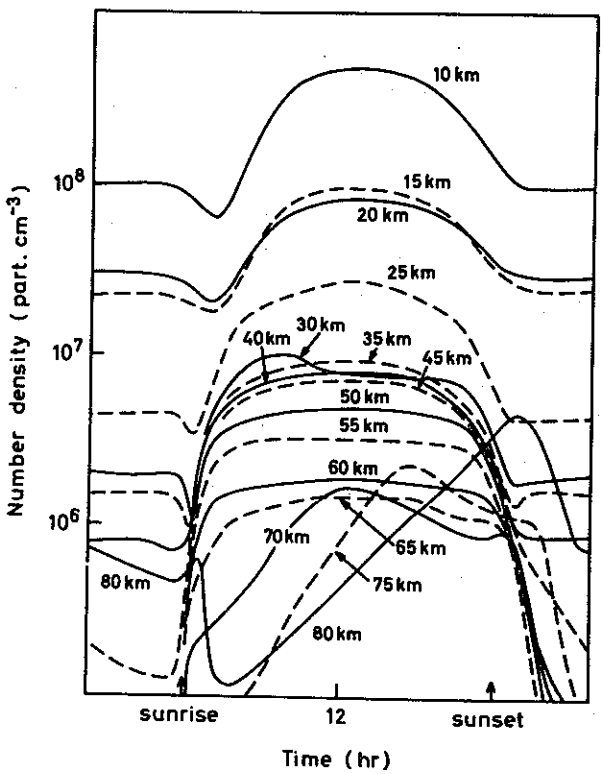

Fig. 4.5. Diurnal variations of hydrogen dioxide, number densities.

HO_2 to OH is very slow due to the low night-time NO values. HO_2 is therefore the main night-time hydrogen component below 45 km. During the day OH is the main component down to about 30 km. Highest odd-hydrogen daytime densities are reached around 40–45 km, with $|OH| \approx 3\text{–}4 \times 10^7$ particles cm^{-3}. Below 30 km, atomic oxygen decreases rapidly, and the balance between OH and HO_2 is determined by the species O_3, CO, CH_4, NO, and NO_2. Hydroxyl is broken down much more rapidly than HO_2. This is very pronounced a few km above the tropopause, where HO_2 densities exceed the OH densities by almost three orders of magnitude by day. At sunset, OH is removed almost instantaneously. Minimum daytime values of OH are obtained at 10–20 km, with $|OH| \approx 5 \times 10^5 cm^{-3}$.

Hydrogen pentoxide has a variation that is opposite to the odd-hydrogen component. The maximum H_2O_2 concentrations are obtained during the night when solar dissociation, the most effective loss process, is absent. Below 40 km, diurnal variations are negligible. H_2O_2 number densities increase downward, with maximum values of 10^{10} particles cm^{-3} at the tropopause.

5. THE FORMATION AND DISTRIBUTION OF NITROGEN OXIDES IN THE STRATOSPHERE AND LOWER MESOSPHERE

There has been an increasing interest in the production and spatial distribution of nitrogen oxides in the atmosphere during the last few years. Recently attention has focussed on the effects of nitrogen oxides on the stratospheric ozone (Crutzen 1971). Hesstvedt (1972) showed that nitrogen dioxide is by far the dominating constituent in removing odd oxygen through the reaction

$$NO_2 + O(^3P) \rightarrow NO + O_2 \qquad k = 9.1 \times 10^{-12} \qquad (5)$$

It should therefore be obvious that reliable information on the distribution of nitrogen is needed.

There are two source regions of odd nitrogen. One upper region above 80 km where production is through ion processes will be discussed in the next chapter. The other region is the lower stratosphere, where nitrogen oxides are produced through the decomposition of N_2O. This region extends upwards to approximately 30 km. Between 30 and 80 km there is no production of nitrogen oxides. The loss of nitrogen oxides to molecular nitrogen is through the reaction:

$$N(^4S) + NO \rightarrow N_2 + O(^3P) \qquad k = 2.2 \times 10^{-11} \qquad (39)$$

Below 60 km the number densities of N decrease rapidly, making reaction (39) extremely slow, and therefore we can also neglect the loss of odd nitrogen in this region. At the tropopause, the loss of nitrogen oxides is due to a downward flux into the troposphere, where they are lost through precipitation processes.

The downward flux is given by:

$$F_{z\downarrow} = -K_z \cdot |M| \cdot \frac{d}{dz}(\delta_{NO_x}), \qquad (5.1)$$

where δ_{NO_x} is the mixing ratio of nitrogen oxides. Since there are no photochemical loss reactions in the lower stratosphere, only production and diffusion terms determine nitrogen oxides. The following equation can therefore be set up:

$$\frac{d}{dt}|NO_x| = -\frac{d}{dz}\left(K_z \cdot |M| \cdot \frac{d}{dz}(\delta_{NO_x})\right) + P_{NO_x} \qquad (5.2)$$

Photochemical production is given by the reaction

$$N_2O + O(^1D) \rightarrow NO + NO \qquad k = 9 \times 10^{-11} \qquad (31)$$

giving

$$P_{NO_x} = 2k_{31} \cdot |N_2O| \cdot |O(^1D)| \qquad (5.3)$$

Diurnal variations are negligible in the stratosphere, and we can therefore, with sufficient accuracy, set

$$\frac{d}{dt}|NO_x| \approx 0$$

We now have to solve the differential equation

$$\frac{d}{dz}\left(K_z \cdot |M| \cdot \frac{d}{dz}(\delta_{NO_x})\right) = +P_{NO_x} \qquad (5.4)$$

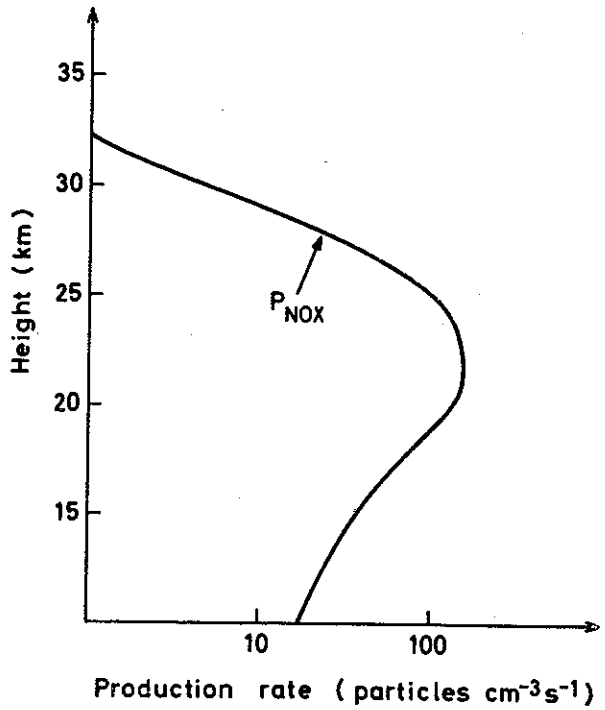

Fig. 5.1. NO_x production rates.

Eduation (5.4) is integrated between the tropopause at 10 km and the upper boundary at 40 km. Boundary fluxes are taken to be: $F_{\downarrow 40} = 0$ and $F_{\downarrow 10} = \sum_{z=10}^{40} P_{NO_x} \cdot \Delta z$. The downward flux at 10 km is thought to be the total production of nitrogen oxides in the height region from N_2O decomposition. We further use a fixed value of δ_{NO_x} at the lower border:

$$\delta_{NO_x T \cdot P} = 3 \times 10^{-9} \qquad (5.5)$$

With these assumptions the mixing ratio of NO_x at height h is:

$$\delta_{NO_x \cdot h} = \delta_{NO_x \cdot TP} + \sum_{z=10}^{h} \frac{1}{K_z \cdot |M|} \cdot \times \left(\sum_{z=10}^{40} P_{NO_x} \cdot \Delta z - \sum_{z=10}^{h} P_{NO_x} \cdot \Delta z \right) \cdot \Delta z \qquad (5.6)$$

The efficiency of reaction (31) in producing odd nitrogen is not very high. Dissociation of N_2O, producing molecular nitrogen, is the dominant loss reaction. Only a few percent of the N_2O loss gives odd nitrogen. This is, however, sufficient to have a marked effect on δ_{NO_x}, since N_2O densities exceed the NO_x densities almost by two orders of magnitude at the tropopause level.

The height profile of δ_{NO_x} depends strongly on at what heights the production takes place. High NO_x production at altitudes where K_z is low gives a marked gradient in the δ_{NO_x} (equation 5.1) in order to keep up the flux. Production rates versus height are shown in Fig. 5.1. Just above the tropopause, loss rates of N_2O are slow, due to the low $O(^1D)$ densities, and therefore we have low production rates of NO_x. Above 30 km the production is also low, as a result of the low N_2O densities. In the region between, where both $O(^1D)$ and N_2O is relatively abundant, NO_x production is more effective. Maximum production rates take place between 20 km and 25 km, with $P_{NO_x} = 200$ particles $cm^{-3}s^{-1}$. Total production above the tropopause is given by.

$$\sum_{z=10}^{40} P_{NO_x} \cdot \Delta z = 1.2 \times 10^8 \text{ particles cm}^{-2}s^{-1} \qquad (5.7)$$

The increase in δ_{NO_x} with height, which is necessary for the downward transport of NO_x produced by reaction (31), is shown in Fig. 5.2. The increase is very pronounced between 18 and

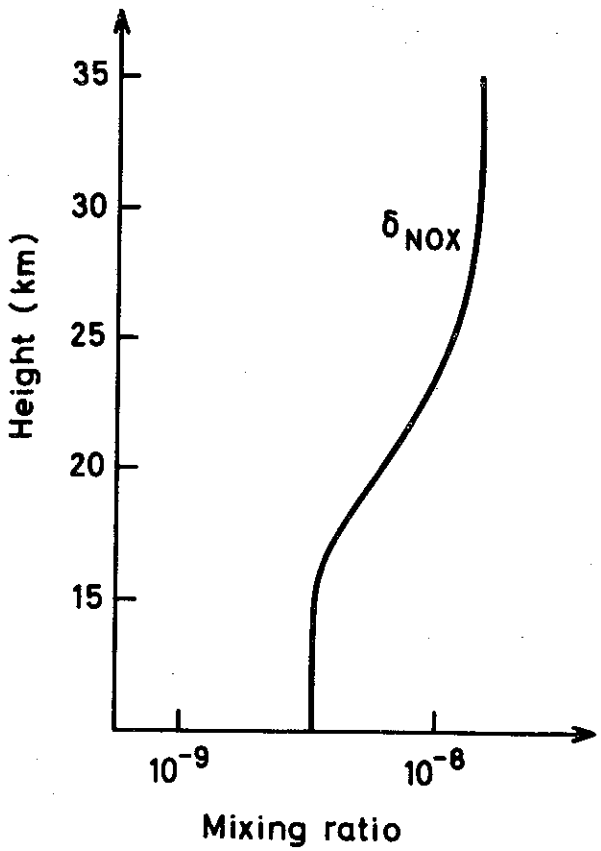

Fig. 5.2 NO_x mixing ratio in the lower stratosphere.

28 km. This is the region where we have high production. In addition eddy transport is slow, due to low K_z values. Below 18 km, the eddy transport increases, and the production decreases rapidly with height, and is negligible above 30 km (Fig. 5.1). In both cases the fluxes are so low that there are very small changes in the mixing ratio.

Mixing ratio increases from its tropopause value 3.0×10^{-9} to its maximum value around 30 km of 1.4×10^{-8}. It should be noticed that the result depends strongly on the model used. Changes in ozone densities would change the $O(^1D)$ densities and therefore also the δ_{NO_x} profile. It would also change the absorption of solar radiation, which results in a changed dissociation of N_2O.

When the height profile of NO_x is obtained, it is of interest to find the internal distribution between the different nitrogen species, since equilibrium between the species is established much faster than equilibrium of NO_x against transport. As we have seen from reaction (31), the initial product of NO_x is nitric oxide. There is, however, a conversion to NO_2 through the reaction:

$$NO+O_3 \rightarrow NO_2+O_2$$
$$k = 9.3\times10^{-13}\cdot e^{-\frac{1235}{T}} \qquad (40)$$

Equilibrium between NO and NO_2 is maintained by the reactions converting NO_2 to NO:

$$NO_2+O(^3P) \rightarrow NO+O_2$$
$$k = 9.1\times10^{-12} \qquad (5)$$

$$NO_2+h\nu \rightarrow NO+O(^3P) \quad \lambda<3975\ \text{A} \qquad (i)$$

Below about 65 km, reaction (40) is fast enough to convert NO to NO_2 during the night, while the reverse reactions are negligible, since there is no dissociation of NO_2 (reaction i), and atomic oxygen is present in very small quantities (reaction 5).

In the stratosphere below about 40 km, the nitrogen scheme has to be extended to include more complex nitrogen species such as NO_3, HNO_3, and N_2O_5. Nitric acid is present in the lower stratosphere as a major nitrogen component. It has been measured in the height region 18 km to 30 km at a zenith distance of 90°, and has a fairly constant mixing ratio of $1\text{–}3\times10^{-9}$ (Murcray et al. 1969, Rhine et al. 1969).

Several reactions proposed as sources and sinks of nitric acid in the stratosphere have turned out to be of little atmospheric interest (Asquith & Tyler 1970, Morris & Niki 1971). At present the reaction sequence proposed by Morley & Smith (1972) seems to be effective in converting nitrogen dioxide to nitric acid (Crutzen 1972):

$$NO_2+OH \rightarrow HNO_3^*$$
$$k = 1.05\times10^{-11}\cdot e^{-\frac{170}{T}} \qquad (41a)$$

$$HNO_3^* \rightarrow NO_2+OH = \frac{10^{13}}{\left(1+\frac{5000}{T}\right)^4} \qquad (41b)$$

$$HNO_3^*+M \rightarrow HNO_3+M$$
$$k = 4\times10^{-11} \qquad (41c)$$

The above sequence produces HNO_3 by a three-body reaction (41a,b) above 30 km, when radiative lifetime is shorter than collisional lifetime. Below 20 km, production is by the binary reactions (41a,c), and collisional lifetime is here short enough to make practically all the excited-state nitric acid production deactivated by collision Altitudes between 20 and 30 km are a transition zone where both processes are important. The production at all altitudes is obtained by combining the equations in a three-body reaction:

$$NO_2+OH+M \rightarrow HNO_3+M$$
$$k = 1.05\times10^{-11}\cdot e^{-\frac{170}{T}} \times \frac{4\times10^{-11}\cdot|M|}{4\times10^{-11}\cdot|M|+\frac{10^{13}}{\left(1+\frac{5000}{T}\right)^4}} \qquad (41)$$

Nitric acid is broken down in the stratosphere, mostly by solar dissociation:

$$HNO_3+h\nu \rightarrow OH+NO_2 \quad \lambda<5460\ \text{A} \qquad (k)$$

$$HNO_3+h\nu \rightarrow HO_2+NO \quad \lambda<3700\ \text{A} \qquad (l)$$

Dissociation cross sections have recently been measured by Graham & Johnston (1972); it is assumed that dissociation at the long wavelength side is given by reaction (k), and at the short wavelength side by reaction (l). Since HNO_3 is

produced by reaction (41) with HO, reaction (*l*) is therefore involved in the conversion form OH and HO_2.

It should be noticed that the dissociation rates (Figs. 2.1) are much less than those obtained by using cross sections given by Leighton (1961). This results in lower loss rates of HNO_3, since the above reactions are the main loss. A minor loss reaction is the reaction with hydroxyl:

$$HNO_3 + OH \rightarrow H_2O + NO_3 \quad k = 10^{-13} \qquad (23)$$

This reaction is, as we have already seen, a loss reaction of odd hydrogen. Nitric acid is also broken down by atomic oxygen:

$$HNO_3 + O(^3P) \rightarrow OH + NO_3 \quad k \leq 10^{-14} \qquad (42)$$

It is, however, only in the upper stratosphere that this reaction effects the HNO_3 densities at heights where HNO_3 densities are small compared to the NO densities.

NO_3 enters the nitrogen cycle through reaction

$$NO_2 + O_3 \rightarrow NO_3 + O_2$$

$$k = 10^{-11} \cdot e^{-\frac{3000}{T}} \qquad (43)$$

This reaction is slow, and since the loss reactions are very fast, the equilibrium densities of NO_3 will be low. NO_3 is expected to be broken down by the reactions:

$$NO_3 + NO \rightarrow NO_2 + NO_2 \quad k = 10^{-11} \qquad (44)$$

$$NO_3 + h\nu \rightarrow NO_2 + O(^3P) \quad \lambda < 5710\ \text{A} \qquad (n)$$

$$NO_3 + h\nu \rightarrow NO + O_2 \quad < \lambda 11\ \mu \qquad (m)$$

Nitric oxide and O_2 are the main product from solar dissociation (Johnston 1972). A considerable part of the NO_3 loss gives dinitrogen pentoxide through the sequence:

$$NO_3 + NO_2 \rightarrow N_2O_5^* \quad k = 7 \times 10^{-12} \qquad (45)$$

$$N_2O_5^* \rightarrow NO_2 + NO_3 \quad k = 2.8 \times 10^{8} \qquad (46)$$

$$N_2O_5^* + M \rightarrow N_2O_5 + M \quad k = 1.7 \times 10^{-10} \qquad (47)$$

Ground-state dinitrogen pentoxide is broken down by solar dissociation

$$N_2O_5 + h\nu \rightarrow N_2O_5 + O(^3P) \quad \lambda < 8000 \qquad (j)$$

Dissociation cross sections are taken from Jones & Wolf (1937), and dissociation rates are given as average daytime values in Fig. 2.1.

N_2O_4 formed in the reaction (*j*) is broken down rapidly by the reaction:

$$N_2O_4 + M \rightarrow NO_2 + NO_2 + M$$

Through all the above reactions diurnal variations of the odd-nitrogen species are calculated. Initial daytime values of the nitrogen components are obtained by steady-state calculations. Equilibrium between the species depends on the loss rates. Rapid changes between two components mean that equilibrium is established rapidly. Fig. 5.3 shows the loss rates of the components NO, NO_2, and HNO_3. Loss rates from NO to NO_2 and vice-versa are fast; equilibrium between the two components is therefore rapidly established. This will take place before HNO_3 has reached its equilibrium value, since the loss rates from NO_2 to HNO_3 are very slow compared to the loss rate to NO.

The loss of NO_2 producing NO_3 is very slow compared to the loss of NO_3 to the NO–NO_2 cycle, which makes NO_3 a negligible nitrogen

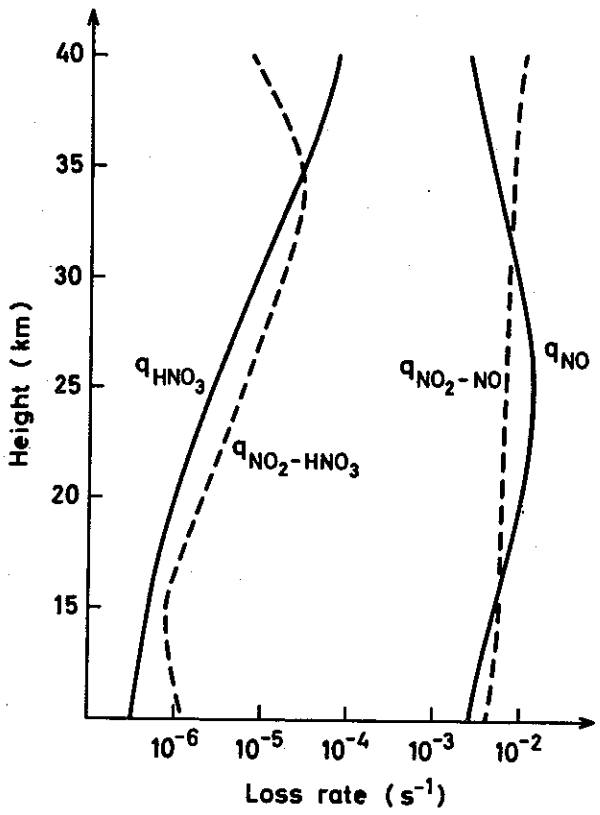

Fig. 5.3. NO, NO_2, and HNO_3 loss rates. The curves q_{NO} and q_{NO_2-NO} give NO and NO_2 loss rates, and the curves q_{HNO_3} and $q_{NO_2-HNO_3}$ give HNO_3 and NO_2 loss rates.

constituent. It acts, however, as a source of N_2O_5 through reaction (45), which is broken down at a slower rate. Since it is limited by the slow NO_3 production, N_2O_5 is also found to be less abundant than the components NO, NO_2, and HNO_3.

Initial values are therefore obtained by assuming that NO, NO_2, and HNO_3 are the main nitrogen components, and that equilibrium between NO and NO_2 is rapidly established. It can then be assumed that equilibrium between NO–NO_2 and HNO_3 is established. When the number density of the total odd-nitrogen components is given by $\delta_{\text{odd N}} \cdot |M|$, equilibrium values of the above species are given by these equilibrium expressions:

$$|NO| = \delta_{\text{odd N}} \cdot |M| \cdot \frac{k_5 \cdot |O(^3P)| + J_{NO_2}}{k_5 \cdot |O(^3P)| + J_{NO_2} + k_{40} \cdot |O_3|} \cdot \frac{J_{HNO_2} + k_{23} \cdot |OH|}{J_{HNO_2} + k_{23} \cdot |OH| + f \cdot k_{41} \cdot |OH|} \tag{5.8}$$

$$|NO_2| = \delta_{\text{odd N}} \cdot |M| \cdot \frac{k_{40} \cdot |O_3|}{k_5 \cdot |O(^3P)| + J_{NO_2} + k_{40} \cdot |O_3|} \cdot \frac{J_{HNO_3} + k_{23} \cdot |OH|}{J_{HNO_3} + k_{23} \cdot |OH| + f \cdot k_{41} \cdot |OH|} \tag{5.9}$$

$$|HNO_3| = \delta_{\text{odd N}} \cdot |M| \cdot \frac{f \cdot k_{41} \cdot |OH|}{J_{HNO_3} + k_{23} \cdot |OH| + f \cdot k_{41} \cdot |OH|} \tag{5.10}$$

The first equilibrium term in the equations of NO and NO_2 determines the equilibrium between the two components, while the last term in all three equations determines the equilibrium between NO–NO_2 and HNO_3.

The letter f gives the efficiency of NO_2 through reaction (41) in converting the species NO–NO_2 to HNO_3. It is given by the equilibrium expression for NO_2.

$$f = \frac{k_{40} \cdot |O_3|}{k_{40} \cdot |O_3| + k_5 \cdot |O(^3P)| + J_{NO_3}} \tag{5.11}$$

When the above species are determined, equilibrium densities of NO_3 and N_2O_5 are given by:

$$|N_2O_5| = \frac{k_{45} \cdot |NO_2| \cdot |NO_3|}{J_{N_2O_5}} \frac{k_{47} \cdot |M|}{k_{47} \cdot |M| + k_{46}} \tag{5.13}$$

Average daytime mixing ratios are given in Fig. 5.4 below 40 km. Above this height NO is the dominant component. Below 35 km, NO_2 and HNO_3 are the main nitrogen species. HNO_3 is present between 20 km and 35 km, with fairly constant mixing ratios, $\delta_{HNO_3} = 3\text{–}5 \times 10^{-9}$. The decrease below 20 km is a result of the decrease in total mixing ratio (Fig. 5.2). NO_2 has its highest mixing ratio around 30 km, where it is the dominant odd-nitrogen component. Mixing ratios of 5×10^{-9} are reached. Below 25 km, the mixing ratio is fairly constant, $\delta_{NO_2} = 10^{-9}$. NO mixing ratio decreases steadily down to 25 km. Below 25 km, NO mixing ratios of 10^{-9} are obtained. To illustrate the distribution between the main odd-nitrogen components, the fractional part of the different species is given in Fig. (5.5) for heights between 40 km and 10 km. From the region above 40 km where nitric oxide occupies more than 80% of the total odd nitrogen, it decreases rapidly below. It is of minor interest compared to NO_2 and HNO_3. Nitrogen dioxide, the main component in the odd-oxygen destruction, is the main odd component around 30 km. Below about 27 km the high ozone densities convert NO effectively to NO_2, which in turn is converted to HNO_3. Since the loss of nitric acid decreases rapidly below 30 km, its relative densities increase rapidly. Around 25 km these effects are very pronounced. HNO_3 dominates strongly with 70% of the total odd nitrogen. Nitric acid dominates less strongly below, but is the main component at all heights. Around 15 km, 40% of odd nitrogen is in the form of HNO_3. Below 15 km HNO_3 increases again, a result of the increase of OH.

It should be obvious that species with lifetimes equal to one day or less will undergo changes

$$|NO_3| = \frac{k_{53} \cdot |O_3| \cdot |NO_2 + k_{23} \cdot |OH| \cdot |HNO_3| + k_{42} \cdot |O(^3P) \cdot |HNO_3|}{k_{44} \cdot |NO| + \frac{k_{47} \cdot |M|}{k_{47} \cdot |M| + k_{46}} \cdot k_{45} \cdot NO_2 + J_{NO_3}} \tag{5.12}$$

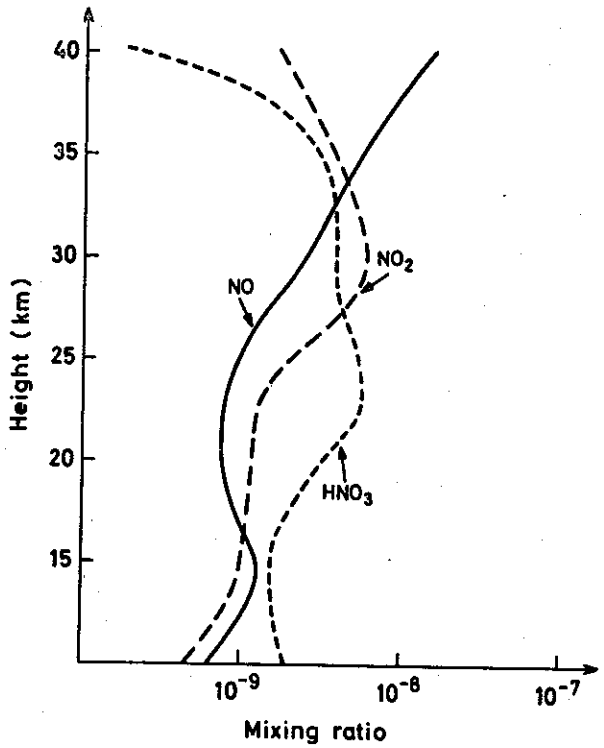

Fig. 5.4. NO, NO_2, and HNO_3 mixing ratios.

during the day. This is found to be true for NO_2, NO_3, and N_2O_5 where the main loss by day is solar dissociation.

The diurnal variations are obtained as for the odd-oxygen and odd-hydrogen components. Minor components are therefore solved by equation (4.6).

Above about 27 km, where either NO or NO_2 are the main components, HNO_3, NO_3, and N_2O_5 are determined with the following production and loss terms:

$$P_{HNO_3} = k_{41} \cdot |NO_2| \cdot |OH| \cdot |M| \quad (5.14)$$

$$Q_{HNO_3} = k_{42} \cdot |O(^3P)| + J_{HNO_3} + k_{23} \cdot |OH| \quad (5.15)$$

$$P_{NO_3} = k_{43} \cdot |NO_2| \cdot |O_3| \quad (5.16)$$

$$Q_{NO_3} = k_{44} \cdot |NO| + J_{NO_3} + k_{45} \cdot |NO_2| \cdot \frac{k_{46}}{k_{46} + k_{47} \cdot |M|} \quad (5.17)$$

$$P_{N_2O_5} = k_{45} \cdot |NO_3| \cdot |NO_2| \cdot \frac{k_{47} \cdot |M|}{k_{47} \cdot |M| + k_{46}} \quad (5.18)$$

$$Q_{N_2O_5} = J_{N_2O_5} \quad (5.19)$$

When NO dominates, NO_2 is calculated from (4.6) with

$$P_{NO_2} = k_{40} \cdot |NO| \cdot |O_3| \quad (5.20)$$

$$Q_{NO_2} = J_{NO_2} + k_5 \cdot |O(^3P)| \quad (5.21)$$

NO is calculated from the total nitrogen oxide:

$$|NO| = \delta_{NO_x} \cdot |M| - |NO_2| - |HNO_3| - |NO_3| - 2 \cdot |N_2O_5| \quad (5.22)$$

When NO_2 is the dominant nitrogen compound, the calculation procedure is changed. NO is now given by eq. (4.6) with the terms:

$$P_{NO} = J_{NO_2} \cdot |NO_2| + k_5 \cdot |O(^3P)| \quad (5.23)$$

$$Q_{NO} = k_{40} \cdot |O_3| ,$$

NO_2 is given by

$$|NO_2| = \delta_{NO_x} \cdot |M| - |NO| - |HNO_3| - |NO_3| - 2 \cdot |N_2O_5| \quad (5.24)$$

Below 27 km, at heights where HNO_3 is the dominant odd component, all components, except HNO_3, are determined by eq. (4.6), with the above production and loss terms. It is found unnecessary to calculate diurnal variations of

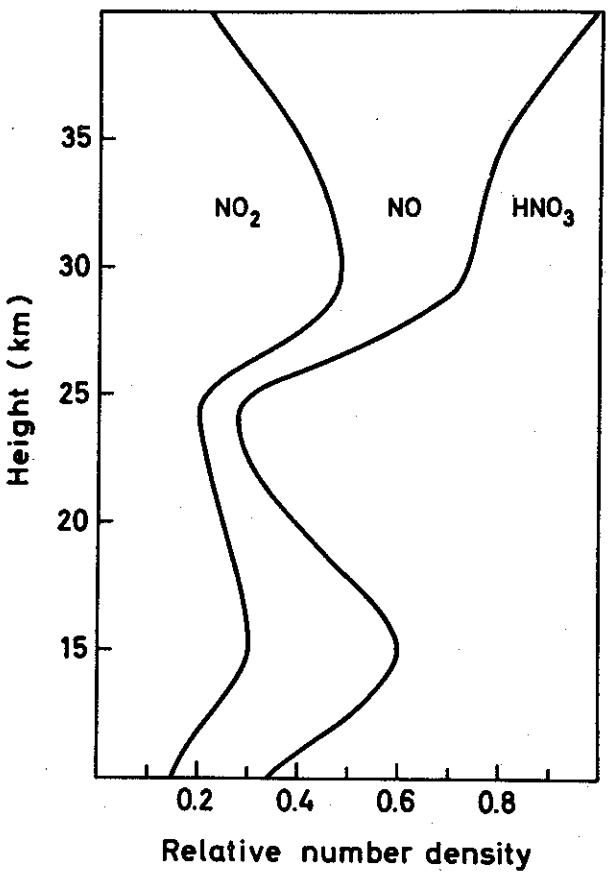

Fig. 5.5. Relative densities of NO, NO_2, and HNO_3.

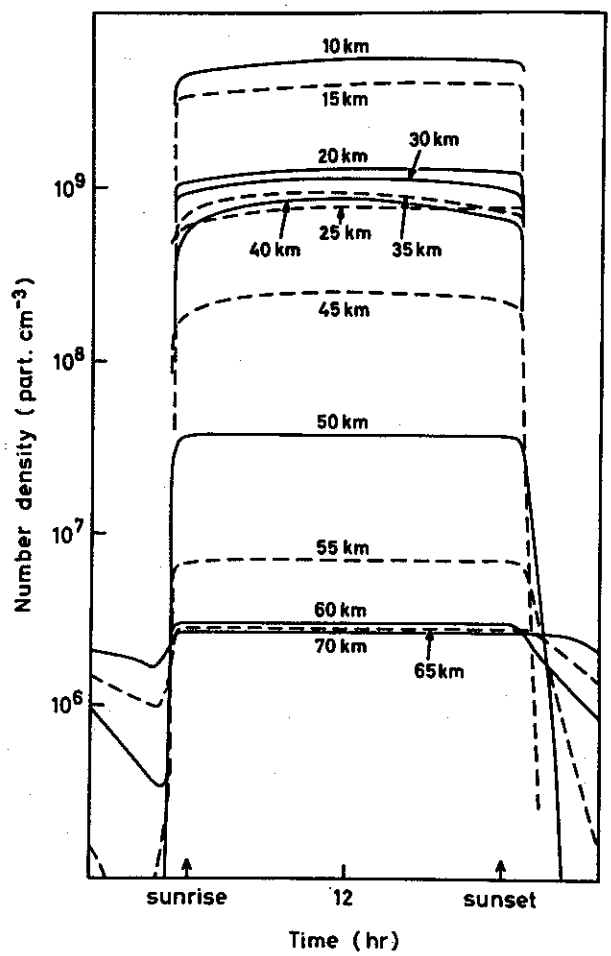

Fig. 5.6. Diurnal variations of NO number densities.

HNO_3. This is a result of the long lifetimes of nitric acid below 27 km. τ increases from approximately 4 days at 27 km to 30 days at 15 km, which gives negligible variations over the day. HNO_3 is therefore given by the steady-state values below 27 km. Diurnal variations of NO and NO_2 are given in Figs. 5.6 and 5.7. Nitric oxide is broken down at night below 70 km, as a result of reaction (40). Above 70 km, ozone densities are too low to effect NO markedly. Below about 60 km, however, the ozone densities are so high that we have an almost instantaneous conversion from NO to NO_2. This is also a result of the rapid changes of atomic oxygen and solar radiation, which convert NO_2 to NO during the day. At sunset we have a fast conversion from NO_2 to NO. Since the sum of NO and NO_2 is almost constant over the day – above 35 km, HNO_3 densities are low, and below, diurnal variations are small – it has, therefore, little effect on the diurnal variation of NO and NO_2. We will, therefore, have a variation in NO_2 which is opposite to the variation in NO. Above 40 km, where daytime NO_2 densities are low, there is a very strong increase after sunset, and decrease after sunrise. In the lower stratosphere, daytime NO_2 densities are approximately the same as the NO densities, and night-time NO_2 densities therefore increase with about a factor of 2.

Calculations of N_2O_5 number densities led to maximum values exceeding 10^8 particles cm^{-3} during the night in the lower stratosphere. Diurnal variations are very pronounced since lifetimes $\tau_{N_2O_5} = \dfrac{1}{J_{N_2O_5}}$ are less than one day. N_2O_5 decreases during the day in the presence of sunlight and minimum values are obtained in the afternoon before sunset. These values are a factor of 10 or more below the maximum night-time values.

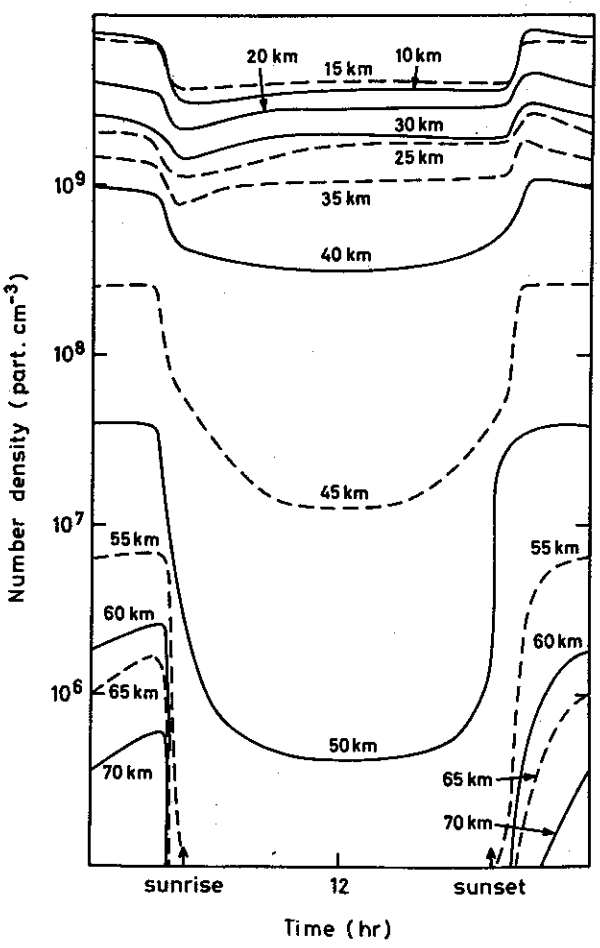

Fig. 5.7. Diurnal variations of NO_2 number densities.

Diurnal variations in NO_3 are similar. Maximum values are obtained during the night. By day the fast reactions (*m*), (*n*), (44), and (45) remove NO_3 rapidly. Number densities are low, even at night, and maximum values will never exceed 10^7 particles cm^{-3}.

6. THE CHEMISTRY OF NITRIC OXIDE IN THE THERMOSPHERE AND MESOSPHERE, AND ITS ROLE IN IONIZATION

The role of nitric oxide as a major source of *D*-region ionization is well known. It has a low ionization potential (9.22 ev), which allows ionization by the strong Ly-α radiation. It is also well established from recent research that NO plays an active role in the complex chemistry of negative ions below approximately 85 km, where it is involved in the chain leading to the terminal ions (Mohnen 1970, Reid 1970).

Measurements of nitric oxide have been performed on various occasions (Pearce 1969, Meira 1970). Pearce's measurement seems to be in error, giving too high number densities, while the measurement of Meira, with much lower number densities below 90 km, is probably more correct. The sun's x-ray fluxes are the primary source of odd nitrogen species. These fluxes are strongly absorbed in the atmosphere (O_2 and N_2); this absorption takes place almost entirely above 90 km.

The only loss of odd nitrogen is by the reaction:

$$N(^4S) + NO \rightarrow N_2 + O(^3P)$$
$$k = 2.2 \times 10^{-11} \quad (39)$$

^4S is the ground state of atomic nitrogen. In the stratospere this loss is strongly reduced. $N(^4S)$ is converted to NO by the reaction with the main atmospheric component O_2:

$$N(^4S) + O_2 \rightarrow NO + O(^3P)$$
$$k = 1.4 \times 10^{-11} \cdot e^{-\frac{3550}{T}} \quad (56)$$

Below about 85 km, ionic reactions have a negligible influence on the NO chemistry. Above 85 km, the ionic scheme is very simple; N_2^+, NO^+ and O_2^+ are the only ions that have to be considered. NO_2 can be neglected, since it is rapidly converted to NO through reaction (5).

Our scheme will contain the following nitrogen species: $N(^4S)$, $N(^2D)$, NO, N_2, NO^+, and NO_2^+. In addition we have O_2^+ and electrons, which are involved in the nitrogen cycle. The model is similar to the previously described diurnal model. Atomic oxygen, which participates in some reactions, is given densities in the steady-state model (Fig. 3.1).

Atomic nitrogen in the ground-state ^4S and in the excited-state ^2D will be considered, since the efficiency in producing excited-state N is the only source of nitric oxide, while ground-state N acts to break down NO.

When the time-dependent differential equations are set up, eddy diffusion has to be included for the species with long lifetimes. In our scheme, two of the species have relatively long lifetimes. $N(^4S)$ has lifetime $\tau_N >$ hour in the lower part of the region, while NO has $\tau_{NO} >$ hour in the whole region. Eddy diffusion is therefore included in the calculation of these species. Steady-state calculation is first made from equations (3.4)–(3.10). The values obtained are used as initial conditions in the time-varying model. Nitric oxide and atomic nitrogen are calculated in the diurnal model from equation (3.2).

$N(^2D)$ is broken down very fast; diffusion will therefore not affect the component. This is also true for NO^+ and O_2^+, which have short lifetimes $\tau < 1$ hour. All three species can be calculated from the time-dependent equation (4.5), with only photochemical terms.

N_2^+ will rapidly undergo charge exchange to the ions O_2^+ and NO^+, and will be a negligible ion constituent at all heights; the number densities are therefore not calculated. It will, however, be an important source for O_2^+ and NO^+, and this is considered in the calculations.

Initial electron number densities, which must be known when ion number densities are calculated, are determined from the equilibrium expression with the assumption of only NO^+ ions:

$$e = \sqrt{P/\alpha_{NO^+}} \quad (6.2)$$

P is the over-all ionization rate (2.11), and α_{NO^+} is the ion-electron recombination rate for NO^+. The accuracy of using the recombination rate of

NO^+ for all ions should be sufficient, since the recombination rate of O_2^+ with electrons is within a factor of 3 (reaction 59).

When the electron densities are obtained, we get the total ion densities by assuming that the atmosphere is neutral.

In these calculations we are not specially interested in the rapid changes that take place during sunset and sunrise in some species, but more in the changes during the day as a result of NO variations. These changes are fairly slow, and the time step Δt is set to 10–20 minutes. The calculations were continued for several days, until there were no changes in the 24 hour cycle from one day to the next.

When we solve the diffusion equation, it is of second order, and we therefore define upper and lower boundary conditions. As will be shown, NO is broken down in the mesosphere by predissociation, which forms $N(^4S)$ through the reaction:

$$NO + h\nu \rightarrow N(^4S) + O(^3P) \quad \lambda < 1910\ \text{A} \qquad (h)$$

Mixing ratios less than 10^{-9} are obtained, which means that there will be an upward flux from the lower stratosphere, where mixing ratios exceed 10^{-8}. It is therefore necessary to set the lower boundary at heights where δ_{NO} has its maximum value in the lower stratosphere. No drop in mixing ratio is found up to 35 km. A lower boundary value at 35 km of $\delta_{NO_x} = 1.4 \times 10^{-8}$ is therefore used. We also find that the upward flux from the stratosphere, due to the low mixing ratios in the mesosphere, is negligible compared to the downward flux into the troposphere. The upward flux will therefore have a negligible effect on the mixing ratios in the lower stratosphere.

At the upper boundary (110 km), the conditions are somewhat more complicated. Calculations are carried out under the assumption that conditions in the first few km above 110 km are similar to those below, and that the excess of production in the 6 km interval above will be transported down into the region, and further that this production is equal to the production in the 6 km interval below. Variations of this flux have shown, however, that it effects only the first few km below 110 km.

This should give a flux of odd nitrogen into the region, where it is converted to molecular nitrogen. The decrease in mixing ratio with height of N_2 to match the odd nitrogen flux is negligible, since the ratio $|N_2|/|N_{odd}|$ is 10^5–10^6.

The primary source of odd nitrogen is the X-ray ionization of N_2 (cc) followed by:

$$\left.\begin{array}{l} (49) \\ N_2^+ + O(^3P) \rightarrow NO^+ + N(^4S) \\ (50) \\ N_2^+ + O(^3P) \rightarrow NO^+ + N(^2D) \end{array}\right\} \quad k = 1.4 \times 10^{-10}$$

These two reactions have to compete with the reaction

$$N_2^+ + O_2 \rightarrow N_2 + O_2^+ \qquad k = 0.7 \times 10^{-10} \qquad (51)$$

in charge exchange from N_2^+. Dissociative recombination of N_2^+ can safely be neglected compared to the fast reactions (49), (50), and (51).

The expression for odd-nitrogen production from reactions (49) and (50) is given by:

$$P_{Nodd} = k_{49.50} \cdot |N_2^+| \cdot |O(^3P)| = \alpha \cdot P_{N_2^+} \qquad (6.3)$$

α gives the efficiency of atomic oxygen in deactivating N_2^+:

$$\alpha = k_{49.50} \cdot |O(^3P)| / (k_{49.50} \cdot |O(^3P)| + k_{51} \cdot |O_2|) \qquad (6.4)$$

and $P_{N_2^+}$ is the ionization of N_2 by X-rays. α drops rapidly below about 90 km, where the number density of $O(^3P)$ decreases with height.

Since O_2^+ is included in the odd-nitrogen cycle, we have to include all the O_2^+ sources of importance in the region. The most pronounced source above 90 km is Ly-β ionization at 1025.7 A:

$$O_2 + h\nu \rightarrow O_2^+ + e \quad \lambda = 1025.7\ \text{A} \qquad (aa)$$

which is about as important as the X-ray ionization. In addition we have the less important $O_2(^1\Delta_g)$ ionization below 90 km:

$$O_2(^1\Delta_g) + h\nu \rightarrow O_2^+ + e \qquad \lambda < 1118\ \text{A} \qquad (dd)$$

All the other reactions, except for the loss reaction (39), are involved in the internal distribution of the species.

We should especially notice the role of O_2^+ in the distribution of odd-nitrogen species by the important reaction

$$O_2^+ + NO \rightarrow O_2 + NO^+ \quad k = 6.3 \times 10^{-10} \quad (52)$$

NO will, through this reaction, determine whether O_2^+ or NO^+ is the dominant ion in the lower *E*-region.

The only efficient production of nitric oxide is by the reaction

$$N(^2D) + O_2 \rightarrow NO + O(^3P)$$

$$k = 6 \times 10^{-12} \quad (53)$$

Therefore, the abundance of NO critically depends on the efficiency of the reactions producing excited-state N. Production by reaction (50) is only important in the region above 100 km, and results of the calculations show that (50) must be the dominant path of reactions (49), (50). If not, $N(^4S)$ number densities will be too dominant above 100 km compared to NO. The calculations are therefore carried out with an efficiency of $N(^2D)$ production, $\eta = 0.9$.

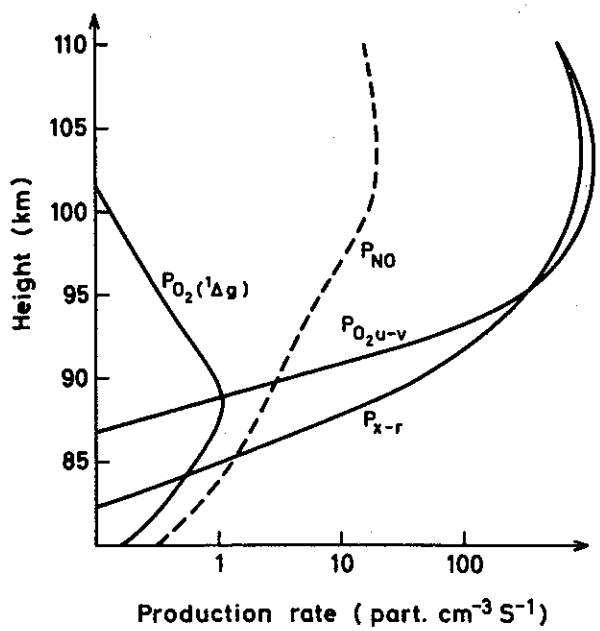

Fig. 6.1. Noon time ion pair production rates from Lyman-α ionization of NO (curve P_{NO}), ionization of $O_2(^1\Delta_g)$ by ultraviolet radiation (curve $PO_2(^1\Delta_g)$), ionization of O_2 by Lyman-β radiation (curve $P_{O_2 u-v}$), and ionization of N_2 and O_2 by x-rays (curve P_{x-r}).

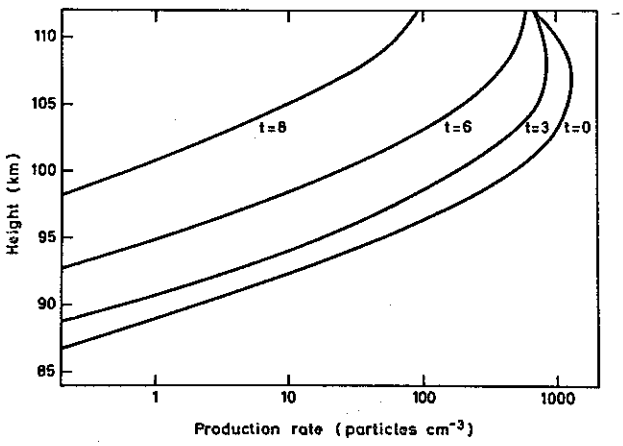

Fig. 6.2. Odd nitrogen production rates. *t* is hours after noon.

Dissociative recombination of NO^+ is an effective source of $N(^2D)$ in the whole height region. It is given by:

$$NO^+ + e \rightarrow N(^4S) + O(^3P) \; (\gamma - 1)$$

$$k = 5 \times 10^{-7} \cdot \left(\frac{300}{T}\right) \quad (54)$$

$$NO^+ + e \rightarrow N(^2D) + O(^3P) \; \gamma \quad (55)$$

The efficiency of producting $N(^2D)$ is given by γ. The only loss process of $N(^2D)$ is reaction (53); from this it follows that the efficiency in producing (^2D), η, and γ, is also the efficiency in producing nitric oxide.

There is also a production of NO fron $N(^4S)$ by the reaction

$$N(^4S) + O_2 \rightarrow NO + O(^3P)$$

$$k = 1.4 \times 10^{-11} \cdot e^{-\frac{3550}{T}} \quad (56)$$

This reaction, however, is a negligible source of NO above 80 km, due to the very high activation energy (Schiff 1968). In the upper stratosphere, with higher O_2 densities, and higher temperatures, reaction (56) effectively reduces the $N(^4S)$ number densities.

Since reactions (54) and (55) have an effect on NO in the whole region, it is of interest to discuss the result for different γ-values. Calculations show that it is reasonable to expect $\gamma = 0.6$–0.9. The results for $\gamma = 0.6$, 0.7, 0.8, and 0.9 will therefore be discussed.

Ionization rates at solar minimum are given in Fig. 6.1. X-ray and Ly-β ionization dominate

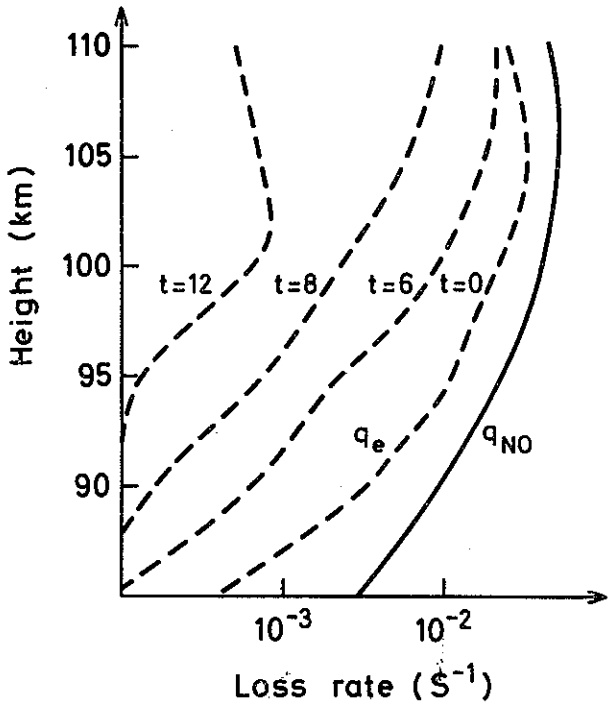

Fig. 6.3. Loss of O_2^+ by the reaction with NO (curve q_{NO}), and by dissociative recombination (curve q_e). t is hours after noon.

above 85 km. Both sources are approximately equally important, Ly-β radiation somewhat higher than the X-rays above 100 km, and X-ray fluxes dominating below 95 km. Maximum ionization rates are between 100–105 km, with about 2000 ion pairs/cm^3 formed pr. second.

Below 85 km, Ly-α ionization of NO is the main ion source. Production rates will depend on the NO profile, and therefore also on the γ-value chosen. An increase in γ values from 0.6 to 0.9 will increase the ion pair production by a factor of 3.

The role of $O_2(^1\Delta_g)$ is less important than other sources at all heights, and has a very limited effect on the total ion production.

We have already pointed out that reactions (49) and (50) are the only effective sources of odd nitrogen. From this it should follow that odd nitrogen is produced by highly variable X-rays, and that this production varies with the solar cycle variation.

Production rates during solar minimum conditions are given in Fig. (6.2). Variations during the day are also indicated on the figure. The production takes place almost entirely above 85 km. The presence of odd nitrogen below this height must therefore be entirely due to the downward transport by eddy diffusion.

NO controls the ionic species through reaction (52). How important this reaction is will to some extent depend on the γ value. For $\gamma = 0.8$, reaction (52) will dominate O_2^+ loss at all heights (Fig. 6.3). For great zenith distances, nitric oxide controls O_2^+ completely, since dissociative recombination (reaction 59) varies strongly during the day.

Similar curves are given for NO in Fig. 6.4. Reaction (52) controls the NO loss above 88 km during the day; at night it is a negligible loss reaction. Below 88 km, NO is broken down mostly by predissociation (reaction (*h*)), and eddy diffusion controls the NO profile only below 50 km.

The loss of NO by reaction (52) is given by the fractional part of reactions (54) and (55), going into ground-state atomic nitrogen:

$$Q_{NO} = k_{54} \cdot O_2^+ \cdot (1-\gamma) \qquad (5.6)$$

while the fractional part going into the excited-state ^2D produces NO through the sequence

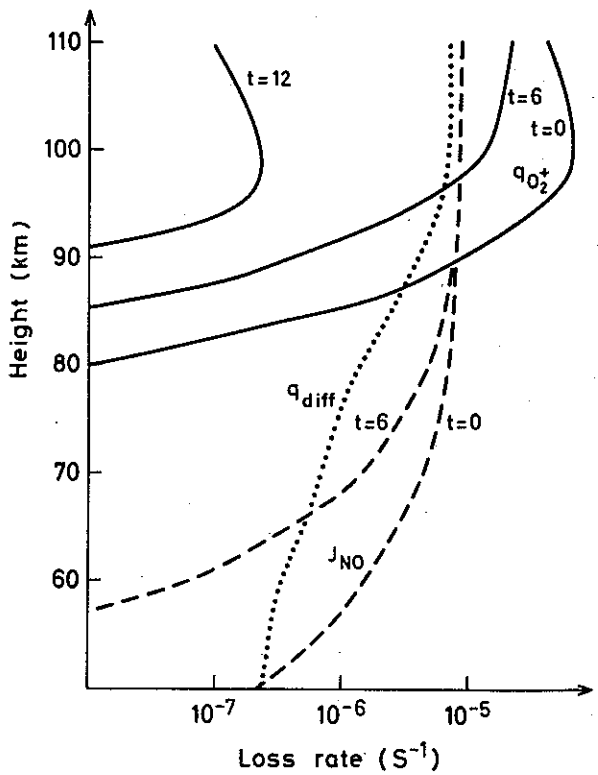

Fig. 6.4. Loss rates of NO by dissociation (curve J_{NO}), by eddy diffusion (curve q_{diff}) and by the reaction with O_2^+ (curve $q_{O_2^+}$). t is hours after noon.

$$O_2^+ + NO \rightarrow NO^+ + O_2$$
$$k = 6.3 \times 10^{-10} \quad (52)$$

$$NO^+ + e \rightarrow N(^2D) + O(^3P)$$
$$k = 5 \times 10^{-7} \cdot \left(\frac{300}{T}\right) \quad (55)$$
$$\text{efficiency} = \gamma$$

$$N(^2D) + O_2 \rightarrow NO + O(^3P) \quad k = 6 \times 10^{-12} \quad (53)$$

A high γ value will therefore make the feedback of NO efficient, and reduce the effect of reaction (52) as a loss term.

Below 88 km, dissociation of nitric oxide is the main production of ground-state atomic nitrogen, and this loss is strong enough to break down NO below the region where ionic reaction is the main loss. The loss processes of O_2^+ (Fig. 6.3) and of NO (Fig. 6.4) clearly show that the two species influence each other in the height region 85–110 km. It should also be pointed out that chemical processes dominate the loss of NO at high solar elevation, but are less important at low solar elevation ($t = 8$), and at night ($t = 12$), compared to the turbulent loss term $\left(Q_{\text{diff}} = \frac{K_z}{H^2}\right)$.

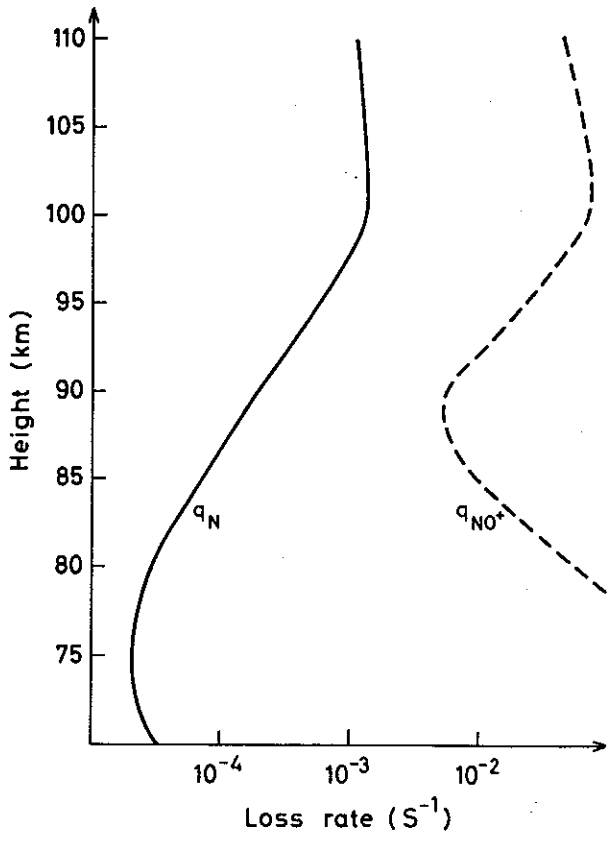

Fig. 6.5. Loss rates of $N(^4S)$ (curve q_N), and of NO^+ (curve q_{NO^+}).

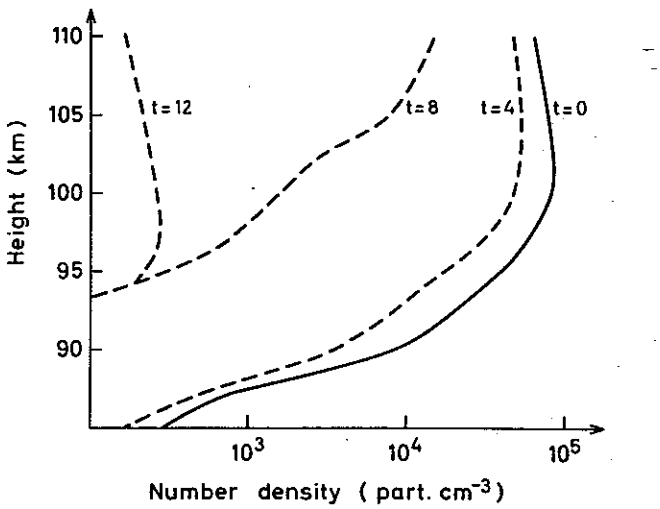

Fig. 6.6 O_2^+ number densities. t is hours after noon.

NO^+ is a terminal ion above 85 km, and the only loss is by dissociative recombination reactions (54) and (55). Lifetimes of NO^+ are minutes or less at all heights (Fig. 6.5), which is in agreement with the assumption we made when the differential equation of NO^+ was set up. $N(^4S)$ has its main loss by reaction (39), with some minor contributions above 95 km from reaction

$$N(^4S) + O(^3P) \rightarrow NO + h\nu$$
$$k = 2 \times 10^{-17} \quad (57)$$

and below 80 km from reaction (56). $N(^4S)$ lifetimes are therefore determined by NO densities, and have maximum lifetimes around 80 km with $\tau_N < 1$ day (Fig. 6.5).

A change in γ value will also influence the ion profiles. In the lower E-region ($z < 90$ km), nitric oxide breaks down O_2^+ (reaction 52), and produces NO^+, and in the D-region the ionization is proportional to the NO densities (reaction 52), a result of the strong Ly-α radiation.

The maximum ion densities are about $10^5 cm^{-3}$ at 100 km. This value is almost independent of γ value. All these figures are for solar minimum conditions, and at high solar elevation (noon).

If we look at the diurnal behaviour of the components, we find that the two ion species have strong diurnal variation. This is a result of the

variation of the ionizing radiation. Ly-β and X-ray fluxes are absorbed by the air, and will decrease with increasing zenith distance. At night ionization will be given by the constant (in time) scattered Ly-α, and Ly-β radiation.

The diurnal variation of O_2^+ is very marked (Fig. 6.6). There is a drop in number densities from day to night by more than a factor of 100 at 100 km, from its daytime value of 8×10^4 particles cm^{-3} to the night-time value of 3×10^2 particles cm^{-3}. NO^+ has a less marked variation; it drops by a factor of approximately 30 in the whole height region (Fig. 6.7).

As we have already seen in Fig. 6.4, (52) is the main reaction in converting O_2^+ to NO^+; O_2^+ and NO^+ number densities depend, therefore, on the γ value chosen. A high γ value effectively converts O_2^+ to NO^+. This effect on O_2^+ and on NO^+ densities varies markedly when γ increases from 0.6 to 0.9. For $\gamma = 0.6$, O_2^+ densities exceed NO^+ by a factor of 3, while $\gamma = 0.9$ gives NO^+ densities slightly higher than O_2^+ densities. This favours a high γ value; $\gamma = 0.8$ seems to be reasonable.

It is of interest to compare the number densities of NO^+ to O_2^+ and their variation by day. From measurements, this ratio approximately reaches unity around 100 km at mid-day, and a value of 0.8 is therefore, according to the last figure, reasonable to use. The calculated ratio is given in Fig. 6.8 for $\gamma = 0.8$ from 110 to 85 km. Below 90 km it increases, and is about 5 at 85 km. During the night the ratio increases at all heights, with more than a factor of 10.

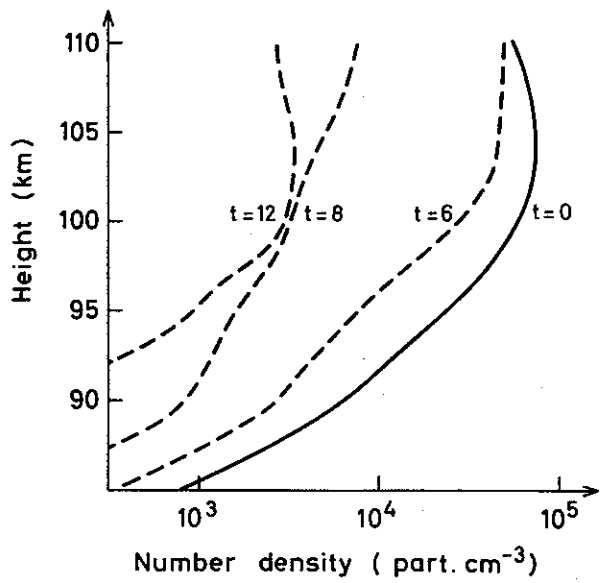

Fig. 6.7. NO^+ number densities. t is hours after noon.

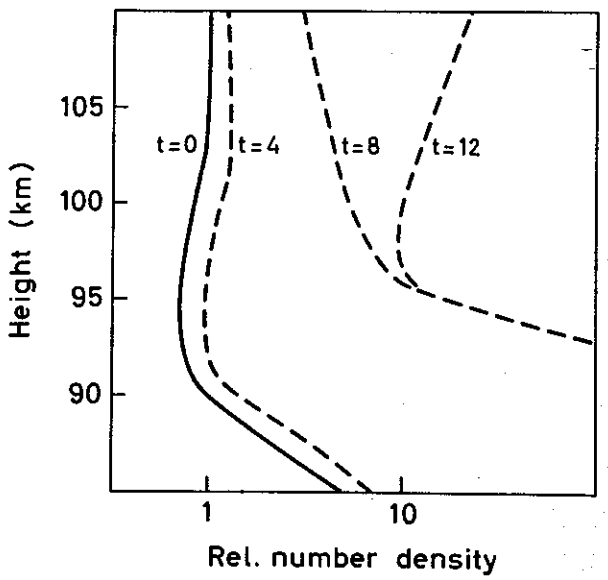

Fig. 6.8. Relative number densities of NO^+ to O_2^+. t is hours after noon.

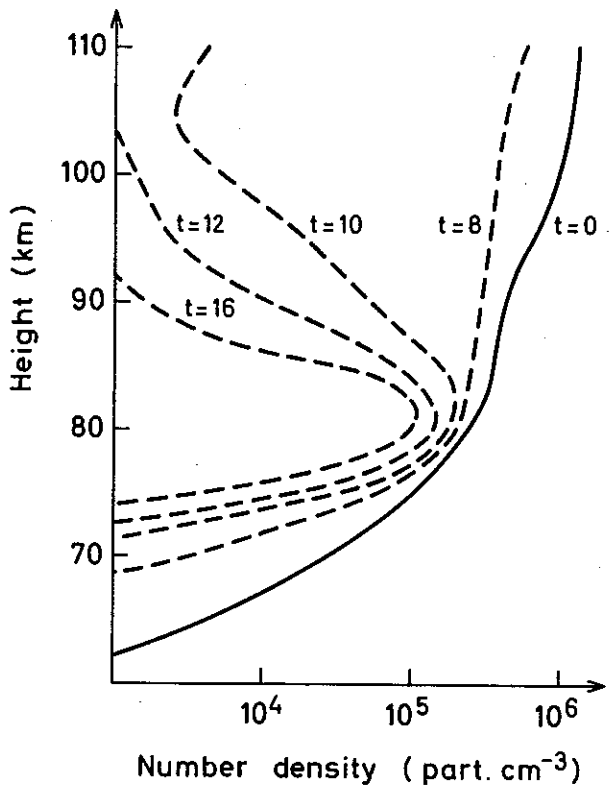

Fig. 6.9. $N(^4S)$ number densities. t is hours after noon.

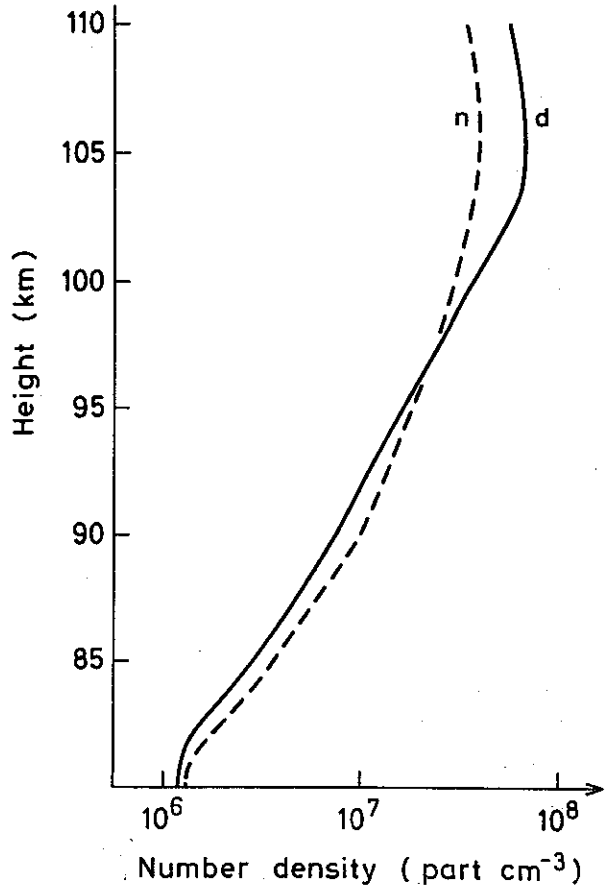

Fig. 6.10. NO number densities at noon (curve *d*), and at midnight (curve *n*).

As we have shown in Fig. 6.2, the odd-nitrogen production has a strong diurnal variation, and when in addition we know that the loss reaction (52) dominates over transport processes above 95 km, we should at least expect diurnal variations in one of the two species N(^4S) and NO.

This is also found in N(^4S). It has a diurnal variation as shown in Fig. 6.9. Diurnal variations are most pronounced in the upper region where NO densities are highest. The night-time drop in densities is several orders of magnitude. Around 80 km, variations are much less. Due to low NO densities, N(^4S) decrease is less than a factor of 3. Maximum daytime densities of 10^6 particles cm^{-3} are at 110 km, and maximum night-time densities of 10^5 particles cm^{-3} are at 80 km.

The dominant odd-nitrogen constituent is NO; it has a diurnal variation that is much less pronounced than that of N(^4S) (Fig. 6.10). Above 100 km, NO densities decrease by approximately a factor of 2 from day to night. Below 95 km, diurnal variations are small. NO densities increase during the night because diffusion is the main night-time process.

These small daytime variations may look surprising, since production is highly variable by day. They can, however, be explained by examining the loss through reaction (39). NO exceeds N(^4S) by more than a factor of 10, and the less abundant constituent N(^4S) will disappear almost entirely before any strong effects are detected on NO.

The calculation of NO, which has been extended to the lower border at 35 km, results in low NO values far below the region where they are controlled by ionic processes (Fig. 6.11). These low NO values, as shown in Fig. 6.4, are a result of NO predissociation. This production leads to N(^4S) densities, which have a marked effect on the NO profile. The transport by eddy

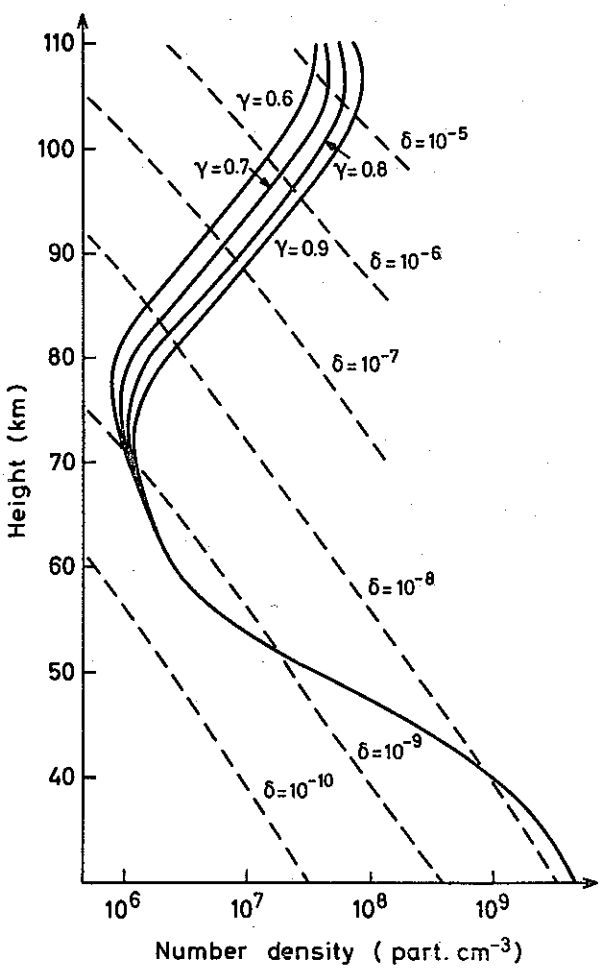

Fig. 6.11. NO number densities for $\gamma = 0.6$, 0.7, 0.8 and 0.9. Dashed lines give constant mixing ratios.

diffusion becomes less important at lower heights due to decreasing eddy diffusion coefficients downward. NO densities decrease down to 76 km, where values as low as 2×10^{6} particles cm^{-3} are obtained. Below, upward transport from the lower stratosphere exceeds the loss by reaction (39).

There is also a drop in mixing ratios down to 60 km, where values as low as 5×10^{-10} are obtained. The variation in NO densities with γ value is also shown on the figure. Variations in γ affect NO down to about 70 km. In the region 110–80 km, an increase in γ from 0.6 to 0.9 increases the NO densities by a factor of 4. We also find here that the NO densities obtained favour a high γ value. These low mesosphere values are in agreement with the low values obtained by Brasseur & Cislek (1972) for these heights.

From the above calculations, it can be concluded that there exists a strong link between O_2^+, NO^+, and NO in the chemically active region between 110 and 90 km. Changes in one of the species automatically lead to changes in the two other species. It is therefore necessary to include O_2^+ in the odd nitrogen scheme, since it controls NO above 85 km–90 km. It is also clear that predissociation of NO makes $N(^4S)$ so abundant that it markedly affects the NO profile in the mesosphere.

7. THE CHEMISTRY OF POSITIVE AND NEGATIVE CLUSTER IONS

Our understanding of *D*-region ion chemistry has developed during the last few years. The nature of the ion present in this region was first indicated by the positive-ion chemistry measurements of Narcisi & Bailey (1965). The surprising result of their measurements was that the water cluster ions H_3O^+ and $H_3O^+.(H_2O)_n$ were the dominating positive ions below 82 km. This unexpected result led to an intensified laboratory research for new reactions.

At present a great number of possible reactions are known (Fehsenfeld & Ferguson 1969, Lineberger & Puckett 1969, 1969*a*, Good et al. 1970, Fehsenfeld et al. 19771, 1971*a*, and Puckett & Teague 1971).

The establishment of the positive-ion reaction scheme was followed by intensified research into negative-ion reactions, which are known to be produced initially in the *D*-region by electron attachment:

$$e+O_2+O_2 \rightarrow O_2^- + O_2$$

$$k = 1.4\times10^{-29}\cdot\left(\frac{300}{T}\right)\cdot e^{-\frac{600}{T}} \qquad (100)$$

$$e+O_3 \rightarrow O^- + O_2 \quad k = 3\times10^{-12} \qquad (101)$$

In the same way as for positive ions, we can expect clustering of negative ions, as shown by laboratory experiments of Pack & Phelps (1971), and Kebarle et al. (1972).

There still exists, however, a great deal of uncertainty in the chemistry of the cluster ions in the lower ionosphere. We know very little about the chain leading to the negative terminal ions.

In this work, a diurnal model of the complex scheme of positve and negative cluster ions in the atmosphere below 88 km, is calculated and discussed on the basis of known reactions and rate constants.

A model in which positive and negative cluster reactions are included becomes rather complicated. Many new processes have to be included, in contrast to the simple electron positive-ion model discussed in the previous chapter.

Ion diffusion can be neglected in the lower ionosphere, and we are left with only chemical processes in the ion model.

When all processes are considered in an electron positive- and negative-ion model, the variation of the electrons is given by:

$$\frac{d}{dt}(e) = \sum_i J_i\cdot m_i - \sum_i \alpha_i\cdot n_i^+\cdot e - \sum_i \beta_i\cdot m_i\cdot e + \sum_i\sum_j \gamma_{ij}\cdot n_i^-\cdot m_j + \sum_i \varrho_i\cdot n_i^- , \qquad (7.1)$$

the variation of positive ions by:

$$\frac{d}{dt}(n_i^+) = J_i\cdot m_i - \alpha_i\cdot n_i^+\cdot e - \sum_j \delta_{ij}\cdot n_j^+\cdot n_i^+ - \sum_j k_{ij}\cdot n_j^+\cdot m_j + \sum_k\sum_{(k+i)} k_{kl}\cdot n_k^+\cdot m_l \qquad (7.2)$$

and the variations of negative ions by:

$$\frac{d}{dt}(n_i^-) = \sum_j \beta \cdot e \cdot m_j - \sum_j \delta_{ij} \cdot n_j^+ \cdot n_i^- + \sum_{\substack{k \\ (k+i)}} \sum_l l_{kl} \cdot n_k^- \cdot m_l - \sum_j l_{ij} \cdot n_i^- \cdot m_j - \varrho_i \cdot n^- - \sum_j \gamma_{ij} \cdot n_i^- \cdot m_j \quad (7.3)$$

Further, it will be assumed that the atmosphere as a whole is neutral.

$$\sum_i n_i^+ = e + \sum_i n_i^- \quad (7.4)$$

In the above equations, e, n^+, n^- are the number densities of electrons, positive ions and negative ions, and m is the number density of a neutral constituent. α is the ion-electron recombination coefficient, and k and l are the charge rearrangement coefficients for positive and negative ions. γ gives the collision-detachment rate, β the electron-attachment rate, ϱ the photodetachment rate, and δ the mutual neutralization coefficient between positive and negative ions.

The time-dependent equation of the number density of the total positive ions, $S_n^+ = \sum_i n_i^+$, is given by the equation

$$\frac{d}{dt}(S_n^+) = \sum_i J \cdot {}_i m_i - \alpha_{av} \cdot (S_n^+)^2 \quad (7.5)$$

where the square of the positive-ion number densities is used, since S_n^+ is equal to the sum of negative ions and electrons (eq. 7.4). The average recombination rate is given by the following expression:

$$\alpha_{av} = \frac{\sum_i \sum_j \delta_{ij} \cdot n_i^+ \cdot n_j^- + \sum_i \alpha_i \cdot n_i^+ \cdot e}{(S_n^+)^2} \quad (7.6)$$

The number density of total positive ions at a time $t+\Delta t$ is given by:

$$S_{n_t+\Delta t}^+ = (S_{ne1}^+ - S_{ne2}^+) \times \frac{\frac{S_{n_t}^+ - S_{nel}}{S_{n_t}^+ - S_{ne2}^+} \cdot e^{-(-\sqrt{4 \cdot \sum_i J_i \cdot m_i \cdot \alpha_{av}} \cdot \Delta t)}}{1 - \frac{S_{n_t}^+ - S_{nel}^+}{S_{n_t}^+ - S_{ne2}^+} \cdot e^{+(-\sqrt{4 \cdot \sum_i J_i \cdot m_i \cdot \alpha_{av}} \cdot \Delta t)}} \quad (7.7)$$

where

$$S_{nel}^+ = \sqrt{\sum_i J_i \cdot m_i / \alpha_{av}}, \text{ and } S_{ne2}^+ = -\sqrt{\sum_i J_i \cdot m_i / \alpha_{av}}.$$

Ion and electron number densities are obtained by solving the equations (7.1), (7.2), and (7.3).

The number densities of positive ions at a time $t+\Delta t$:

$$n_{i(t+\Delta t)}^+ = n_{iet}^+ + (n_{i_t} - n_{i_{et}}) \cdot e^{-(\alpha_i \cdot e + \sum_j \delta_{ij} \cdot n_j^- + \sum_j k_{ij} \cdot m_j) \cdot \Delta t} \quad (7.8)$$

with

$$n_{ie}^+ = (J_i \cdot m_i + \sum_{\substack{k \\ k \neq i}} \sum_l k_{kl} \cdot n_k^+ \cdot m_l) / (\alpha_i \cdot e + \sum_j \delta_{ij} \cdot n_j^- + \sum_j k_{ij} \cdot m_j) \quad (7.9)$$

Number density of the dominant positive ion is determined from the number density of the total positive ions:

$$n_{it+\Delta t}^+ = S_{nt+\Delta t}^+ - \sum_{(j \neq i)} n_{jt+\Delta t}^+ \quad (7.10)$$

Number densities of negative ions are similarly given by:

$$n_{it+\Delta t}^- = n_{iet} + (n_{i_t} - n_{iet}) \times e^{-(\sum_j \delta_{ij} \cdot n_j^+ + \sum_j l_{ij} \cdot m_j + \sum_j \cdot \gamma_{ij} \cdot m_j + \rho_i) \cdot \Delta t} \quad (7.11)$$

with the equilibrium value:

$$n_{ie}^- = (\sum_j \beta \cdot e \cdot m_j + \sum_{\substack{k \\ k \neq i}} \sum_l l_{kl} \cdot n_k \cdot m_l) / (\sum_j \delta_{ij} \cdot n_j^+ + \sum_j l_{ij} \cdot m_j + \sum_j \gamma_{ij} \cdot m_j + \varrho_i) \quad (7.12)$$

At heights where electrons dominate negative ions, the number densities of electrons are determined from the simple relation in (7.4):

$$e_{t+\Delta t} = \sum_i n_{it+\Delta t}^+ - \sum_i n_{it+\Delta t}^- \quad (7.13)$$

When $e_t < n_i^-$, the number densities are calculated from equation (7.1):

$$e_{t+\Delta t} = e_{et} + (e_t - e_{et}) \cdot e^{-(\sum_i \alpha_i \cdot n_i^+ + \sum_i \beta_i \cdot m_i) \cdot \Delta t} \quad (7.14)$$

The equilibrium densities are given by:

$$e_e = (\sum_i J_i \cdot m_i + \sum_i \sum_j \gamma_{ij} \cdot n_i^- \cdot m_j + \sum_i \varrho_i \cdot n_i^-) / (\sum_i \alpha_i \cdot n_i^+ + \sum_i \beta_i \cdot m_i) \quad (7.15)$$

Under these conditions the main negative constituent n_i^- is calculated from:

$$n^-_{i\,t+\Delta t} = \sum_j n^+_{j\,t+\Delta t} - \sum_{\substack{k \\ (k \neq i)}} n^-_{k\,t+\Delta t} - e_{t+\Delta t} \quad (7.16)$$

The time step in this model is the same as we used in the neutral model: $t = 60$ seconds. A lot of the positive and negative-ion species, as well as the electrons, have short lifetimes, due to charge rearrangement when they collide with neutral species (given by the terms, $\sum_j k_{ij} \cdot m_j$, $\sum_j l_{ij} \cdot m_j$, and $\sum_j \beta_i \cdot m_j$, respectively). When the lifetimes $\tau < 0.15$, the number densities at time $t + \Delta t$ are given by the equilibrium values (7.9), (7.12), and (7.15). All equations showing the variations of electrons and ions can be simplified, since only a limited number is important for each constituent. We will, therefore, simplify the equation for each component by considering the reactions that are expected to be important; and to simplify expressions, all types of loss rates will be denoted by k_l.

The ionization rate J_i becomes very simple below 60 km, where the only ion source is the very energetic galactic cosmic rays (GCR) that ionize N_2 and O_2. It is given by the simple expression:

$$P_{\mathrm{GCR}} = J_{\mathrm{GCR}} \cdot |M| \quad (7.21)$$

The initial ions are N_2^+ and O_2^+, where the N_2^+ ions are rapidly converted to O_2^+ by the reaction

$$N_2^+ + O_2 \rightarrow O_2^+ + N_2$$
$$k = 0.7 \times 10^{-10} \quad (51)$$

In our calculations we can therefore use O_2^+ as the primary ion.

Zero is used as initial value for all ion components, and calculations are carried out until no variations in ion densities from one 24 hour cycle to the next occurred. Four days turned out to be sufficient, due to the short ion lifetime.

8. POSITIVE CLUSTER IONS

Since the first measurements of water cluster ions by Narcisi & Bailey (1965), *D*-region investigations have been focused on the problem of formation and distribution of hydrated ions. Kebarle et al. (1967) showed that the hydration takes place through the reaction sequence:

$$H^+ \cdot (H_2O)_{n-1} + H_2O + M \rightarrow H^+ \cdot (H_2O)_n + M \quad (70\text{–}76)$$

and they gave equilibrium constants $K = \frac{k_f}{k_r}$ for the degree n of hydration.

It has also been shown that molecular oxygen ions are rapidly converted to water cluster ions (Fehsenfeld & Ferguson 1969, Good et al. 1970, and Fehsenfeld et al. 1971). The critical link in the chain from O_2^+ to water cluster ions is the three-body reaction

$$O_2^+ + O_2 + M \rightarrow O_4^+ + M \quad k = 2.4 \times 10^{-30} \quad (58)$$

To be efficient, it has to be compared with the loss by the charge exchange reaction

$$O_2^+ + NO \rightarrow NO^+ + O_2 \quad k = 6.3 \times 10^{-10} \quad (52)$$

and with the loss by dissociative recombination and mutual neutralization:

$$O_2^+ + e \rightarrow O(^3P) + O(^3P) \quad k = 2 \times 10^{-7} \frac{\sqrt{300}}{T} \quad (59)$$

$$O_2^+ + \sum_i n_i^- \rightarrow O_2 + \sum_i n_i \quad k = 2 \times 10^{-7} \quad (60)$$

Lifetimes from these three reactions are given in Fig. 8.1 as $\tau_{O_2^+} = 1/q_{O_2^+}$, where $q_{O_2^+}$ is the loss rate of O_2^+. In the height interval of interest ($z < 88$ km), the three-body reaction (58) represents the main loss of O_2^+. τ is approximately 10 seconds at 80 km, and less than a second below 75 km. Loss by dissociative recombination is represented by the maximum daytime value. At night, this loss is more than one order of magnitude slower, due to low electron concentrations (Fig. 9.6). Charge exchange to NO^+ is also ineffective, since NO densities are very small in the *D*-region (Fig. 6.11).

The ion O_4^+ formed by the three-body reaction (58) will never reach number densities of interest in the *D*-region, since it is removed rapidly by the fast binary reaction with water vapour:

$$O_4^+ + H_2O \rightarrow O_2^+(H_2O) + O_2 \quad k = 2.2 \times 10^{-9} \quad (61)$$

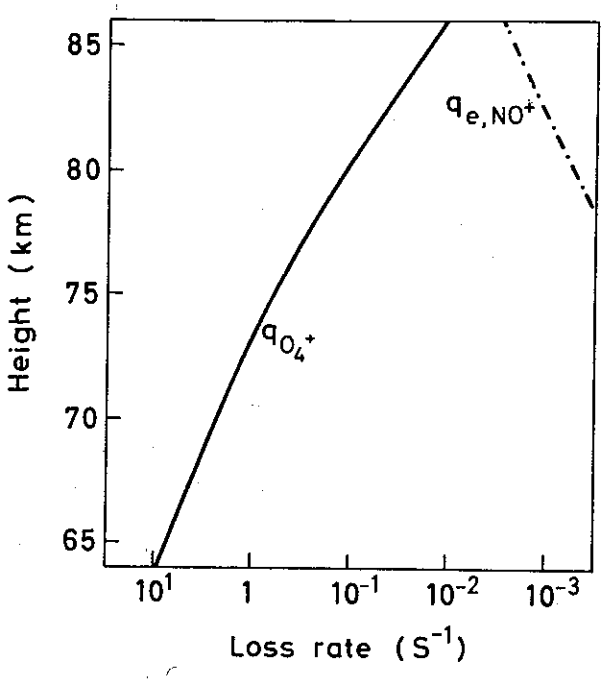

Fig. 8.1. Loss rates of O_2^+ by reaction (58) curve $q_{O_4^+}$, and by reactions (52) and (59) curves q_{e,NO^+}.

which proceeds with no activation energy (Fesenfeld et al. 1971).

There is also an important conversion of O_4^+ back to O_2^+ by the reaction with atomic oxygen

$$O_4^+ + O(^3P) \rightarrow O_2^+ + O_3 \quad k = 3 \times 10^{-10} \quad (62)$$

This reaction makes the production of cluster ions from O_2^+ strongly dependent on the atomic-oxygen profile. Since this component increases rapidly above 82 km (Fig. 3.1), there is a sharp decrease in cluster-ion production from O_2^+ above 82 km. O_4^+ is also expected to be converted to O_2^+ by the reaction with $O_2(^1\Delta_g)$ (Ferguson 1971).

$$O_4^+ + O_2(^1\Delta_g) \rightarrow O_2^+ + O_2 + O_2 \quad k = 10^{-10} \quad (63)$$

The rate constant has not been measured, but is expected to be fast; the above value has therefore been adopted. This reaction is, however, of minor interest, since the reaction with atomic oxygen is the main reaction converting O_4^+ to O_2^+. Lifetimes of O_4^+ are less than one second at all heights. As we have already seen, (Fig. 8.1), lifetimes of O_2^+ are also very short in the *D*-region. Chemical equilibrium between the two components is therefore rapidly established.

The real loss is therefore through the reaction (61), which forms cluster ions. This loss has to compete with dissociation, recombination and mutual neutralization of O_2^+, reactions (59) and (60), and of O_4^+:

$$O_4^+ + e \rightarrow O_2 + O_2 \quad k = 1 \times 10^{-6} \quad (64)$$

$$O_4^+ + \sum_i n_i^- \rightarrow O_2 + O_2 + \sum_i n_i$$

$$k = 4 \times 10^{-7} - 1 \times 10^{-6} \quad (65)$$

The neutralization coefficient is $k_{65} = 4 \times 10^{-7}$ for the simple negative ions, and $k_{65} = 10^{-6}$ for negative cluster ions.

The only reaction of importance is the cluster reaction (61). Loss by other reactions (Fig. 8.1) is too slow.

It is obvious that reaction (61), which forms water cluster ions, is very effective in the charge exchange from O_4^+. Below 86 km, it is safe to say that all O_2^+ produced will undergo charge exchange and form water cluster ions.

These numbers are for daytime conditions. Below about 80–82 km, both $O(^3P)$ and $O_2(^1\Delta_g)$ are absent during the night. This results in a more effective cluster formation.

As soon as the ion $O_2^+ \cdot (H_2O)$ is formed, charge exchange reactions rapidly form H_3O^+ and $H_3O^+ \cdot (H_2O)$ (Fehsenfeld et al. 1971):

$$O_2^+ \cdot (H_2O) + H_2O \rightarrow H_3O^+ + OH + O_2$$

$$k = 3 \times 10^{-10} \quad (66)$$

$$O_2^+ \cdot (H_2O) + H_2O \rightarrow H_3O^+ \cdot OH + O_2$$

$$k = 1.9 \times 10^{-9} \quad (67)$$

$$H_3O^+ \cdot OH + H_2O \rightarrow H_3O^+ \cdot (H_2O) + OH$$

$$k = 3 \times 10^{-9} \quad (68)$$

The lifetimes of the ions $O_2^+ \cdot (H_2O)$ and $H_3O^+ \cdot OH$ will be approximately the same as for O_4^+, and their number densities are therefore negligible. Since the last ion is converted to the cluster ion $H_3O^+ \cdot (H_2O)$, it follows that there will be an almost instantaneous conversion from O_2^+ via O_4^+ to ions H_3O^+ and $H_3O^+ \cdot (H_2O)$.

$O_2^+ \cdot (H_2O)$ may also be produced directly from O_2^+ by the three-body reaction:

$$O_2^+ + H_2O + M \rightarrow O_2^+ \cdot (H_2O) + M$$

$$k = 2.8 \times 10^{-28} \quad (69)$$

This is, however, a very ineffective reaction, compared to reaction (58). Even if the rate constant of the last reaction is almost 2 orders of magnitude higher than the rate constant of reaction (58), the number densities of O_2 exceed that of H_2O by more than four orders of magnitude. Reaction (69) can therefore safely be neglected in these calculations.

Higher cluster formations take place, as we have already seen, through the three-body reactions

$$H_3O^+ \cdot (H_2O)_{n-1} + H_2O + M \rightarrow H_3O^+ \cdot (H_2O)_n + M \quad (70\text{-}76)$$

Rate constants are given by Good et al. (1970), and n has the values 1, 2, 3, 4. The following rate constants have been used:

$$\begin{aligned} n &= 1,\ k_{70} = 3.4\times10^{-27},\\ n &= 2,\ k_{71} = 2.3\times10^{-27}\\ n &= 3,\ k_{72} = 2.4\times10^{-27},\\ n &= 4,\ k_{73} = 0.9\times10^{-27} \end{aligned} \quad (8.1)$$

When the clustering process proceeds, there will, however, be an increasing rate constant of the reverse reactions (Good et al. 1970*a*):

$$H_3O^+ \cdot (H_2O)_n + M \rightarrow H_3O^+ \cdot (H_2O)_{n-1} + H_2O + M \quad n = 1,2,3,4\ldots \quad (77\text{–}83)$$

In the *D*-region, where water vapour densities are of the order 10^9 particles cm^{-3} (Fig. 3.2), the above reactions may be of importance even for the slow rate constants when n is small. Reverse rate constants have been measured at temperatures 300 °K (Good et al. 1970, 1970a, Puckett & Teaque 1970, Fehsenfeld et al. 1971, 1971a).

Summer temperatures at mesopause level are, however, very low, and since the reverse reactions are strongly temperature-dependent (Kebarle et al. 1967), these have to be included in the rate constants. Equilibrium constants $K_{n-1,n}$ have been given for $n = 1$–7. When forward reactions are known, reverse reactions are given by $k_r = \frac{k_f}{K}$. Rate constants for forward reactions are known for $n = 1-4$ (eq. (8.1)), and for $n>4$ the following reactions have been adopted for $n = 5, k_{74} = 5\times10^{-28}$, $n = 6, k_{75} = 3\times10^{-28}$, and for $n = 7, k_{76} = 2\times10^{-28}$.

Equilibrium constants $K_{n-1\ n}$ for $n = 1-7$ are determined from the expression $K_{n-1,n} = \frac{A}{T} \cdot 1000 - B$, where A and B are constants given by Kebarle et al. (1967). With k_f and $K_{n-1,n}$ known, reverse reactions k_r for all hydration steps are determined as a function of temperature. At the temperature 300 °K the following values for $n = 5,6,7$ are obtained: $k_{81} = 1.4\times10^{-11}$, $k_{82} = 4\times10^{-11}$, and $k_{83} = 6\times10^{-11}$.

As already pointed out, three-body reactions where water vapour is involved are not very efficient in the *D*-region. The importance of hydration depends, therefore, on how fast the three-body reactions (70–76) are, compared to the recombination with electrons, and mutual neutralization with negative ion, which is the net loss of positive ions. Whether a neutralization or a further clustering takes place depends on the rate constants used. Fig. 8.2 shows loss rates for hydronium cluster. Cluster ions are formed

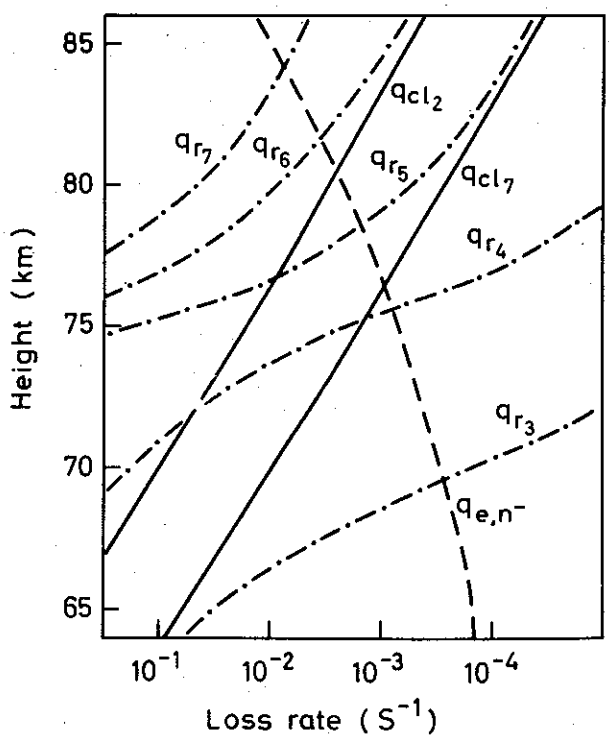

Fig. 8.2. Loss rates by hydronium cluster ions. Curve $q_{e,n-}$ gives loss rates by dissociation and neutralization, curve q_{cl_2} and q_{cl_7} give loss rates by the clustering reactions (71) and (76), and curves q_{r3}–q_{r7} give loss rates by the reverse reactions (79)–(83).

effectively below 82 km, where three-body clustering proceeds faster than recombination. The temperature dependence of the reverse reactions is clearly demonstrated in the figure, where reverse reactions for $n>2$ are included.

Below 80 km there is a sharp temperature increase, which makes reverse reactions proceed fast. Higher clusters (n = 6–7) are not stable in the *D*-region. Reverse reactions are much faster than forward reactions. Below 70 km, this is even true for all $n>3$, a result of the high temperature in the lower mesosphere. Below 77 km, equilibrium of the cluster ions is established before loss by dissociative recombination or mutual neutralization takes place. It is also obvious that in the lower *D*-region, reverse reactions for n = 1 and 2 are too slow to make H_3O^+ and $H_3O^+.H_2O$ the main ion components. It should be mentioned that only water cluster-ion formation is important below 70 km, where there are no diurnal variations. Number densities are therefore determined only by the value of the equilibrium constant $K_{n-1,n}$. It is only the relative value of k_f to k_r which is of interest.

The most important ion source in the *D*-region is, however, the Ly-α ionization of nitric oxide. This source exceeds all other sources at heights between 85 km and 70 km (Fig. 2.2).

It has been shown (Puckett & Teague 1971, and Fehsenfeld et al. 1971a) that a formation of water cluster ions, starting with NO^+ takes place, similar to that of H_3O^+. NO^+ is therefore the main precursor of cluster ions in the *D*-region. The cluster ions $NO^+.(H_2O)_n$ are formed through the three-body reactions

$$NO^+ \cdot (H_2O)_{n-1} + H_2O + M \rightarrow NO^+ \cdot (H_2O)_n + M \qquad n = 1,2,3 \qquad (84\text{–}86)$$

with the following rate constants (Fehsenfeld et al. 1971a):

$$k_{84} = 1.6\times10^{-28},$$
$$k_{85} = 1.0\times10^{-27},$$
and $$k_{86} = 2.0\times10^{-27} \qquad (8.2)$$

As mentioned before, three-body reactions, where water vapour is involved, are not very effective above 80 km.

NO^+ is removed much faster when three-body reactions with more abundant atmospheric constituents, like CO_2 and N_2, are involved (Dunkin et al. 1971, Niles & Heimerl 1972, and Heimerl 1972):

$$NO^+ + CO_2 + M \rightarrow NO^+ \cdot CO_2 + M \qquad k = 2.5\times10^{-29} \qquad (87)$$

$$NO^+ + N_2 + M \rightarrow NO^+ \cdot N_2 + M \qquad k = 2.4\times10^{-31} \qquad (88)$$

Due to the high N_2 densities, the last reaction is the most effective.

The ions $NO^+ \cdot N_2$ and $NO^+ \cdot CO_2$ will rapidly undergo charge exchange to form $NO^+.(H_2O)$:

$$NO^+ \cdot N_2 + CO_2 \rightarrow NO^+ \cdot CO_2 + N_2 \qquad k = 10^{-9} \qquad (89)$$

$$NO^+ \cdot CO_2 + H_2O \rightarrow NO^+ \cdot H_2O + CO_2 \qquad k = 10^{-9} \qquad (90)$$

Clustering of NO^+ is found to proceed until the ion $NO^+.(H_2O)_3$ is formed. $NO^+.(H_2O)_4$ has not been observed (Ferguson 1971). This is because there is a fast binary switching reaction with water vapour:

$$NO^+ \cdot (H_2O)_3 + H_2O \rightarrow H_3O^+ \cdot (H_2O)_2 + HNO_2 \qquad k = 8\times10^{-11} \qquad (91)$$

The importance of this reaction is, however, limited, since the clustering reactions (85, 86) are too slow above 80 km to produce higher NO^+ clusters.

Nitric oxide cluster ions have reverse reactions similar to hydronium cluster ions (Puckett & Teaque 1970, Fehsenfeld et al. 1971a). $NO^+ \cdot (H_2O)_n$ ions are present only in the *D*-region, and are lost through switching reactions (91) and (95), and by dissociative recombination before higher hydrates are formed. Reactions (92) and (93) are therefore considered unimportant in the *D*-region.

Several reactions have been proposed as responsible for the switch over from nitric oxide cluster ions to hydronium cluster ions. Burke (1970) has suggested that atomic hydrogen reacts with singly hydrated NO^+:

$$NO^+ \cdot H_2O + H \rightarrow H_3O^+ + NO$$
$$k < 10^{-11} \qquad (94)$$

The above upper limit on the rate constant (Ferguson 1971) makes the reaction too slow around 80 km to form H_3O^+ effectively. Niles & Heimerl (1972) have suggested that the switching takes place through the reaction with hydroxyl:

$$NO^+ \cdot H_2O + OH \rightarrow H_3O^+ + NO_2$$
$$k = 2 \times 10^{-9} \qquad (95)$$

Unfortunately the rate constant has not been measured; the above rate is an adopted value to explain the switch over from $NO^+.(H_2O)$ to H_3O^+, which has been used in these calculations. In order to be efficient, the above reaction has to exceed the loss by dissociative recombination, and the loss by mutual neutralization with negative ions:

$$NO^+ \cdot (H_2O)_n + e \rightarrow NO + (H_2O)_n$$
$$k = 10^{-6} - 10^{-5} \qquad (98)$$
$$NO^+ \cdot (H_2O)_n + \sum_i n_i^- \rightarrow NO + (H_2O)_n + \sum_i n_i$$
$$k = 4 \times 10^{-7} - 1 \times 10^{-6} \qquad (99)$$

Rate constants for dissociative recombination are similar to rate constants used for hydronium clusters. For mutual neutralization, values of $4 \times 10^{-7} cm^{-3} s^{-1}$ are used for simple negative ions, and $1 \times 10^{-6} cm^{-3} s^{-1}$ for negative cluster ions, the same as for hydronium cluster ions. The different loss reactions for NO^+ ions are shown in Fig. 8.3. The three-body clustering reaction (88) is effective in converting NO^+ to NO^+ cluster ions, when it is faster than the loss by dissociative recombination and mutual neutralization, which is below 85 km. OH reduces $NO^+ \cdot H_2O$ effectively below 83 km, where the loss rate exceeds the loss by dissociative recombination.

Calculations of positive-ion densities are carried out in a similar way as for neutral species, with production terms P and loss terms Q.

Diurnal variations of the main D-region ions are given in Fig. 8.4 in the height region 85 km–70 km. O_2^+ and NO^+ are important ions during the day around 85 km. They have very marked diurnal variations, and are negligible compared with cluster ions during the night. At this height

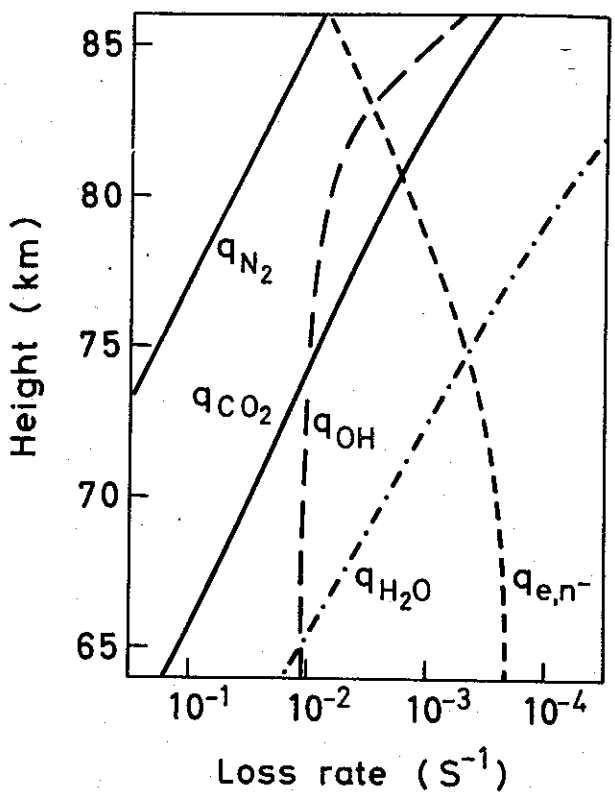

Fig. 8.3. Loss rates of NO^+. Curves q_{N_2}, q_{CO_2}, and q_{H_2O} give loss rates by reactions (84), (87) and (88), curves $q_{e,n-}$ by reactions (98) and (99), and curve q_{OH} by reaction (95).

$NO^+ \cdot H_2O$ is the main daytime cluster ion, a result of the efficient reaction (88). H_3O^+ and $H_3O^+ \cdot H_2O$ are the main hydronium ions. Higher cluster formation of hydronium ions are not effective due to the slow three-body reactions (Fig. 8.2). Diurnal variations are very pronounced with an increase of more than a factor of 10 in total ion densities from night to day.

At 80 km, three-body reactions become efficient in producing heavier ion clusters. $H_3O^+ \cdot H_2O$ is, however, the main positive ion during the day, when high electron densities (Fig. 9.6) effectively netralize positive ions before heavier clusters are formed. At night, however, low loss rates allow higher hydrates to be formed; the ions, $H_3O^+ \cdot (H_2O)_2$, $H_3O^+ \cdot (H_2O)_3$, and $H_3O^+ \cdot (H_2O)_4$ are the main components. Diurnal variation in total ion density is much less pronounced than it was at 85 km; a result of less variation in ionization rates, and of higher loss rates during the day when electrons dominate the negative ions. At 75 km, $H_3O^+ \cdot (H_2O)_3$ and

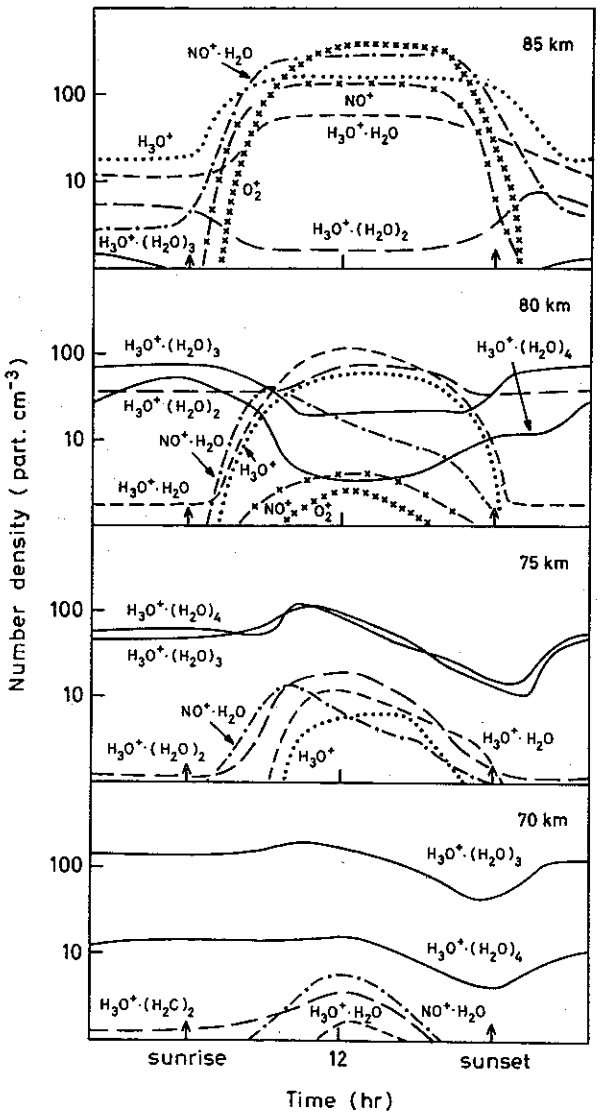

Fig. 8.4. Diurnal variations of positive ion number densities in the *D*-region.

$H_3O^+ \cdot (H_2O)_4$ are the main components over the whole day. Maximum ion densities are reached a couple of hours before noon, and there is a marked decrease in total ion densities in the afternoon, with minimum densities around sunset. This can be explained by the variation in electron densities. Electrons are built up slowly before noon, reaching high densities after noon, and decreasing slowly in the afternoon. Since electron densities exceed the negative ion densities in the afternoon (Fig. 9.7), positive ions are broken down much more effectively in the afternoon. The same effect is found at 70 km, but at this height $\lambda < 1$ only for a short period in the afternoon (Fig. 9.7). The drop in positive ion densities is therefore less pronounced at 70 km than it is at 75 km. For $z = 65$ km this effect is negligible, since $\lambda > 1$ over the whole day. At 70 km, $H_3O^+ \cdot (H_2O)_3$ is the dominant component; its densities exceed $H_3O^+ \cdot (H_2O)_4$ densities by almost a factor of 10. This high $H_3O^+ \cdot (H_2O)_3$ density can be explained by the variations of temperatures with height in the *D*-region. At 75–80 km low temperatures ($T < 200$ K) make reverse reactions (77–80) very slow. Below 75 km the temperature increases rapidly, and reverse reaction (80) becomes fast, and breaks up $H_3O^+ \cdot (H_2O)_4$ effectively.

It should be noticed that NO^+ and its hydrates are important atmospheric species only above 75 km. From 75 km and down they decrease rapidly.

Below 60 km the ion scheme can be simplified. Galactic cosmic rays are the only important source and they are, as we know, constant over the day. In addition positive and negative cluster ions are the only ions to be considered. Since we have used a mutual neutralization rate constant, which is the same for all cluster ions, loss rates will also be constant and we will have no diurnal variations in the ion species. Total positive ion densities are, therefore, given by eq. (7.5) with $\frac{d}{dt}[S_n^+] = 0$. The ion pair production is given in eq. (7.12), with $J_{GCR} = 2 \times 10^{-17}$, and since mutual neutralization is the only effective loss process, total ion densities are given by:

$$[S_n^+] = \sqrt{\frac{P_{GCR}}{\delta_{ei}}} \approx 4.5 \times 10^{-6} \cdot \sqrt{M} \qquad (8.3)$$

$\delta_{ei} = 1 \times 10^{-6}$ is the mutual neutralization coefficient.

From this expression we can see that the total ion density is proportional to the square root of the air density. Ion pair production is expected to be given by the above expression down to about 35 km. Below 35 km, increased GCR absorption leads to ionization rates which are constant with height (George 1970).

Since there are small diurnal variations, height profiles of the positive cluster ions for heights between 70 km and 10 km are given in Fig. 8.5.

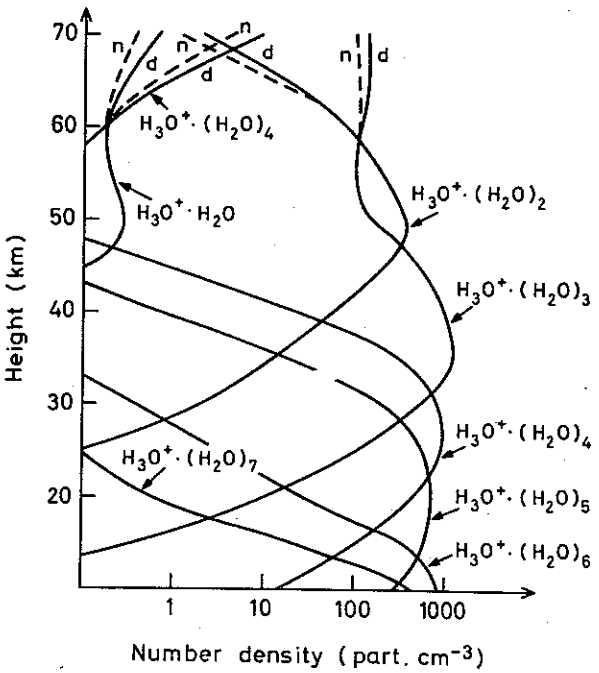

Fig. 8.5. Number densities of positive cluster ions between 70 km and 10 km. Dashed lines give values at midnight.

$H_3O^+ \cdot (H_2O)_2$ increases strongly down to 50 km, and between 60 and 50 km it is the main component. This is a result of high temperatures, which makes the reaction (79) an effective loss reaction for $H_3O^+ . (H_2O)_3$ ions. The high stratopause temperatures, therefore, lead to a fast break-up of heavier cluster ions. The drop in temperature in the stratosphere has a marked effect on the ion profiles. Below 50 km, heavier clusters ($n > 2$) increase rapidly. There is a steady increase towards heavier ions all the way down to the tropopause as a result of decrease in temperature and increase in H_2O number densities. Between approximately 50 km and 30 km, $H_3O^+ \cdot (H_2O)_3$ is the main component. Around 30 km, $H_3O^+ \cdot (H_2O)_4$ is the main positive ion component; around 20 km, $H_3O^+ \cdot (H_2O)_5$ dominates, and around tropopause level ($z =$ 10 km), $H_3O^+ \cdot (H_2O)_6$ dominates. $H_3O^+ \cdot (H_2O)_7$ also becomes a significant ion component at the lower boundary. Total ion densities increase downward toward 35 km, to the value 1.4×10^3 particles cm^{-3}.

In Fig. 8.8 we see clearly that the ion profiles depend strongly on temperatures. Modest changes in the temperature will result in marked changes in the ion profiles.

9. NEGATIVE IONS

As already mentioned, the presence of negative ions in the *D*-region has been known for only a few years, but at present there is an intensified study of these ions, and of the rate constants of the negative-ion reactions. We know, however, very little about the reaction chains leading to the terminal ions. Measurements of Narcisi et al. (1972), and Arnold et al. (1971), indicate that the negative ions, in the same way as the positive ions, form stable water cluster-ions, as could be expected (Ferguson 1971).

In the *D*-region, only two electron attachment reactions have to be considered. The main negative-ion production is through three-body electron attachment to O_2:

$$e + O_2 + O_2 \rightarrow O_2^- + O_2$$

$$k = 1.4 \times 10^{-29} \cdot \left(\frac{300}{T}\right) e^{-\frac{600}{T}} \qquad (100)$$

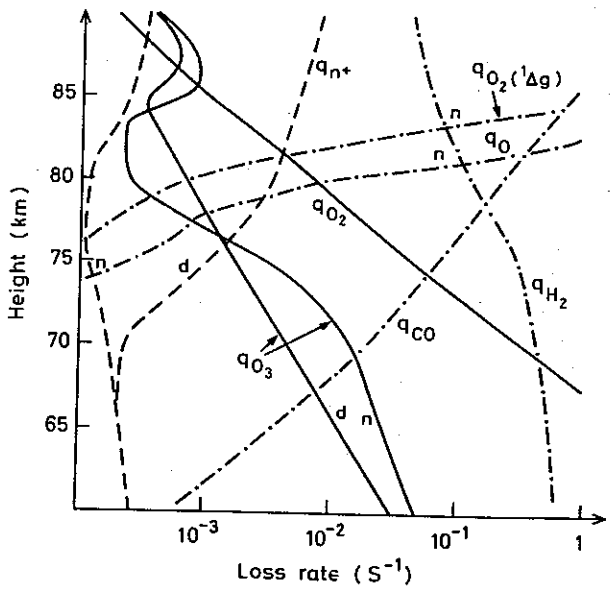

Fig. 9.1. Electron and negative-ion loss rates. Full lines give electron loss rates, curve q_{O_2} gives loss rates by reaction (100) and curve q_{O_3} by reaction (101). Dashed lines and dashed-dotted lines give negative-ion loss rates. Curve q_{n+} gives loss rates by reaction (97), and curves q_O, $qO_2(^1\Delta_g)$, q_{H_2}, and curve q_{CO} give electron detatchment rates by reactions (103)–(106). *d* gives noon-time, and *n* midnight values.

There is also a minor contribution from dissociative attachment of ozone:

$$O_3 + e \rightarrow O^- + O_2$$
$$k = 3 \times 10^{-12} \qquad (101)$$

Dissociative attachment of other neutral species is too slow to contribute to negative-ion production in the lower ionosphere. Electron loss rates are shown in Fig. 9.1. Since O_3 varies by day, loss rates by reaction (101) also vary. In the figure, this variation is represented by night-time and daytime O_3 values. Below 80 km, the three-body reaction with O_2 is the main reaction converting electrons to negative ions. It is only above 85 km that the reaction with O_3 becomes comparable to three-body attachment. These are, however, heights where negative ions are of minor interest in our calculations. Negative ions should dominate over electrons, when the above loss reactions exceed the loss of electrons by dissociative recombination with positive ions. From Fig. 9.1 this should be approximately below 80 km during the day and below 90 km during the night. This is really not what happens in the atmosphere, since the efficiency of negative-ion production is strongly reduced by fast reverse reactions. Several associative detachment reactions of the type

$$X^- + Y \rightarrow XY + e$$

with rate constants exceeding 10^{-10} (Bortner & Kummler 1968, Ferguson 1970) are known to take place in the ionosphere. The most important reactions are found to be:

$$O^- + O(^3P) \rightarrow O_2 + e$$
$$k = 1.4 \times 10^{-10} \qquad (102)$$

$$O_2^- + O(^3P) \rightarrow O_3 + e$$
$$k = 3 \times 10^{-10} \qquad (103)$$

$$O^- + O_2(^1\Delta_g) \rightarrow O_3 + e$$
$$k = 3 \times 10^{-10} \qquad (104)$$

None of these ratios are of importance below 80 km during the night. Reactions with H_2 and CO have therefore been included since neither of these components have diurnal variations:

$$O^- + H_2 \rightarrow H_2O + e$$
$$k = 6.7 \times 10^{-10} \qquad (105)$$

$$O^- + CO \rightarrow CO_2 + e$$
$$k = 8 \times 10^{-10} \qquad (106)$$

When these loss reactions are considered, the initial negative ions, O_2^- and O^-, can be rapidly converted back to electrons. This process is specially effective during the day when $O(^3P)$ and $O_2(^1\Delta_g)$ are relatively abundant. The negative-ion loss exceeds the electron loss down to about 65 km, with lifetimes $\tau < 1$ sec. During the night, conditions are quite different. $O(^3P)$ and $O_2(^1\Delta_g)$ drop off rapidly below 85 km, and the efficiency of reactions (100)–(101) is, therefore, strongly reduced. This leads to an efficient negative-ion production below about 80 km. Even if the negative-ion reaction with CO and H_2 is effective down to 75–70 km, these components include only O^-, which is a minor initial component compared with O_2^-.

The above considerations show that the primary ions O_2^- and O^- are highly unstable during the day. Formation of more stable ions depends on how fast reactions producing other negative ions are. Charge-exchange reactions of the type

$$X^- + Y \rightarrow Y^- + X$$

are known to take place (Bortner & Kummler 1968). The following reactions have been considered.

$$O^- + NO_2 \rightarrow NO_2^- + O(^3P)$$
$$k = 1 \times 10^{-9} \qquad (107)$$

$$O_2^- + NO_2 \rightarrow NO_2^- + O_2$$
$$k = 1.8 \times 10^{-9} \qquad (108)$$

$$O^- + O_3 \rightarrow O_3^- + O(^3P)$$
$$k = 5.3 \times 10^{-10} \qquad (109)$$

$$O_2^- + O_3 \rightarrow O_3^- + O_2$$
$$k = 4 \times 10^{-10} \qquad (110)$$

Even though all rate constants are fast, the two first reactions are not effective. During the day, NO_2 densities are very low in the *D*-region, and only below about 70 km are night-time values of

NO_2 high enough to be of interest. O_3, on the other hand, is present in the *D*-region and below, with much higher number densities. It is also necessary to consider the three-body associative reaction of O_2^- with O_2:

$$O_2^- + O_2 + O_2 \rightarrow O_4^- + O_2$$
$$k = 4 \times 10^{-31} \qquad (111)$$

This reaction will be the main O_2^- loss in the lower ionosphere. The relative importance of the two reactions (111) and (110) is shown in Fig. 9.2. Loss of O_2^- to form more stable negative ions will be through reaction with O_3 in the *D*-region. Above 85 km, three-body loss by reaction (111) is negligible. Below 85 km, this reaction is responsible for approximately 10% of O_2^- loss. There will, however, be variations during the day due to variations in O_3, which are also shown in the figure. The O_4^- production exceeds the production of O_3^- only for $z < 55$ km.

There is also a fast charge-exchange reaction converting O^- to O_2^-:

$$O^- + O_2(^1\Delta_g) \rightarrow O_2^- + O(^3P)$$
$$k = 10^{-10} \qquad (112)$$

and a reverse reaction:

$$O_2^- + O(^3P) \rightarrow O^- + O_2$$
$$k = 10^{-11} \qquad (113)$$

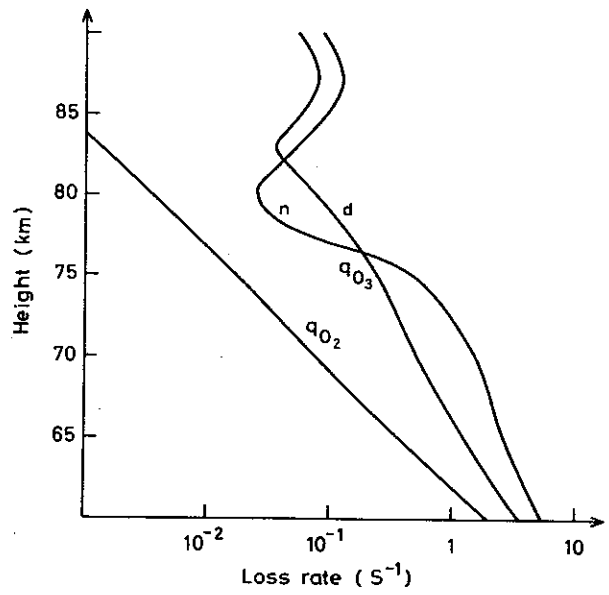

Fig. 9.2. Loss rates of O_2^- by reaction (110) (curve q_{O_3}) and by reaction (111) (curve q_{O_2}). *d* is noontime and *n* midnight values.

$O(^3P)$ and $O_2(^1\Delta_g)$ are, as we have already mentioned, active only during the day, and at night above 80 km, and are therefore of minor interest due to other fast reactions.

As soon as the ions O_3^- and O_4^- are formed, a large number of possible ion-molecule reactions can take place. The following ion-molecule reactions are found to be of aeronomic interest:

$$O_3^- + CO_2 \rightarrow CO_3^- + O_2$$
$$k = 4 \times 10^{-10} \qquad (114)$$

$$O_3^- + NO \rightarrow NO_3^- + O(^3P)$$
$$k = 10^{-10} \qquad (115)$$

$$O_4^- + CO_2 \rightarrow CO_4^- + O_2$$
$$k = 4.3 \times 10^{-11} \qquad (116)$$

$$O_4^- + O(^3P) \rightarrow O_3^- + O_2$$
$$k = 4 \times 10^{-10} \qquad (117)$$

$$CO_3^- + O(^3P) \rightarrow O_2^- + CO_2$$
$$k = 10^{-11} \qquad (118)$$

$$CO_4^- + O(^3P) \rightarrow CO_3^- + O_2$$
$$k = 1.5 \times 10^{-11} \qquad (119)$$

$$CO_3^- + NO \rightarrow NO_2^- + CO_2$$
$$k = 8 \times 10^{-12} \qquad (120)$$

$$NO_2^- + O_3 \rightarrow NO_3^- + O_2$$
$$k = 1.8 \times 10^{-11} \qquad (121)$$

$$O_4^- + NO \rightarrow NO_3^-{}^* + O_2$$
$$k = 2.5 \times 10^{-10} \qquad (122)$$

$$CO_4 + NO \rightarrow NO_3^-{}^* + CO_2$$
$$k = 4.8 \times 10^{-11} \qquad (123)$$

$$NO_3^-{}^* + NO \rightarrow NO_2^- + NO_2$$
$$k = 1.5 \times 10^{-11} \qquad (124)$$

In the *D*-region, CO_2 densities exceed those of NO by several orders of magnitude, and reactions where CO_2 are involved are fast. There will, therefore, be a fast conversion from O_3^- and O_4^- via CO_4^- to CO_3^-. Whether NO_2^- or NO_3^- become important negative species depends on how fast the reactions with NO are, compared to mutual neutralizations of CO_3^- and CO_4^-. In this model, mesospheric NO densities are low ($2-3 \times 10^6$ particles cm^{-3}), and NO_3^- production

becomes effective only around 80 km at sunrise.

Electron detachment by solar photons takes place through the following type of reaction:

$$X^- + h\nu \rightarrow X + e$$

The efficiency of electron detachment depends on the electron affinity of the negative ions. Low energy threshold allows energetic radiation at longer wavelength to detach the electrons, resulting in a high detachment rate. This will be the case for O^- and O_2^-. NO_2^-, on the other hand, and presumably NO_3^-, have higher electron affinities and lower detachment rates. Table 9.1 gives the electron affinities and detachment rates for some of the negative ions:

Table 9.1.

	E.A. (e.v.)	Detachment rate (s^{-1})
O^-	not known	1.4
O_2^-	0.43	0.33
CO_4^-	1.22	not known
O_3^-	1.9	6×10^{-2}
NO_2^-	2.7	4×10^{-2}
NO_3^-	~3.7	not known

For O_4^- and CO_3^-, neither electron affinities nor detachment rates are given.

The above rates are of minor interest since associative detachment reactions (102) and (103) are the main negative ion loss during the day. Photo-detachment may be of importance for NO_3^- ions after sunrise since they are lost only by mutual neutralization with positive ions. A photo-detachment rate of 1×10^{-4} is used for NO_3^-.

The above reaction scheme leads, as we have noticed, to NO_3^- as the terminal ion. Below 80 km, densities of neutral constituents become high, and therefore three-body clustering reactions are likely to take place. In the last year, several measurements on negative cluster ion reactions have been reported (Pack & Phelps 1971, McKnight & Sawina 1971, Kebarle et al. 1972, Phelps 1972). The following clustering sequence of O_2^- is taken from Pack & Phelps (1971):

$$O_4^- + H_2O \rightarrow O_2^- \cdot (H_2O) + O_2 \qquad k = 1.4\times10^{-9} \qquad (125)$$

$$O_2^- + H_2O + O_2 \rightarrow O_2^- \cdot (H_2O) + O_2 \qquad k = 3\times10^{-28} \qquad (126)$$

$$O_2^- \cdot (H_2O) + H_2O + O_2 \rightarrow O_2^- \cdot (H_2O)_2 + O_2 \qquad k = 4\times10^{-28} \qquad (127)$$

O^- and O_3^- cluster ions are also formed through three-body reactions with water vapour.

$$O^- + H_2O + O_2 \rightarrow O^- \cdot (H_2O) + O_2 \qquad k = 1.0\times10^{-28} \qquad (128)$$

$$O_3^- + H_2O + O_2 \rightarrow O_3^- \cdot (H_2O) + O_2 \qquad k = 2.1\times10^{-28} \qquad (129)$$

O_3^- is produced from O^- through the three-body reaction:

$$O^- + O_2 + O_2 \rightarrow O_3^- + O_2 \qquad k = 1.2\times10^{-30} \qquad (130)$$

In the same way as positive cluster ions, negative cluster ions are found to be broken down by reverse reactions. The negative water cluster ion $O_2^- \cdot (H_2O)_2$ is broken down by O_2 to form $O_2^- \cdot (H_2O)$ (Pack & Phelps 1971):

$$O_2^- \cdot (H_2O)_2 + O_2 \rightarrow O_2^-(H_2O) + H_2O + O_2 \qquad k = 7.1\times10^{-15} \qquad (131)$$

and O_4^- is broken down to give O_2^-:

$$O_4^- + O_2 \rightarrow O_2^- + O_2 + O_2 \qquad k = 2.7\times10^{-14} \qquad (132)$$

$O_2^- \cdot (H_2O)$ is a very unstable negative ion; it is broken down rapidly in the *D*-region by the two fast reactions (Parkes 1971, Adams & al. 1970):

$$O_2^- \cdot (H_2O) + O_2 \rightarrow O_4^- + H_2O \qquad k = 2.5\times10^{-15} \qquad (133)$$

$$O_2^- \cdot (H_2O) + CO_2 \rightarrow CO_4^- + H_2O \qquad k = 5.8\times10^{-10} \qquad (134)$$

Since $|CO_2| \sim 10^{-3}|O_2|$ in the atmosphere, the last reaction is the main loss reaction of $O_2^- \cdot (H_2O)$.

Puckett & Lineberger (1970) measured rate constants of NO_2^- hydration in an H_2O–NO mixture:

$$NO_2^- + H_2O + NO \rightarrow NO_2^- \cdot (H_2O) + NO \qquad k = 1.3\times10^{-28} \qquad (135)$$

The same rate constant will be adopted here for N_2 as third body. They have also suggested the following reaction to take place:

$$NO_2^- \cdot (H_2O) + HNO_2 \rightarrow NO_2^- \cdot (HNO_2) + H_2O$$
$$k = 1 \times 10^{-9} \qquad (136)$$

since bond strength of $NO_2^- \cdot (HNO_2)$ is greater than bond strength of $NO_2^- \cdot (H_2O)$. Unfortunately we know very little about the number densities of HNO_2. We have, however, expected it to be produced and broken down in a similar way as HNO_3. With these assumptions, HNO_2 is present in the *D*-region with so small densities that it is of no interest for ion reactions. The same argument can be used against HNO_3 in ionic reactions in the *D*-region.

NO_3^- cluster ions are produced effectively through the sequence (Ferguson 1971)

$$NO_3^- + O_2 + M \rightarrow NO_3^- \cdot O_2 + M$$
$$k = 10^{-32} \qquad (137)$$

$$NO_3^- \cdot O_2 + H_2O \rightarrow NO_3^- \cdot (H_2O) + O_2$$
$$k = 10^{-9} \qquad (138)$$

rather than by three-body association:

$$NO_3^- + H_2O + M \rightarrow NO_3^- \cdot (H_2O) + M$$
$$k = 2 \times 10^{-28} \qquad (139)$$

The argument here is similar to what was used for positive water cluster formation. Even if the rate constant of reaction (139) is more than three orders of magnitude faster than the rate constant of reaction (137), the O_2 number density exceeds the number density of H_2O almost by a factor of 10^5, which makes reaction (137) the main reaction for NO_3^- cluster production.

We have already mentioned, we expect all negative ions in the *D*-region and below to form stable water cluster ions. We have therefore used reactions of the type:

$$X^- \cdot (H_2O)_{n-1} + H_2O + M \rightarrow X^- \cdot (H_2O)_n + M$$
$$n = 1,2,3 \ldots \qquad (139\text{–}141)$$

on the main negative ions NO_3^-, CO_3^-, and CO_4^-. Rate constants are expected to be similar to the rate constants of reactions (126), (129), and (139); the following value is therefore used: $k = 2 \times 10^{-28}$. CO_4^- cluster ions might be broken down by the binary reaction (Kebarle et al. 1972):

$$CO_4^- \cdot (H_2O) + H_2O \rightarrow O_2^- \cdot (H_2O)_2 + CO_2$$

This reaction would be of great importance to the negative ions in the lower stratosphere, where CO_4^- cluster ions dominate the negative ions. There might be other reactions of the same type as above, with other neutral components than water, which could affect all the cluster ions. We have, however, neglected this in these calculations, and only used the binary reactions with known rate constants.

In addition, we must expect reverse reactions for higher water cluster formation for all negative ions similar to the reverse reaction (131):

$$X^- \cdot (H_2O)_n + M \rightarrow X^- \cdot (H_2O)_{n-1} + H_2O + M$$
$$n = 2,3, \ldots$$

Since we know very little about the rate constants, and the activation energies associated with them, we have found it necessary to simplify the negative cluster-ions calculations, and calculate only one cluster component of each negative ion. These ions are given by $O_2^-(H_2O)_n$, $O_3^-(H_2O)_n$, $CO_3^-(H_2O)_n$, $CO_4^-(H_2O)_n$, $NO_2^-(H_2O)_n$, and $NO_3^-(H_2O)_n$. Each calculated component will therefore be the sum of all the clusters of one negative ion.

How effectively cluster ions are produced, depends on how fast the three-body reactions, producing cluster ions, are compared to the ion mutual neutralization reactions, and the binary ion-molecule reactions, forming other negative ions. Mutual neutralization is given by

$$n_i^- + \sum_j n_j^+ \rightarrow n_i + \sum_j n_j \quad k = 10^{-6} \qquad (97, 99)$$

Loss by the terminal negative ions is given by mutual neutralization with positive ions. When life times are hours, there will be marked delay in the negative-ion variations. This effect is pronounced in the *D*-region, where ion densities are low, specially during the night. The diurnal variation of τ_{n-} is illustrated in Fig. 9.3. At night lifetimes are greater than two hours at all heights. After sunrise there is a slow decrease in lifetimes at all heights, except around 85 km, where it

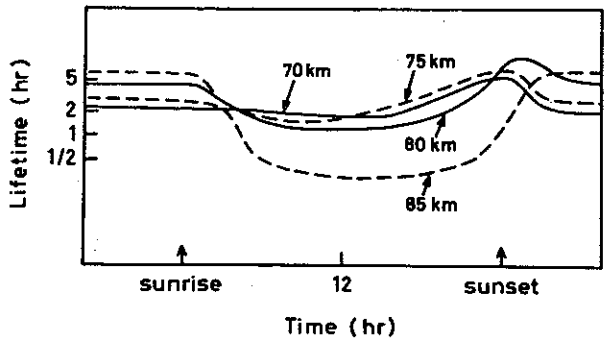

Fig. 9.3. Diurnal variations of the lifetimes of negative ions in the *D*-region.

decreases markedly during the day. Below 85 km, however, lifetimes of two hours or more are maintained almost for three hours after sunrise, and even at noon lifetimes exceed one hour in most of the *D*-region. There is a pronounced increase in τ in the afternoon, reaching maximum values shortly after sunset. This is a result of the build-up of electron densities in the afternoon which are not broken down until after sunset. Since electrons remove positive ions effectively, negative ions are most abundant after sunset.

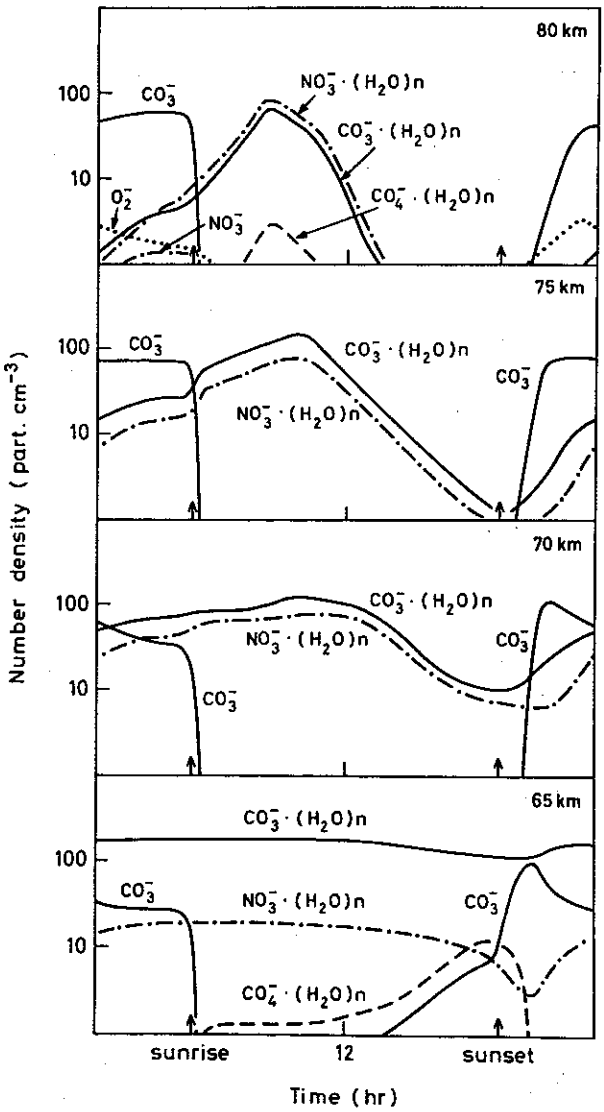

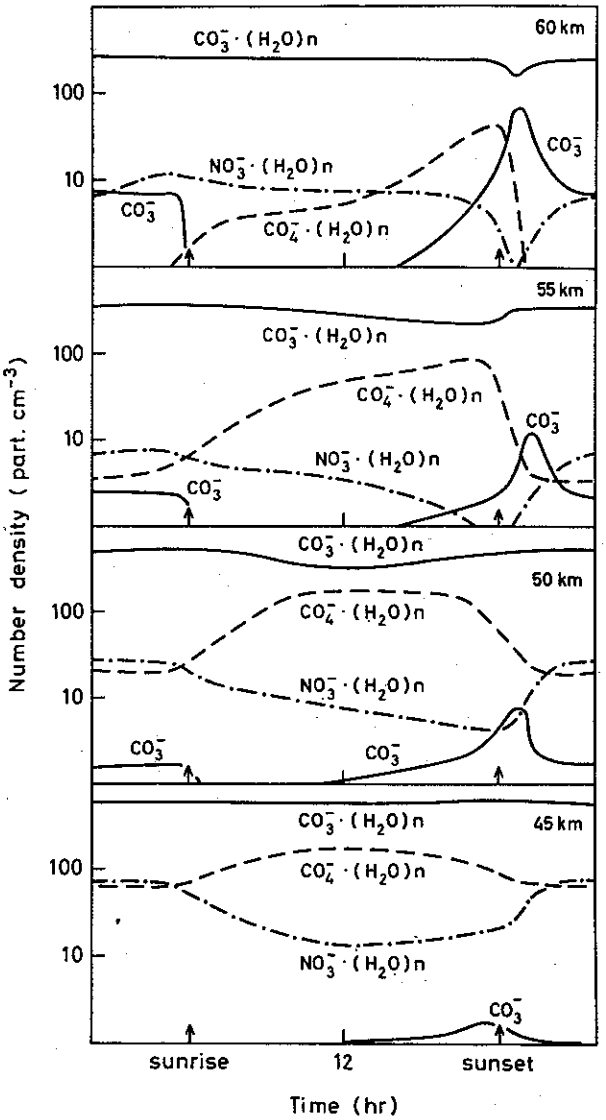

Fig. 9.4. Diurnal variations of negative ion number densities between 80 km and 45 km.

These long lifetimes will therefore lead to marked delay in the breakdown of terminal negative ions, especially after sunrise. Fig. 9.4 gives the diurnal variations of the main negative ions. The figure is extended down to 45 km, since there will be marked diurnal variations of the main components down to this height.

The diurnal variations of the negative ions are very pronounced even in the upper stratosphere.

In the *D*-region there is a pronounced time delay before daytime and night-time ion densities are obtained, which is, as we have already pointed out, a result of the long lifetimes in this region. Above 80 km, negative-ion densities decrease rapidly. The variations of negative ions are therefore given for heights from 80 km and down. At 80 km and 75 km, CO_3^- is the main night-time ion. In increases rapidly after sunset, reaching values of $5-6\times10^2$ particles cm^{-3}. At sunrise, CO_3^- drops rapidly, and becomes a negligible negative component during the day. The cluster ions $CO_3^-\cdot(H_2O)_n$ and $NO_3^-\cdot(H_2O)_n$, however, continue to rise for several hours since they are terminal ions, and are broken down only by neutralization with positive ions. When electron densities become comparable to negative-ion densities, there is a fast drop in negative-ion densities. The low daytime values are therefore not reached until after noon. In the first few hours after sunset, O_2^- is a main negative-ion component. NO_3^- is always a negligible component, since it is effectively converted to NO_3^- clusters through the reaction (137). CO_4^- and its cluster ions are of minor interest in the *D*-region. At 70 km, negative-ion densities exceed the electron densities over the whole day. There is, therefore much less diurnal variation in total negative-ion densities, and below 70 km it is negligible.

In the height region above 45 km, where pronounced diurnal variations take place, CO_3^- and its hydrates are the main ion components. Above 65 km, CO_3^- increases rapidly at sunset, and is the main component for some hours. Below 65 km, $CO_3^-\cdot(H_2O)_n$ ions are the main ions over the whole day, and have very small diurnal variations. $CO_4^-\cdot(H_2O)_n$ becomes an important negative-ion component in the lower stratosphere. It has a diurnal variation which is opposite to the variation of CO_3^- and NO_3^- cluster ions, with low night-time values, and maximum values before sunset. NO_3^- cluster ion densities are low below 70 km, a result of the low NO mixing ratios in the mesosphere and upper stratosphere. Below 50 km, ion densities increase, but NO_3^- cluster ions will not become a main ion component in the stratosphere.

Below 45 km, diurnal variations of the main components are small. It is therefore convenient to present ion densities with their average daytime values for heights between 45 km and 10 km (Fig. 9.5). $CO_3^-\cdot(H_2O)_n$ is the main component down to 35 km, while $CO_4^-\cdot(H_2O)_n$ is the main negative-ion component below 35 km. Total ion densities increase down to 35 km, with an approximately constant value of 1.4×10^3 particles cm^{-3} below 35 km.

Electron densities vary strongly by day (Fig. 9.6). At 85 km, variation is fairly symmetrical, with a strong increase after sunrise, and a similar decrease around sunset.

Below 85 km, there is an increased delay in the electron build-up after sunrise upon entry into the mesosphere ($z>60$ km). Around 65 km, maximum electron densities are obtained at sunset. Maximum electron densities decrease downward from 10^3 particles cm^{-3} at 85 km to 10^{-1} particles cm^{-3} at 50 km.

The diurnal variation in λ is also very unsymmetrical above 50 km (Fig. 9.7). Maximum

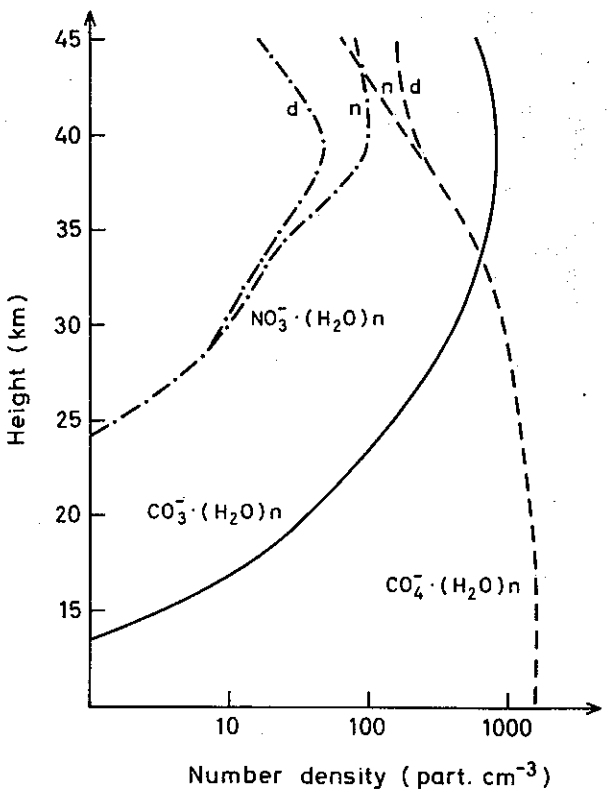

Fig. 9.5. Number densities of negative cluster ions between 45 km and 10 km. *d* gives noon-time, and *n* midnight values.

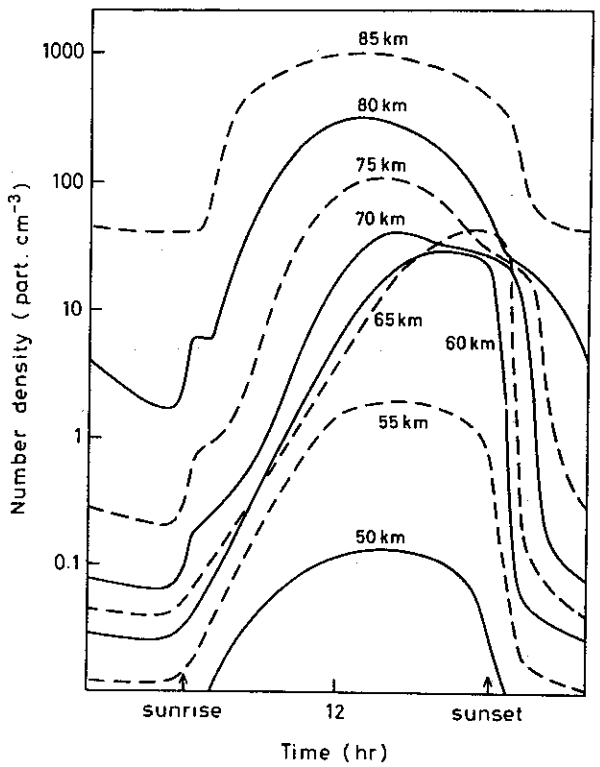

Fig. 9.6. Diurnal variations of electron number densities.

values are obtained in the late night, just before sunrise. This tendency is very pronounced around 80 km, while the night-time values in the lower mesosphere are almost constant. A similar variation is found during the day. Minimum λ values are obtained in the afternoon, shortly before sunset. At 80 km, there is a very marked decrease from sunrise until sunset, of several orders of magnitude. At lower altitude, diurnal variation in λ becomes less pronounced.

The number density of total negative ions is found to exceed the number density of electrons ($\lambda > 1$) at about 68 km in the afternoon, when λ has its lowest value, and around 82 km before sunrise, when λ has its maximum value. Noon-time values will, as we can see from the figure, differ quite markedly from the minimum value in the afternoon, since λ varies so strongly in the sunlight period.

10. DISCUSSION OF THE MODEL

As we have already pointed out, the result of the calculations depends strongly on the model chosen. Calculations are carried out for mid-latitude (45°) summer conditions. Several parameters of importance to atmospheric species are known to vary very strongly with latitude and season, such as the turbulent diffusion coefficient, absorption of solar photons, and temperature. It is therefore obvious that the same calculations as above would give different results if they were carried out for other latitudes or seasons.

There is, however, one more serious problem—the great uncertainty of many of the rate constants. This is specially true for rate constants of nitrogen reactions, and reactions with cluster ions.

Since many of the main components in this model have been measured, a comparison between observed and calculated profiles should be a valuable check of the reliability of this model.

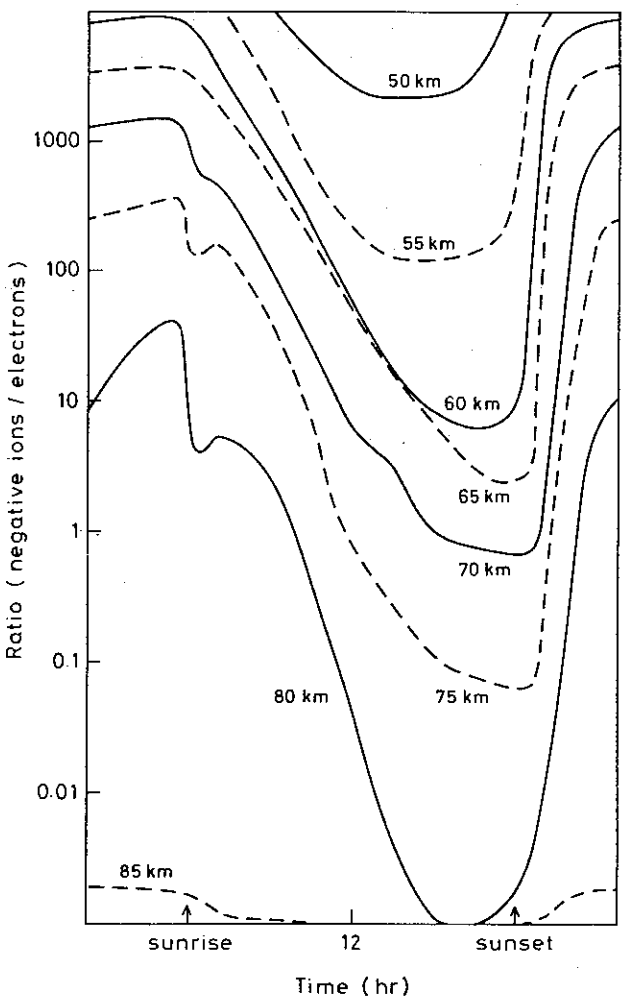

Fig. 9.7. Diurnal variations of λ.

There are, however, very few measurements performed, and seasonal and latitudinal variations are not known.

We should therefore keep in mind that differences between observations and this calculation might be due to the fact that most of the observations are performed under different atmospheric conditions than those used in this model.

Ozone is, as we have already seen, a main participant in the negative-ion chemistry of the *D*-region. Reliable negative-ion profiles therefore depend strongly on the diurnal variations of O_3. Below 70 km, daytime and night-time ozone have been measured (Hilsenrath 1972). These measurements agree very well with our calculations (Fig. 10.1). Below 50 km, ozone is by far the most dominant odd-oxygen component, with negligible diurnal variations. Above 50 km, there is an increasing difference between daytime and night-time ozone densities, in good agreement with the observation. At 65 km, ozone is twice as abundant during the night as it is during the day.

In the height region around 80 km, where odd-hydrogen components control $O(^3P)$ and O_3, we should notice the very marked drop in ozone densities during the night (Fig. 4.2), a result of OH and HO_2 removing odd oxygen. We should also notice the very unsymmetric variation between 70 and 80 km in both ozone and atomic oxygen in the sunlight period, since $O(^3P)$ and O_3 are in photochemical equilibrium. Maximum densities are reached well before noon, and there is a marked decrease in the afternoon. Both night-time and daytime height profiles of $O_2(^1\Delta_g)$ have been measured several times (Evans et al. 1968, Wood et al 1969, Evans et al. 1972). A comparison with these calculations should therefore be of interest. Fig. 10.2 gives observed night-time and afternoon profiles (Evans et al. 1972, and Evans et al 1968), respectively, compared to calculated height profile of $O_2(^1\Delta_g)$ for the same time. $O_2(^1\Delta_g)$ is present during the night only for $z > 80$ km, since it is probably produced during the night by reactions with $O(^3P)$, (reactions 1 and 4,*b*). These reactions are both uncertain (Bates 1954, Wood 1972), but they have been adopted since they seem to give a night-time profile in agreement with observations. It should be noticed that only 10% of reaction (4) is re-

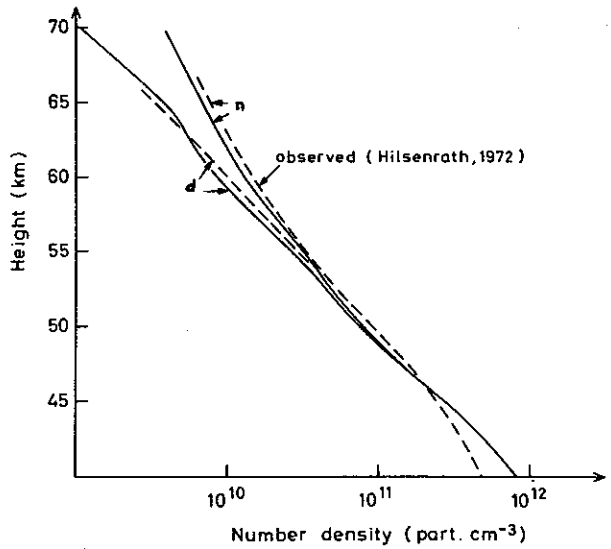

Fig. 10.1. Calculated (full lines) and observed (dashed lines) ozone profiles between 70 km and 40 km. *d* gives daytime, and *n* night-time values.

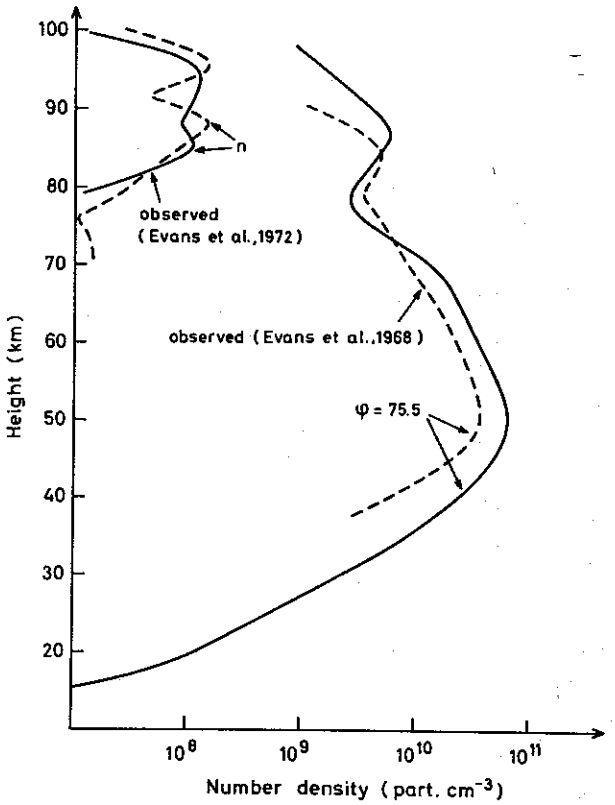

Fig. 10.2. Calculated (full lines) and observed (dashed lines) $O_2(^1\Delta_g)$ profiles between 100 km and 10 km. *n* gives night-time values, and φ gives the sun's zenith-distance for the daytime profile.

quired to give observed $O_2(^1\Delta_g)$ densities. During the day, calculations give the secondary maximum around 85 km, in good agreement with observations. The calculated profile is taken for the same solar elevation as in the observation, $\phi = 75.5°$. This is highly necessary when comparisons are made, since $O_2(^1\Delta_g)$, in the same way as $O(^3P)$ and O_3, vary in a most irregular fashion by day above 70 km (Fig. 4.3). This is also clearly demonstrated in the height profiles given for morning and evening conditions by Wood (1969).

Discrepancies between observations and calculations, especially below 60 km, are probably due to the observed profile representing conditions during autumn at lower latitudes (October at 30°), while calculations are made for summer conditions at 45°. Hydroxyl has turned out to be a very important component in atmospheric chemistry. In the mesosphere, OH and HO_2 through reactions (3) and (4) control odd oxygen, and, with the rate constant $k_{95} = 2 \times 10^{-9}\text{cm}^{-3}\text{s}^{-1}$, OH through reaction (95) determines the main-ion component in the *D*-region. Furthermore, it is the main component in breaking down CO and CH_4, and therefore also in determining their height profiles. It is therefore obvious that reliable information on the abundance of OH in the atmosphere is of the greatest importance to atmospheric chemistry. OH measurements have, however, been reported only a couple of times (Anderson 1971), giving height profiles for late afternoon ($\phi = 86°$) in the height region 45–70 km. Since OH has a pronounced variation during the day (Fig. 4.4), a calculated height profile for $\phi = 86°$ is given in the Figure along with the observed height profile. Between 70 and 55 km, calculated values are within experimental error of the result. Below 55 km, the calculation gives a somewhat higher value than what could be expected from observations. Below 55 km, the given profile is for a time when there is a fast drop in OH densities (Fig. 4.4). Small changes in the atmospheric conditions could, therefore, result in marked changes in the profile.

In the lower stratosphere, OH is also an important component in the odd nitrogen cycle, since it rapidly converts NO_2 to HNO_3 through

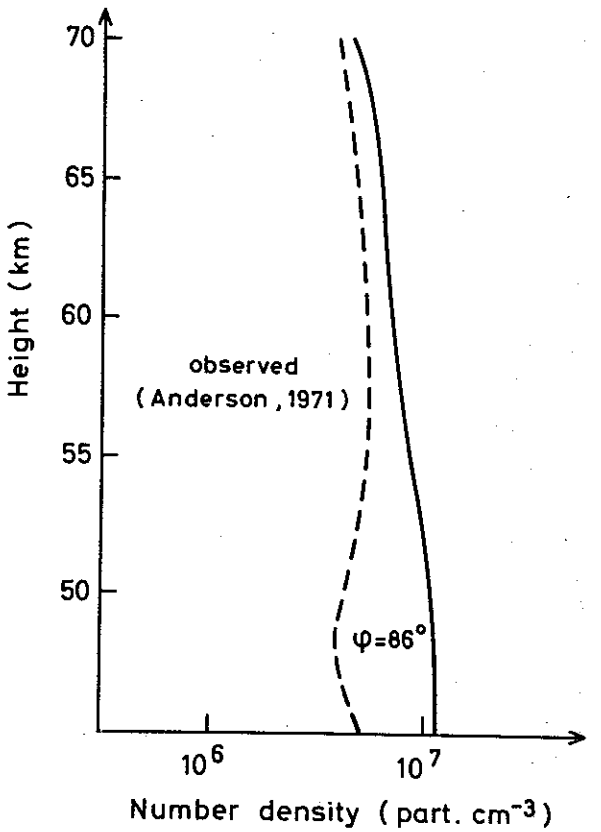

Fig. 10.3. Calculated (full line) and observed (dashed line) hydroxyl profiles between 70 km and 45 km for a zenith distance φ.

reaction (41). Unfortunately, some rate constants in the main reactions of hydroxyl production and destruction are uncertain. Reaction (26), producing OH, might be as much as one order of magnitude faster at tropopause temperatures, while reaction (28), which destroys OH, is possibly two orders of magnitude faster. Reaction (28) would then be the main loss reaction of OH almost down to the tropopause.

Our knowledge of atmospheric nitrogen oxides has increased rapidly in the last few years, and reliable measurements on nitric oxide in the lower thermosphere and nitrogen dioxide and nitric acid in the lower stratosphere are now available.

Fig. 10.4 gives the calculated NO height profile, compared to the observed profile of Meira (1970). Calculated NO densities have a variation with height in good agreement with observations, maximum density around 100 km, minimum density around 80 km. Calculated densities are, however, much too low to explain the observations. The discrepancy can be explained as

follows. First of all, the calculated NO profile is for summer conditions at 45°, while the observed profile is for winter conditions at 38°. In the winter, a more effective downward transport below about 90 km would be expected, since eddy diffusion coefficients are much higher (Lindzen 1971). Secondly, the calculated NO profile is for minimum solar activity, while observations are made during maximum solar activity. This will result in a high NO production during the time of observation since the primary source of NO is solar X-ray radiation (Isaksen 1971). The calculated NO profile therefore represents summer conditions at mid-latitude, during minimum solar activity. We must expect an increase in NO densities, especially at *D*-region heights in the winter, and at maximum solar activities.

Nitric oxide is the main component in the nitrogen oxide cycle down to 70 km during the night, and down to 35 km during the day. Below 35 km, both NO_2 and HNO_3 become important nitrogen components. NO_2 has been measured between 12 and 29 km at zenith distances $\phi > 91°$ by Ackerman & Muller (1972), and their results are given in Fig. 10.5 along with the calculated height profile for the same zenith distances.

Calculated NO_2 mixing ratios vary with height in the lower stratosphere in agreement with

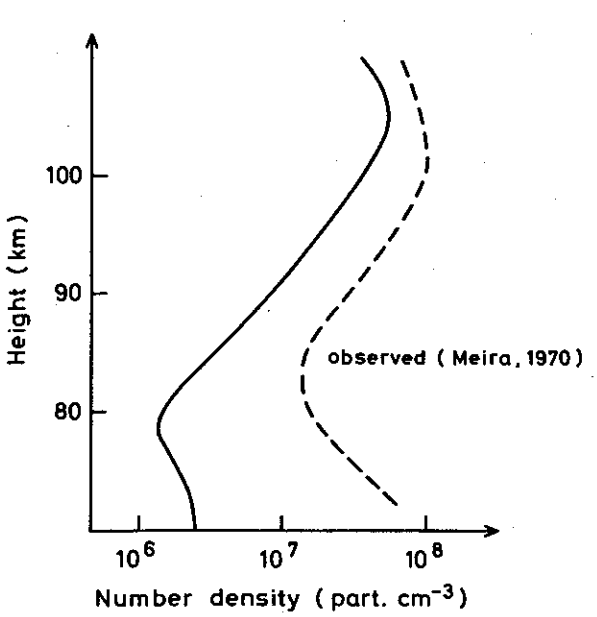

Fig. 10.4. Calculated (full line) and observed (dashed line) NO profiles between 110 km and 70 km.

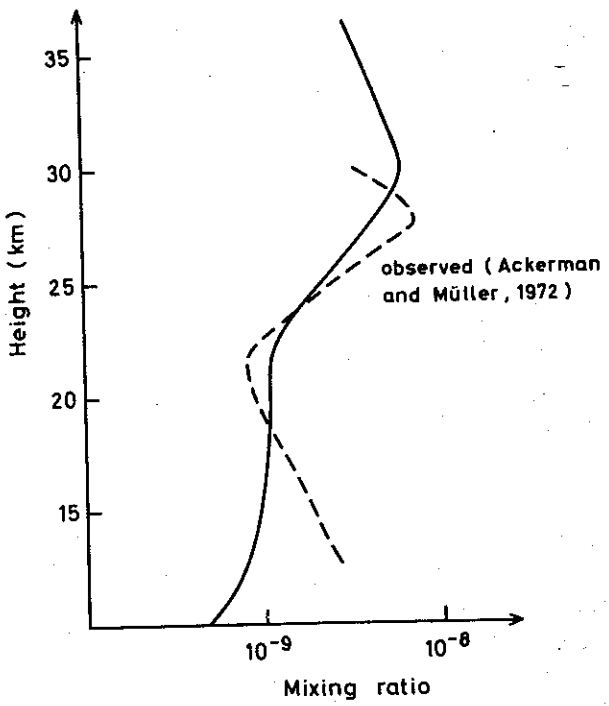

Fig. 10.5. Calculated (full line) and observed (dashed line) NO_2 profiles between 35 km and 10 km.

observations. Maximum mixing ratio occurs above the ozone maximum, around 30 km. There is a slow decrease above, due to ozone decrease, and a decrease below, since NO_2 is converted to HNO_3 below 30 km. Below 20 km, NO_2 mixing ratio is fairly constant, in contrast to observations which show an increase in δ_{NO_2} downward from 20 km, reaching a value of 3×10^{-9} at 12 km. It is, however, possible that this discrepancy is due to the fact that the observations at low heights, which are at the greatest zenith distance, have daytime NO partly converted to NO_2. It is also possible that the difference between observations and calculations is due to variations in ozone densities, since NO is converted to NO_2 through reaction (40). O_3 is known to vary strongly with latitude, and also with time, around tropopause level, sometimes with a low secondary maximum (Herring & Borden 1964). In these calculations only average conditions for the summer months at 45° are used.

HNO_3 is measured with a fairly constant mixing ratio between 18 km and 30 km, $\delta_{HNO_3} = 1 - 2 \times 10^{-9}$ (Rhine et al. 1969). The calculated height profile of HNO_3 shows variation in mixing ratio within a factor of 2.5 between 18 km and

30 km, with values somewhat higher than observed, $\delta_{HNO_3} = 2-5\times10^{-9}$ (Fig. 5.3). Maximum HNO_3 mixing ratio is obtained between 20 km and 25 km. It should also be mentioned that the odd nitrogen component depends on OH. Changes in OH will, therefore, give changes in odd-nitrogen components.

When the calculated ion densities are compared with observed ion densities, it should be remembered that total ion densities depend on the NO profile, since Ly-α ionization of NO is the main ion source in the *D*-region. The low nitric oxide densities obtained in the *D*-region, therefore, give low total ion densities. If we compare these calculations with *D*-region ion measurements (Narcisi 1972, Goldberg & Aikin 1971, Johannesen & Krankowsky 1972), we find that the observed profiles give higher *D*-region densities than the calculations. And since the observations are performed at different latitudes and seasons, this is what we can expect, according to our previous remarks about the NO height profile.

As we have seen from the calculations in the *D*-region, the simple ions O_2^+ and NO^+ are effectively converted to water cluster ions. The reliability of the reaction scheme forming cluster ions can be checked by comparing the calculated with the observed relative densities of water cluster ions present in the *D*-region. This has been done in Fig. 10.6, giving calculated relative densities of cluster ions at noon, and observed densities by Narcisi (1972), and by Johannesen & Krankowsky (1972). Calculated relative densities are represented by two profiles. First, only hydronium cluster ions are considered, and next nitric oxide clusters are included. If we consider only hydronium cluster ions, variations in densities with height are in fair agreement with the result of Johannesen & Krankowsky (1972).

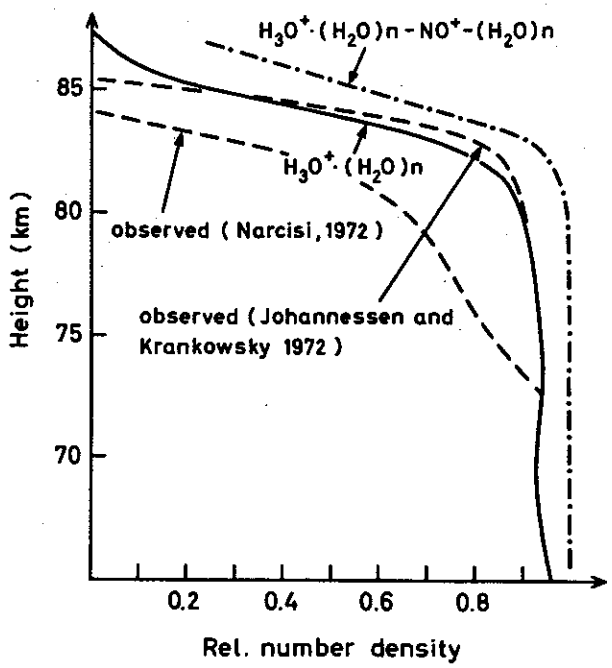

Fig. 10.6. Calculated (full line, dashed dotted line) and observed (dashed lines) cluster ion profiles. Full line, only hydronium cluster ions. Dashed-dotted line, NO cluster ions included.

When nitric oxide cluster ions are included, there is a much slow decrease in cluster ions above about 82–83 km. Hydronium cluster ions are inversely proportional to atomic oxygen, since reaction (63) which converts O_4^+ back to O_2^+, and reaction (95) producing hydronium cluster ions from $NO^+\cdot(H_2O)$ determine hydronium cluster ions. Nitric oxide cluster ions are produced by three-body reaction from NO^+, and are lost either by dissociative recombination with electrons or by three-body reactions forming higher cluster ions, in addition to reaction (95). These loss reactions are too slow to give a sharp cut-off in NO^+ clusters above 82 km, in agreement with observations. The observed profiles would be explained if there was a binary reaction with $O(^3P)$ on the sequence from NO^+ to $NO^+\cdot H_2O$ breaking up the cluster in the same way as for O_4^+ ions (reaction 63). The variations in cluster ion cut-off may therefore be due to variations in the $O(^3P)$ profile. The profile by Narcisi (Fig. 10.6), giving a lower cut-off, would then be a result of a lower $O(^3P)$ profile.

The low mesopause temperature allows higher hydrates to be stable. Around 80 km, the cluster ions $H_3O^+\cdot H_2O$ and $H_3O^+\cdot(H_2O)_2$ are the main daytime components. At 75 km, the cluster ions $H_3O^+\cdot(H_2O)_3$ and $H_3O^+\cdot(H_2O)_4$ are the main components, and at 70 km, high temperatures make the reverse reaction (80) so fast that $H_3O^+\cdot(H_2O)_4$ is converted back to $H_3O^+\cdot(H_2O)_3$.

If we compare these calculated values with observed ion densities, high cluster formations are found to be present in the region between

80 and 85 km, with $H_3O^+ \cdot H_2O$, $H_3O^+ \cdot (H_2O)_2$, and $H_3O^+ \cdot (H_2O)_3$ the main components in high latitude, summer, when mesopause temperatures are low (Johannesen & Krankowsky 1972). It is difficult to explain why observations in every case give $H_3O^+ \cdot H_2O$ and $H_3O^+ \cdot (H_2O)_2$ as the main components; calculations give $H_3O^+ \cdot (H_2O)_3$ and $H_3O^+ \cdot (H_2O)_4$ as the main components.

It is, however, possible that the ions lose one or more water molecules before observations, due to increased shock-layer temperature (Narcisi 1972).

Negative ions vary strongly by day (Fig. 9.4), and if we want to compare observations with a calculated height profile, the result depends strongly on what time of the day the profile is taken. Fig. 10.7 gives observed negative-ion densities at midnight, and the calculated height profile at the same time. From the observed profile, only components which are calculated are included. Observations also show the ions Cl^-, HCO_3^- below 80 km and heavy cluster ions with mass 111 ± 1 and 125 ± 1 present above 80 km. It is not possible to explain these ions by the present model, and they are not included in the Figure.

CO_3^- is the main negative ion below 80 km in the observations and in these calculations. There is a rapid decrease in ion densities above 80 km, where O_2^- is comparable to CO_3^-. Below 70 km, calculations give $CO_3^- . (H_2O)_n$ as the dominating negative ion. There is, however, a great discrepancy between observation and calculation for NO_3^-. Observations give NO_3^- densities between 80 km and 75 km almost ten times higher than what is obtained in the calculations, and below 75 km, observed NO_3^- exceeds calculated $NO_3^- . (H_2O)_n$ by the same magnitude. This can be explained by the low NO densities in the *D*-region, since NO_3^- is produced by reactions with NO. We can therefore expect NO densities to be one order of magnitude higher under the observed conditions, than in our calculations.

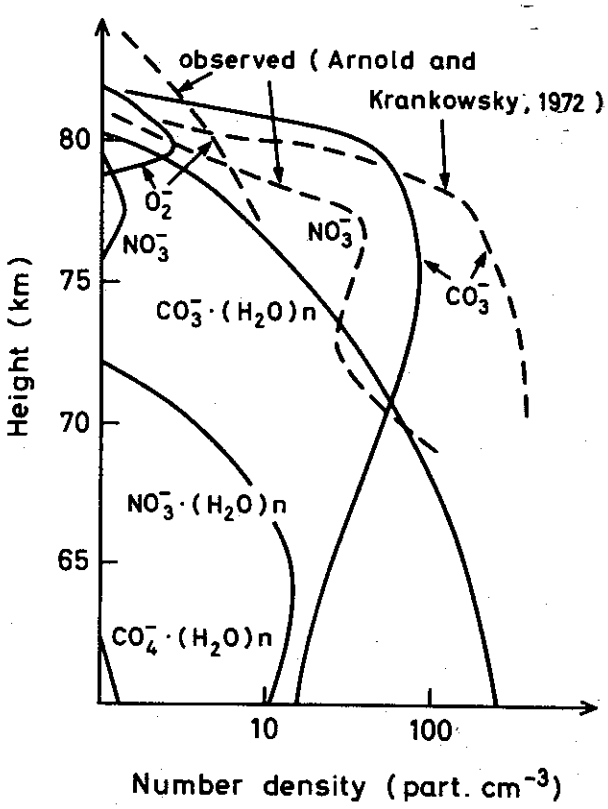

Fig. 10.7. Calculated (full lines) and observed (dashed lines) negative ion profiles.

The calculations show that most of the atmospheric species can be calculated from the reaction rates and diffusion coefficient known at present. It is, however, clear that some of the main species, such as NO and OH, may have seasonal and latitudinal variations. This work will be continued by calculating NO profiles for different latitudes and seasons to find how NO varies with variation in the diffusion coefficient and in solar activity. It would also be interesting to show the influence of NO variations on the *D*-region ion chemistry, since NO influences both positive and negative ions. Plans are also underway to extend the calculations downward into the troposphere, to obtain diurnal variations of atmospheric species. Reliable background information is needed before models, including sources of air pollution, are included.

APPENDIX

DISSOCIATION SCHEME

$O_2+h\nu \rightarrow O(^3P)+O(^3P)$	$\lambda<2424$ Å	Ackerman (1971) Kockarts (1971)	(*a*)
$O_2+h\nu \rightarrow O(^1D)+O(^3P)$	$\lambda<1750$ Å		(*b*)
$O_3+h\nu \rightarrow O(^3P)+O_2(^3\sum_g^-)$	$\lambda<11800$ Å		(*c*)
$O_3+h\nu \rightarrow O(^1D)+O_2(^1\Delta_g)$	$\lambda<3110$ Å		(*d*)
$H_2O+h\nu \rightarrow OH+H$	$\lambda<2420$ Å	Watanabe (1958)	(*e*)
$H_2O_2+h\nu \rightarrow OH+OH$	$\lambda<5650$ Å	Schumb et al. (1965)	(*f*)
$HO_2+h\nu \rightarrow OH+O(^3P)$	$\lambda<4540$ Å	$J_{HO_2}=J_{H_2O_2}$	(*g*)
$NO+h\nu \rightarrow N+O(^3P)$	$\lambda<1910$ Å	Strobel (1971)	(*h*)
$NO_2+h\nu \rightarrow NO+O(^3P)$	$\lambda<3975$ Å	Tuesday (1961)	(*i*)
$N_2O_5+h\nu \rightarrow N_2O_4+O(^3P)$	$\lambda<80000$ Å	Jones & Wolfe (1937)	(*j*)
$HNO_3+h\nu \rightarrow OH+NO_2$	$\lambda<5460$ Å	Johnston & Graham (1972)	(*k*)
$HNO_3+h\nu \rightarrow HO_2+NO$	$\lambda<4700$ Å		(*l*)
$NO_3+h\nu \rightarrow NO+O_2$	$\lambda<11\ \mu$	Jones & Wolfe (1937)	(*m*)
$NO_3+h\nu \rightarrow NO_2+O(^3P)$	$\lambda<5710$ Å		(*n*)
$N_2O+h\nu \rightarrow N_2+O(^3P)$	$\lambda<3370$ Å	Bates & Hays (1967)	(*o*)
$CH_4+h\nu \rightarrow CH_3+H$	$\lambda<1650$ Å	Inn & Tannaka (1953)	(*p*)
$CO_2+h\nu \rightarrow CO+O(^3P)$	$\lambda<1800$ Å		(*q*)
$CH_2O+h\nu \rightarrow CO+H_2$		Calvert et al. (1972)	(*r*)
$CH_2O+h\nu \rightarrow CHO+H$			(*s*)

IONIZATION SCHEME

$O_2+h\nu \rightarrow O_2^+ + e$	$\lambda = 1025.7$ Å	Huffman (1968)	(*aa*)
$NO+h\nu \rightarrow NO^+ + e$	$\lambda = 1215.7$ Å	Watanabe (1958)	(*bb*)
$N_2+h\nu \rightarrow N_2^+ + e$	2 Å $<\lambda<$ 100 Å	Friedman (1960)	(*cc*)
$O_2+h\nu \rightarrow O_2^+ + e$			
$O_2(^1\Delta_g)+h\nu \rightarrow O_2^+ + e$	$1027<\lambda<1118$ Å	Wayne (1968) Huffman et al. (1971)	(*dd*)

REACTION SCHEME

$$O(^3P)+O(^3P)+M \rightarrow O_2+M$$

$$k = 3.3\times10^{-33}\cdot\left(\frac{300}{T}\right) \quad \text{Nicolet (1972)} \qquad (1)$$

$$O(^3P)+O_3 \rightarrow O_2+O_2$$

$$k = 2\times10^{-11}\cdot e^{-\frac{2395}{T}} \quad \text{Schiff (1969)} \qquad (2)$$

$$O(^3P)+OH \rightarrow H+O_2$$

$$k = 2.5\times10^{-11} \quad \text{Kaufman (1969)} \qquad (3)$$

$$O(^3P)+HO_2 \rightarrow OH+O_2$$

$$k = 7\times10^{-11} \quad \text{Hochanadel et al. (1972)} \qquad (4)$$

$O(^3P) + NO_2 \rightarrow NO + O_2$

$k = 9.1 \times 10^{-12}$ Davies (1972) (5)

$H_2O + O(^1D) \rightarrow OH + OH$

$k = 3 \times 10^{-10}$ Nicolet (1972) (6)

$H_2 + O(^1D) \rightarrow OH + H$

$k = 3 \times 10^{-10}$ Nicolet (1972) (7)

$CH_4 + OH \rightarrow CH_3 + H_2O$

$k = 5.5 \times 10^{-12} \cdot e^{-\frac{1886}{T}}$ Greiner (1970) (8)

$CH_4 + O(^1D) \rightarrow CH_3 + OH$

$k = 3 \times 10^{-10}$ Nicolet (1972) (9)

$CH_3 + O_2 + M \rightarrow CH_3O_2 + M$

$k = 1.3 \times 10^{-31}$ Basco et al. (1971) (10)

$CH_3 + O(^3P) \rightarrow CH_2O + H$

$k = 3 \times 10^{-13}$ Nicolet (1970) (11)

$CH_3O_2 + NO \rightarrow CH_3O + NO_2$

$k = 2.7 \cdot 10^{-12} \cdot e^{-\frac{500}{T}}$ See ref. by Crutzen (1972) (12)

$CH_3O_2 + CH_3O_2 \rightarrow CH_3 + CH_3O + O_2$

$k = 2.6 \times 10^{-13}$ Heiklen (1968) (13)

$CH_3O + O_2 \rightarrow CH_2O + HO_2$

$k = 1.0 \times 10^{-12} \cdot e^{-\frac{3300}{T}}$ See ref. by Crutzen (1972) (14)

$CH_2O + OH \rightarrow CHO + H_2O$

$k = 1.4 \times 10^{-11}$ Morris & Niki (1971*b*) (15)

$CHO + O_2 \rightarrow CO + HO_2$

$k = 10^{-13}$ McMillan & Calvert (1965) (16)

$OH + HO_2 \rightarrow H_2O + O_2$

$k = 2 \times 10^{-10}$ Hochanadel et al. (1972) (17)

$OH + OH \rightarrow H_2O + O(^3P)$

$k = 1.4 \times 10^{-11} \cdot e^{-\frac{500}{T}}$ Kaufman (1969) (18)

$H + HO_2 \rightarrow H_2O + O(^3P)$

$k = 1.5 \times 10^{-12} \cdot T^{1/2} \cdot e^{-\frac{2000}{T}}$ Nicolet (1970) (19)

$H + HO_2 \rightarrow H_2 + O_2$

$k = 5 \times 10^{-12} \cdot T^{1/2} \cdot e^{-\frac{1000}{T}}$ Nicolet (1970) (20)

$H + H + M = H_2 + M$

$k = 1.0 \times 10^{-32}$ Bennett & Blackmore (1968) (21)

$H_2O_2 + OH \rightarrow H_2O + HO_2$

$k = 4 \times 10^{-13} \cdot T^{1/2} \cdot e^{-\frac{600}{T}}$ Greiner (1968) (22)

$HNO_3 + OH \rightarrow H_2O + NO_3$

$k = 1 \times 10^{-13}$ Morley & Smith (1972) (23)

$H + O_2 + M \rightarrow HO_2 + M$

$k = 3 \times 10^{-32}$ Kaufman (1969) (24)

$H + O_3 \rightarrow HO + O_2$

$k = 2.6 \times 10^{-11}$ Kaufman (1964) (25)

$HO_2 + NO \rightarrow OH + NO_2$

$k = 5 \times 10^{-11} \cdot e^{-\frac{1600}{T}}$ See Wofsy et al. (1972) (26)

$OH + CO \rightarrow H + CO_2$

$k = 2.1 \times 10^{-13} \cdot e^{-\frac{115}{T}}$ Greiner (1969) (27)

$OH + O_3 \rightarrow HO_2 + O_2$

$k \leq 10^{-16}$ Langly & McGrath (1971) (28)

$CO + O(^3P) \rightarrow CO_2 + M$

$k = 2.2 \times 10^{-36}$ Stuhl & Niki (1971) (29)

$N_2O + O(^1D) \rightarrow N_2 + O_2$

$k = 9 \times 10^{-11}$ Greenberg & Heiklen (1970) (30)

$N_2O + O(^1D) \rightarrow NO + NO$

$k = 9 \times 10^{-11}$ Greenberg & Heiklen (1970 (31)

$O(^1D) + M \rightarrow O(^3P) + M$

$k = 6 \times 10^{-11}$ Noxon (1970) (32)

$O(^3P) + O_2 + M \rightarrow O_3 + M$

$k = 1.2 \times 10^{-34} \cdot e^{+\frac{500}{T}}$ Davis et al. (1972) (33)

$O_2(^1\Delta_g) \rightarrow O_2(^3\sum_g^-) + M$

$k = 2.8 \times 10^{-4}$ Badger et al. (1965) (34)

$O_2(^1\Delta_g) + M \rightarrow O_2(^3\sum_g^-) + M$

$k = 4.4 \times 10^{-19}$ Wayne (1972) (35)

$O_2(^1\Delta_g) + O_3 \rightarrow O_2(^3\sum_g^-) + O_3$

$k = 10^{-15}$ Wayne (1972) (36)

$HO_2 + HO_2 \rightarrow H_2O_2 + O_2$

$k = 5 \times 10^{-11} \cdot e^{-\frac{800}{T}}$ Kaufman (1969) (37)

$H_2O_2 + O(^3P) \rightarrow OH + OH$

$k = 10^{-15}$ Foner & Hudson (1962) (38)

$N(^4S) + NO \rightarrow N_2 + O(^3P)$

$k = 2.2 \times 10^{-11}$ Phillips & Schiff (1962) (39)

$NO + O_3 \rightarrow NO_2 + O_2$

$k = 9.3 \times 10^{-13} \cdot e^{-\frac{1235}{T}}$ Clyne et al. (1964) (40)

$NO_2 + OH + M \rightarrow HNO_3 + M$

$$k = 1.05 \times 10^{-11} \cdot e^{-\frac{170}{T}} \cdot \frac{4 \times 10^{-11} \cdot |M|}{4 \times 10^{-11} \cdot |M| + \frac{10^{13}}{\left(1 + \frac{5000}{T}\right)^4}}$$ Crutzen (1972) (41)

$HNO_3 + O(^3P) \rightarrow OH + NO_2$

$k \leq 10^{-14}$ Morris & Niki (1971) (42)

$NO_2 + O_3 \rightarrow NO_3 + O_2$

$k = 10^{-11} \cdot e^{-\frac{3500}{T}}$ Schofield (1967) (43)

$NO_3 + NO \rightarrow NO_2 + NO_2$

$k = 10^{-11}$ Berces & Förgeteg (1970) (44)

$NO_3 + NO_2 \rightarrow N_2O_5^*$

$k = 7 \times 10^{-12}$ Johnston (1951) (45)

$N_2O_5^* \rightarrow NO_2 + NO_3$

$k = 2.0 \times 10^{8}$ Johnston (1951) (46)

$N_2O_5^* + M \rightarrow N_2O_5 + M$

$k = 1.7 \times 10^{-10}$ Johnston (1951) (47)

$N_2O_5 + M \rightarrow N_2O_5^* + M$

$k = 2 \times 10^{-5} \cdot e^{-\frac{9650}{T}}$ Johnston (1951) (48)

$N_2^+ + O(^3P) \rightarrow NO^+ + N(^4S)$

$k = 3.0 \times 10^{-11}$ Fehsenfeld et al. (1970) (49)

$N_2^+ + O(^3P) \rightarrow NO^+ + N(^2D)$

$k = 1.1 \times 10^{-10}$ Fehsenfeld et al. (1970) (50)

$N_2^+ + O_2 \rightarrow O_2^+ + N_2$

$k = 7 \times 10^{-11}$ Ferguson (1971) (51)

$O_2^+ + NO \rightarrow NO^+ + O_2$

$k = 6.3 \times 10^{-10}$ Fehsenfeld et al. (1970) (52)

$N(^2D) + O_2 \rightarrow NO + O(^3P)$

$k = 6 \times 10^{-12}$ Black et al. (1969) (53)

$NO^+ + e \rightarrow N(^4S) + O(^3P)\ (\gamma - 1)$

$k = 5 \times 10^{-7} \cdot \left(\frac{300}{T}\right)$ Biondi (1968) (54)

$NO^+ + e \rightarrow N(^2D) + O(^3P)\ \gamma$ (55)

$N(^4S) + O_2 \rightarrow NO + O(^3P)$

$k = 1.4 \times 10^{-11} \cdot e^{-\frac{3550}{T}}$ Schiff (1968) (56)

$N(^4S) + O(^3P) \rightarrow NO + h\nu$

$k = 2 \times 10^{-17}$ Kenesha (1968) (57)

$O_2^+ + O_2 + M \rightarrow O_4^+ + M$

$k = 2.4 \times 10^{-30}$ Good et al. (1970) (58)

$$O_2^+ + e \rightarrow O(^3P) + O(^3P)$$

$$k = 2\times 10^{-7}\left(\frac{300}{T}\right) \quad \text{Biondi (1968)} \tag{59}$$

$$O_2^+ + \sum_i n_i^- \rightarrow O + O_4 + \sum_i n_i$$

$$k = 2\times 10^{-7} \quad \text{See text} \tag{60}$$

$$O_4^+ + H_2O \rightarrow O_2^+ \cdot (H_2O) + O_2$$

$$k = 2.2\times 10^{-9} \quad \text{Fehsenfeld et al. (1971)} \tag{61}$$

$$O_4^+ + O(^3P) \rightarrow O_2^+ + O_3$$

$$k = 3\times 10^{-10} \quad \text{Ferguson (1971)} \tag{62}$$

$$O_4^+ + O_2(^1\Delta_g) \rightarrow O_2^+ + O_2 + O_2$$

$$k = 10^{-10} \quad \text{Ferguson (1971)} \tag{63}$$

$$O_4^+ + e \rightarrow O_2 + O_2$$

$$k = 10^{-6}\left(\frac{300}{T}\right) \quad \text{See text} \tag{64}$$

$$O_4^+ + \sum_i n_i^- \rightarrow O_2 + O_2 + \sum_i n_i$$

$$k = 4\times 10^{-7} - 10^{-6} \quad \text{See text} \tag{65}$$

$$O_2^+ \cdot H_2O + H_2O \rightarrow H_3O^+ + OH + O_2$$

$$k = 3\times 10^{-10} \quad \text{Fehsenfeld et al. (1971)} \tag{66}$$

$$O_2^+ \cdot H_2O + H_2O \rightarrow H_3O^+ \cdot OH + O_2$$

$$k = 1.9\times 10^{-9} \quad \text{Fehsenfeld et al. (1971)} \tag{67}$$

$$H_3O^+ \cdot OH + H_2O \rightarrow H_3O^+ \cdot H_2O + OH$$

$$k = 3\times 10^{-9} \quad \text{Fehsenfeld et al. (1971)} \tag{68}$$

$$O_2^+ + H_2O + M \rightarrow O_2^+ \cdot H_2O + M$$

$$k = 2.8\times 10^{-28} \quad \text{Fehsenfeld et al. (1971)} \tag{69}$$

$$H_3O^+ + H_2O + M \rightarrow H_3O^+ \cdot H_2O + M$$

$$k = 3.4\times 10^{-27} \quad \text{Good et al. (1970)} \tag{70}$$

$$H_3O^+ \cdot H_2O + H_2O + M \rightarrow H_3O^+ \cdot (H_2O)_2 + M$$

$$k = 2.3\times 10^{-27} \quad \text{Good et al. (1970)} \tag{71}$$

$$H_3O^+ \cdot (H_2O)_2 + H_2O + M \rightarrow H_3O^+ \cdot (H_2O)_3 + M$$

$$k = 2.4\times 10^{-27} \quad \text{Good et al. (1970)} \tag{72}$$

$$H_3O^+ \cdot (H_2O)_3 + H_2O + M \rightarrow H_3O^+ \cdot (H_2O)_4 + M$$

$$k = 9\times 10^{-28} \quad \text{Good et al. (1970)} \tag{73}$$

$$H_3O^+ \cdot (H_2O)_4 + H_2O + M \rightarrow H_3O^+ \cdot (H_2O)_5 + M$$

$$k = 5\times 10^{-28} \quad \text{See text} \tag{74}$$

$$H_3O^+ \cdot (H_2O)_5 + H_2O + M \rightarrow H_3O^+ \cdot (H_2O)_6 + M$$

$$k = 3\times 10^{-28} \quad \text{See text} \tag{75}$$

$$H_3O^+ \cdot (H_2O)_6 + H_2O + M \rightarrow H_3O^+ \cdot (H_2O)_7 + M$$

$$k = 2\times 10^{-28} \quad \text{See text} \tag{76}$$

$$H_3O^+\cdot(H_2O)+M \rightarrow H_3O^+ + H_2O + M$$
$$k = 7\times10^{-26} \text{ at } 307 \text{ K} \quad \text{Good et al. (1970)} \tag{77}$$

$$H_3O^+\cdot(H_2O)_2+M \rightarrow H_3O^+\cdot H_2O + H_2O + M$$
$$k = 7\times10^{-18} \text{ at } 307 \text{ K} \quad \text{Good et al. (1970)} \tag{78}$$

$$H_3O^+\cdot(H_2O)_3+M \rightarrow H_3O^+\cdot(H_2O)_2 + H_2O + M$$
$$k = 4\times10^{-14} \text{ at } 307 \text{ K} \quad \text{Good et al. (1970)} \tag{79}$$

$$H_3O^+\cdot(H_2O)_4+M \rightarrow H_3O^+\cdot(H_2O)_3 + H_2O + M$$
$$k = 6\times10^{-12} \text{ at } T = 307 \text{ K} \quad \text{Good et al. (1970)} \tag{80}$$

$$H_3O^+\cdot(H_2O)_5+M \rightarrow H_3O^+\cdot(H_2O)_4 + H_2O + M$$
$$k = 1.4\times10^{-11} \text{ at } T = 300 \text{ K} \quad \text{See text} \tag{81}$$

$$H_3O^+\cdot(H_2O)_6+M \rightarrow H_3O^+\cdot(H_2O)_5 + H_2O + M$$
$$k = 4\times10^{-11} \text{ at } T = 300 \text{ K} \quad \text{See text} \tag{82}$$

$$H_3O^+\cdot(H_2O)_7+M \rightarrow H_3O^+\cdot(H_2O)_6 + H_2O + M$$
$$k = 7\times10^{-11} \quad \text{See text} \tag{83}$$

$$NO^+ + H_2O + M \rightarrow NO^+\cdot H_2O + M$$
$$k = 1.6\times10^{-28} \quad \text{Fehsenfeld et al. (1971}a\text{)} \tag{84}$$

$$NO^+\cdot H_2O + H_2O + M \rightarrow NO^+\cdot(H_2O)_2 + M$$
$$k = 1\times10^{-27} \quad \text{Fehsenfeld et al. (1971}a\text{)} \tag{85}$$

$$NO^+\cdot(H_2O)_2 + H_2O + M \rightarrow NO^+\cdot(H_2O)_3 + M$$
$$k = 2.0\times10^{-27} \quad \text{Fehsenfeld et al. (1971}a\text{)} \tag{86}$$

$$NO^+ + CO_2 + M \rightarrow NO^+\cdot CO_2 + M$$
$$k = 2.5\times10^{-29} \quad \text{Dunkin et al. (1969)} \tag{87}$$

$$NO^+ + N_2 + M \rightarrow NO^+\cdot N_2 + M$$
$$k = 2.4\times10^{-31} \quad \text{Niles \& Heimerl (1972)} \tag{88}$$

$$NO^+\cdot N_2 + CO_2 \rightarrow NO^+\cdot CO_2 + N_2$$
$$k = 10^{-9} \quad \text{See text} \tag{89}$$

$$NO^+\cdot CO_2 + H_2O \rightarrow NO^+\cdot H_2O + CO_2$$
$$k = 10^{-9} \quad \text{Dunkon et al. (1969)} \tag{90}$$

$$NO^+\cdot(H_2O)_3 + H_2O \rightarrow H_3O^+\cdot(H_2O)_2 + HNO_2$$
$$k = 8\times10^{-11} \quad \text{Fehsenfeld et al. (1971}a\text{)} \tag{91}$$

$$NO^+\cdot(H_2O)_2 + M \rightarrow NO^+\cdot H_2O + H_2O + M$$
$$k = 1.4\times10^{-14} \quad \text{Puckett \& Teague (1971)} \tag{92}$$

$$NO^+\cdot(H_2O)_3 + M \rightarrow NO^+\cdot(H_2O)_2 + H_2O + M$$
$$k = 1.3\times10^{-12} \text{ at } 300\ T \quad \text{Fehsenfeld et al. (1971}a\text{)} \tag{93}$$

$$NO^+\cdot H_2O + H \rightarrow H_3O^+ + NO$$
$$k < 10^{-11} \quad \text{Ferguson (1971)} \tag{94}$$

$$NO^+\cdot H_2O + OH \rightarrow H_3O^+ + NO_2$$
$$k = 2\times10^{-9} \quad \text{See text} \tag{95}$$

$H_3O^+ \cdot (H_2O)_n + e \rightarrow$ products $10^{-6} - 10^{-5}$

Adopted values (96)

$H_3O^+ \cdot (H_2O)_n + \sum_i n_i^- \rightarrow$ products 10^{-6}

Adopted values (97)

$NO^+ \cdot (H_2O)_n + e \rightarrow$ products $10^{-6} - 10^{-5}$

Adopted values (98)

$NO^+ \cdot (H_2O)_n + \sum_i n_i^- \rightarrow$ products 10^{-6}

Adopted values (99)

$e + O_2 + O_2 \rightarrow O_2^- + O_2$

$k = 1.4 \times 10^{-29} \left(\frac{300}{T}\right) e^{-\frac{600}{T}}$ Phelps (1968) (100)

$e + O_3 \rightarrow O^- + O_2$ $k = 3 \times 10^{-12}$ Phelps (1968) (101)

$O^- + O(^3P) \rightarrow O_2 + e$

$k = 1.4 \times 10^{-10}$ Fehsenfeld et al. (1966) (102)

$O_2^- + O(^3P) \rightarrow O_3 + e$

$k = 3 \times 10^{-10}$ Fehsenfeld et al. (1966) (103)

$O^- + O_2(^1\Delta_g) \rightarrow O_3 + e$

$k = 3 \times 10^{-10}$ Fehsenfeld et al. (1969) (104)

$O^- + H_2 \rightarrow H_2O + e$ $k = 6.7 \times 10^{-11}$ Fehsenfeld et al. (1966) (105)

$O^- + CO \rightarrow CO_2 + e$ $k = 4.4 \times 10^{-10}$ Fehsenfeld et al. (1966) (106)

$O^- + NO_2 \rightarrow NO_2^- + O(^3P)$

$k = 1 \times 10^{-9}$ Fehsenfeld et al. (1966) (107)

$O_2^- + NO_2 \rightarrow NO_2^- + O_2$

$k = 1.8 \times 10^{-9}$ Fite (1968) (108)

$O^- + O_3 \rightarrow O_3^- + O(^3P)$

$k = 5.3 \times 10^{-10}$ Fite (1968) (109)

$O_2^- + O_3 \rightarrow O_3^- + O_2$ $k = 4 \times 10^{-10}$ Fite (1968) (110)

$O_2^- + O_2 + O_2 \rightarrow O_4^- + O_2$

$k = 4 \times 10^{-31}$ Pack & Phelps (1971) (111)

$O^- + O_2(^1\Delta_g) \rightarrow O_2^- + O(^3P)$

$k = 10^{-10}$ Ferguson (1971) (112)

$O_2^- + O(^3P) \rightarrow O^- + O_2$

$k = 10^{-11}$ Borthner & Kummler (1968) (113)

$O_3^- + CO_2 \rightarrow CO_3^- + O_2$

$k = 4 \times 10^{-10}$ Ferguson (1970) (114)

$O_3 + NO \rightarrow NO_3^- + O$

$k = 10^{-11}$ Fite (1969) (115)

$$O_4^- + CO_2 \rightarrow CO_4^- + O_2$$
$$k = 4.3 \times 10^{-10} \quad \text{Fehsenfeld et al. (1969)} \tag{116}$$

$$O_4^- + O(^3P) \rightarrow O_3^- + O_2$$
$$k = 4 \times 10^{-11} \quad \text{Ferguson (1971)} \tag{117}$$

$$CO_3^- + O(^3P) \rightarrow O_2^- + CO_2$$
$$k = 8.1 \times 10^{-11} \quad \text{Fite (1968)} \tag{118}$$

$$CO_4^- + O(^3P) \rightarrow CO_3^- + O_2$$
$$k = 1.5 \times 10^{-11} \quad \text{Ferguson (1971)} \tag{119}$$

$$CO_3^- + NO \rightarrow NO_2^- + CO_2$$
$$k = 8 \times 10^{-12} \quad \text{Fite (1968)} \tag{120}$$

$$NO_2^- + O_3 \rightarrow NO_3^- + O_2$$
$$k = 1.8 \times 10^{-11} \quad \text{Ferguson (1972)} \tag{121}$$

$$O_4^- + NO \rightarrow NO_3^{-*} + CO_2$$
$$k = 2.5 \times 10^{-10} \quad \text{Ferguson (1972)} \tag{122}$$

$$CO_4 + NO \rightarrow NO_3^{-*} + CO_2$$
$$k = 4.8 \times 10^{-11} \quad \text{Ferguson (1972)} \tag{123}$$

$$NO_3^{-*} + NO \rightarrow NO_2 + NO_2$$
$$k = 1.5 \times 10^{-11} \quad \text{Ferguson (1972)} \tag{124}$$

$$O_4^- + H_2O \rightarrow O_2^- \cdot H_2O + O_2$$
$$k = 1.4 \times 10^{-9} \quad \text{Pack \& Phelps (1971)} \tag{125}$$

$$O_2^- + H_2O + O_2 \rightarrow O_2^- \cdot H_2O + O_2$$
$$k = 1.3 \times 10^{-28} \quad \text{Pack \& Phelps (1971)} \tag{126}$$

$$O_2^- \cdot H_2O + H_2O + O_2 \rightarrow O_2^- \cdot (H_2O)_2 + O_2$$
$$k = 4 \times 10^{-28} \quad \text{Pack \& Phelps (1971)} \tag{127}$$

$$O^- + H_2O + O_2 \rightarrow O^- \cdot H_2O + O_2$$
$$k = 1.2 \times 10^{-28} \quad \text{Pack \& Phelps (1971)} \tag{128}$$

$$O_3^- + H_2O + O_2 = O_3^- \cdot H_2O + O_2$$
$$k = 2.1 \times 10^{-28} \quad \text{Pack \& Phelps} \quad (1971) \tag{129}$$

$$O^- + O_2 + O_2 \rightarrow O_3^- + O_2$$
$$k = 1.2 \times 10^{-30} \quad \text{Pack \& Phelps (1971)} \tag{130}$$

$$O_2^- \cdot (H_2O)_2 + O_2 \rightarrow O_2 \cdot H_2O + H_2O + O_2$$
$$k = 7.1 \times 10^{-15} \quad \text{Pack \& Phelps (1971)} \tag{131}$$

$$O_4^- + O_2 \rightarrow O_2^- + O_2 + O_2$$
$$k = 2.7 \times 10^{-14} \quad \text{Pack \& Phelps (1971)} \tag{132}$$

$$O_2^- \cdot H_2O + O_2 \rightarrow O_4^- + H_2O$$
$$k = 2.5 \times 10^{-15} \quad \text{Parkes (1971)} \tag{133}$$

$$O_2^- \cdot H_2O + CO_2 \rightarrow CO_4^- + H_2O$$
$$k = 5.8 \times 10^{-10} \quad \text{Adams et al. (1970)} \tag{134}$$

$$NO_2^- + H_2O + NO \rightarrow NO_2^- \cdot H_2O + NO$$
$$k = 1.3 \times 10^{-28} \quad \text{Puckett \& Lineberger (1970)} \qquad (135)$$

$$NO_2^- \cdot H_2O + HNO_2 \rightarrow NO_2^- \cdot HNO_2 + H_2O$$
$$k = 1 \times 10^{-9} \quad \text{Puckett \& Lineberger (1970)} \qquad (136)$$

$$NO_3^- + O_2 + M \rightarrow NO_3^- \cdot O_2 + M$$
$$k = 10^{-31} \quad \text{Ferguson (1970)} \qquad (137)$$

$$NO_3^- \cdot O_2 + H_2O + M \rightarrow NO_3 \cdot H_2O + M$$
$$k = 10^{-9} \quad \text{See text} \qquad (138)$$

$$NO_3^- + H_2O + M \rightarrow NO_3^- \cdot H_2O + M$$
$$k = 2 \times 10^{-28} \quad \text{See text} \qquad (139)$$

$$CO_3^- + H_2O + M \rightarrow CO_3^- \cdot H_2O + M$$
$$k = 2 \times 10^{-28} \quad \text{See text} \qquad (140)$$

$$CO_4^- + H_2O + M \rightarrow CO_4^- \cdot H_2O + M$$
$$k = 2 \times 10^{-28} \quad \text{See text} \qquad (141)$$

$$NO_3^- + h\nu \rightarrow NO_3 + e$$
$$k = 1 \times 10^{-4} \qquad (142)$$

REFERENCES

Ackerman, M. 1971. pp. 149–159 in *Mesospheric Models and Related Experiments*. Reidel.

Ackerman, M. & Müller, C. 1972. *Aeronomic Acta*. No. 105.

Adams, N. G., Bohme, D. K., Dunkin, D. B., Fehsenfeld, F. C. & Ferguson, E. E. 1970. *J. Chem. Phys. 52*, 3133–3140.

Anderson, J. G. 1971. *J. Geophys. Res. 76*, 7820–7824.

Arnold, F., Krankowsky, D. & Wieder, H. 1971. Proceedings of the Advanced Study Institute. pp. 18–28 in *Magnetospheric-Ionospheric Interactions*. Universitetsforlaget, Oslo.

Arnold, F. & Krankowsky, D. 1972. pp. 229-235 in *Cospar Symposium on D- and E- Region Chemistry*. Aeronomy Report 48.

Asquith, P. L. & Tyler, B. J. 1970. *Chem. Commun.* 744–745.

Badger, R. A., Wright, A. C. & Witlock, R. F. 1965. *J. Chem. Phys. 43*, 4345–4350.

Bainbridge, A. E. & Heidt, L. E. 1966. *Tellus 18*, 221–225.

Basco, N., James, D. & James, F. 1971. *Chem. Phys. Lett. 8*, 265–266.

Bates, D. R. 1960. pp. 219–267 in *Physics of the Upper Atmosphere*. Academic Press, New York.

Bates, D. R. & Hays, P. B. 1967. *Planet. Space Sci. 15*, 189–197.

Bates, D. R. & Nicolet, M. 1950. *J. Geophys. Res. 55*, 301–327.

Benett, J. E. & Blackmore, D. R. 1968. *Proc. Roy. Soc. A. 305*, 553–574.

Bérces, T. & Förgeteg, S. 1970. *Trans. Faraday Soc. 66*, 633–639.

Biondi, M. A. 1968. pp. 2–17 in *Symposium on Laboratory Measurements of Atmospheric Interest*. York University, Canada.

Black, G., Slanger, T. G., St. John, G. A. & Young, R. A. 1969. *J. Chem. Phys. 51*, 116–121.

Bortner, M. H. & Kummler, R. H. 1968. Ch. 19 in *Dasa Reaction Rate Handbook*, DASA 1948.

Brasseur, G. & Cislek. 1972. Presented at the Ozone Symposium in Arosa, Switzerland.

Burke, R. R. 1970. *J. Chem. Phys. 75*, 1343–1347.

Calvert, J. G., Kerr, J. A. & Demerjian, K. L. 1972. *Science 175*, 751–752.

Clark, I. D. & Wayne, R. P. 1970. *J. Geophys. Res. 75*, 699.

Clyne, M. A. A., Thrush, B. A. & Wayne, R. P. 1964. *Trans. Faraday Soc. 60*, 359–370.

Craig, R. C. 1965. p. 160 in *The Upper Atmosphere. Meteorology and Physics*. Academic Press, New York and London.

Crutzen, P. J. 1971. *J. Geophys. Res. 76*, 7311–7327.

Crutzen, P. J. 1972. Report AP. 10. Institute of Meteorology, University of Stockholm, Sweden.

Davis, D. D. 1972. Presented at the Second Conference at the CIAP meeting, Boston, U.S.A.

Ditchburn, R. W. & Young, P. A. 1962. *J. Atmos. Terr. Phys. 24*, 127–139.

Dunkin, D. B., Fehsenfeld, F. C., Schmeltekopf, A. L. & Ferguson, E. E. 1971. *J. Chem. Phys. 54*, 3817–3822.
Evans, W. F. J., Hunten, D. M., Llewellyn, E. J. & Valance Jones, A. 1968. *J. Geophys. Res. 73*, 2885–2895.
Evans, W. F. J., Llewellyn, E. J. & Valance Jones, A. 1972. *J. Geophys. Res. 77*, 4899–4901.
Fehsenfeld, F. C., Ferguson, E. E. & Schmeltekopf, A. L. 1966. *J. Chem. Phys. 45*, 1844–1845.
Fehsenfeld, F. C. & Ferguson, E. E. 1969. *J. Geophys. Res. 74*, 1217.
Fehsenfeld, F. C., Albritton, D. L., Burt, J. A. & Schiff, H. I. 1969. *Can. J. Chem. 47*, 1793–1795.
Fehsenfeld, F. C., Dunkin, D. B. & Ferguson, E. E. 1970. *Planet Space Sci. 18*, 1267–1269.
Fehsenfeld, F. C., Moseman, M. & Ferguson, E. E. 1971. *J. Chem. Phys. 55*, 2115–2119.
Fehsenfeld, F. C., Moseman, M. & Ferguson, E. E. 1971a. *J. Chem. Phys. 55*, 2120–2125.
Ferguson, E. E. 1970. *Account. Chem. Res. 3*, 402–408.
Ferguson, E. E. 1971. *Rev. Geophys. Space Phys. 9*, 997–1008.
Ferguson, E. E. 1972 in Cospar symposium on *D*- and *E*-region ion chemistry. *Aeronomy report 48*, pp. 217–220.
Fite, W. L. 1968. Ch. 13 in *Dasa Reaction Rate Handbook*. DASA 1948.
Foner, S. N. & Hudson, R. L. 1962. *J. Chem. Phys. 36*, 2681–2688.
Friedman, H. 1960. pp. 133–218 in *Physics of the Upper Atmosphere*. Academic press, New York.
George, M. J. 1970. *J. Geophys. Res. 75*, 3693–3705.
Goldberg, R. A. & Aikin, A. C. 1971. *J. Geophys. Res. 76*, 8352–8364.
Good, A., Durden, D. A. & Kebarle, P. 1970. *J. Chem. Phys. 52*, 212–221.
Good, A., Durden, D. A. & Kebarle, P. 1970. *J. Chem. Phys. 52*, 222–229.
Graham & Johnston, H. C. 1972. Private communications.
Greenberg, R. I. & Heikelen, J. 1970. *Int. J. Chem. Kin. 2*, 185.
Greiner, N. R. 1968. *J. Phys. Chem. 72*, 406–410.
Greiner, N. R. 1969. *J. Chem. Phys. 51*, 5049–5051.
Greiner, N. R. 1970. *J. Chem. Phys. 53*, 1070–1076.
Gudiksen, P. H., Fairhall, A. W. & Reed, R. J. 1968. *J. Geophys. Res. 77*, 4461–4473.
Hall, L. A. & Hinteregger, H. E. 1970. *J. Geophys. Res. 75*, 6959–6968.
Hampson, J. 1965. *Carde. tekn. rapp.*, No. 1690.
Heiklen, J. 1968. Advances. *Chem. Ser. 76*, 23–39.
Heimerl, J. M. 1972. Summer advanced study institute. Physics and Chemistry of Upper Atmospheres. Orleans, France.
Herring, W. S. & Borden, T. S. 1964 V2. Environmental Research Papers, Mo. 38.
Hesstvedt, E. 1965. *Geofys. Publ. 26*, No. 1.
Hesstvedt, E. 1968. *Geofys. Publ. 27*, No. 4.
Hesstvedt, E. 1970. Inst. Report. Institute of Geophysics. University of Oslo, Norway.
Hesstvedt, E. 1971. pp. 51–64 in *Mesospheric Models and Related Experiments*. Reidel.
Hesstvedt, E. 1972. Water, Air, Soil Pollution. To be published.
Hilsenrath, E. L. 1972. Private communications.
Hocanadel, C. J., Ghormley, J. A. & Orgren, P. 1972. *J. Chem. Phys. 56*, 4426–4432.
Huffman, R. E. 1968. pp. 95–120 in *Symposium on Laboratory Measurements of Atmospheric Interest*. York University, Canada.
Huffman, R. E., Paulsen, D. E., Larabee, D. C. & Cairns, R. B. 1971. *J. Geophys. Res. 76*, 1028–1038.
Hunten, D. M. 1954. *J. Atm. Terr. Phys. 5*, 44–56.
Inn, E. C. & Tannaka, Y. 1953. *J. Opt. Soc. Amer. 43*, 870–973.
Isaksen, I. S. A. 1971. Proceedings of the Advanced Study Institute. *Magnetospheric-Ionospheric Interactions*. Universitetsforlaget, Oslo.
Johannesen, A. & Krankowsky, D. 1972. *J. Geophys. Res. 77*, 2888–2901.
Johnston, H. F. 1951. *J. Amer. Chem. Soc. 73*, 4542–4546.
Johnston, H. F. 1971. *Science 173*, 511–522.
Johnston, H. F. 1972. Private communications.
Jones, E. J. & Wulf, O. R. 1937. *J. Chem. Phys. 5*, 873–877.
Kaufman, F. 1964. *Ann. Géophys. 20*, 106–144.
Kaufman, 1969. *Can. J. Chem. 47*, 1917–1924.
Kebarle, P., Searles, S. K., Zolla, A., Scarborough, J. & Ashadi, M. 1967. *J. Am. Chem. Soc. 89*, 6393–6399.
Kebarle, P., French, M. & Payzaret, J. D. 1972. pp. 252–258 in *Cospar Symposium on D- and E-Region Chemistry*. Aeronomy Report 48.
Kellogg, W. W. 1964. *Space Sci. Rev. 3*, 275–316.
Keneshea, T. J. 1968. Meteorological and Chemical Factor in *D*-Region Aeronomy. Aeronomy Report No. 32, pp. 400–413 in *Third Aeronomy Conference*.
Kockarts, G. 1971. pp. 160–176 in *Mesospheric Models and Related Experiments*. Reidel.
Langly, K. F. & McGrath, W. D. 1971. *Planet. Space Sci. 19*.
Leighton, P. A. 1961. pp. 52–59 in *Photochemistry of Air Pollution*. 52–59.
Lineberger, W. C. & Puckett, J. L. 1969, *Phys. Rev. 186*, 116–127.
Lineberger, W. C. & Puckett, L. J. 1969*a*. *Phys. Rev. 187*, 286–291.
Lindzen, R. S. 1971. pp. 122–130 in *Mesospheric Models and Related Experiments*. Reidel.
McKnight, L. C. & Sawina, J. M. 1971. *Phys. Rev. 3*, 1043–1046.

McMillan, G. R. & Calvert, J. G. 1965. *Oxidation Com. Rev. 1*, 83.
Meira, L. G. 1970. Ph. D. thesis. University of Colorado, U.S.A.
Mohnen, C. A. 1970. *J. Geophys. Res. 75*, 1717–1721.
Morley, C. & Smith, I. W. M. 1972. *J. Chem. Soc. Far. Trans. II. 68*, 1016–1030.
Morris, E. D., Jr. & Niki, H. 1971. *J. Phys. Chem. 75*, 3193–3194.
Morris, E. D., Jr. & Niki, H. 1971a. *J. Chem. Phys. 55*, 1991–1992.
Murcray, D. G., Kyle, T. G., Murcray, F. H. & Williams, W. J. 1969. *J. Opt. Soc. Am. 59*, 1131–1134.
Narcisi, R. S. 1972. Summer Advanced Study Institute. *Physics and Chemistry of Upper Atmospheres*. Orléans, France.
Narcisi, R. S. & Bailey, A. D. 1965. *J. Geophys. Res. 70*, 3687–3700.
Narcisi, R. S., Bailey, A. D., Wlodyka, H. E. & Philbrick, C. R. 1972. *J. Atmosph. Terr. Phys. 34*, 647–658.
Nicolet, M. 1970. *Planet. Space Sci. 18*, 1111–1118.
Nicolet, M. 1970a. Aeronomic Acta. No. 79.
Nicolet, M. 1972. Proceedings of the CIAP Conference, February, Cambridge, U.S.A.
Niles, F. R. & Heimerl, J. M. 1972. *Trans. Am. Geophys. Union 53*, 456.
Norton, R. B. & Barth, C. A. 1970. *J. Geophys. Res. 75*, 3903–3909.
Noxon, J. F. 1970. *J. Chem. Phys. 52*, 1852–1873.
Pack, J. L. & Phelps, A. V. 1966. *J. Chem. Phys. 45*, 4316.
Pack, J. L. & Phelps, A. V. 1971. *Bull. Am. Phys. Soc. 16*, 214.
Parkes, D. H. 1971. *Trans. Faraday Soc. 67*, 579.
Pearce, J. B. 1969. *J. Geophys. Res. 74*, 853–861.
Phelps, A. V. 1968. ch. 12 in *Data Reaction Handbook*. DASA 1948.
Phelps, A. V. 1972. pp. 278–280 in *Cospar Symposium on D- and E-Region Ion Chemistry*. Aeronomy Report No. 48.
Phillips, L. F. & Schiff, H. I. 1962. *J. Chem. Phys. 36*, 1509–1517.
Preston, K. F. & Barr, R. F. 1971. *J. Chem. Phys. 54*, 3347–3348.
Puckett, L. J. & Lineberger, W. C. 1970. *Phys. Rev. 6*, 1635–1641.
Puckett, L. J. & Teague, M. W. 1971. *J. Chem. Phys. 54*, 2564–2572.
Reid, G. C. 1970. *J. Geophys. Res. 75*, 2551–2562.
Rhine, P. E., Tubbs, L. D. & Williams, D. 1969. *Applied Opt. 8*, 1500–1501.
Richtmyer, R. D. 1957. In *Difference Methods for Initial Value Problems*. Interscience Publishers, Inc., New York.
Schiff, H. I. 1968. pp. 201–233 in *Symposium on Laboratory Measurements of Atmospheric Interest*. York University, Canada.
Schiff, H. I. 1969. *Can. J. Chem. 47*, 1903–1916.
Schofield, K. 1967. *Planet. Space Sci. 15*, 643–670.
Schumb, W. C., Gathefield, C. N. & Wentworth, R. L. 1955. p. 287 in *Hydrogen Peroxide*. Reinhold.
Schütz, K., Junge, C., Beck, R. & Albrecht, B. 1970. *J. Geophys. Res. 15*, 2230–2246.
Seiler, W. & Warneck, P. 1972. *J. Geophys. Res. 77*, 3204–3214.
Strobel, D. F., Hunten, D. M. & McElroy, M. B. 1970. *J. Geophys. Res. 75*, 4307–4321.
Stuhl, F. & Niki, H. *J. Chem. Phys. 55*, 3943–3953.
Watanabe, K. 1958. *Advances in Geophys. 5*, 153–221.
Wayne, R. P. 1972. Presented at the Ozone Symposium in Arosa, Switzerland.
Wilkes, M. V. 1954. *Proc. Phys. Soc. 43*, 483–501.
Wofsy, S. C., McConnel, J. C. & McElroy, M. B. 1972. *J. Geophys. Res. 77*, 4477–4493.
Wood, H. C. 1969. M. Sc. Thesis. University of Saskatchewan, Canada.
Wood, H. C. 1972. Ph. D. Thesis. University of Saskatchewan, Canada.

Instructions to Authors

GEOPHYSICA NORVEGICA

publishes papers in English. When preparing manuscripts for submission, authors should consult 1973 copies of the journal and follow its style as closely as possible.

MANUSCRIPTS

Manuscript must be typewritten, double spaced throughout, on one side of the paper, with a wide margin. Authors should submit the *original* manuscript (preferably with one copy) to the editor, whose address is shown on page 2 of the cover.

Separate sheets should be used for the following: 1) title page, with the author's name and institution, and, if the title is longer than 40 letters and spaces, a short title not exceeding this limit for use in the running heads; 2) an abstract not exceeding 12 lines (910 letters and spaces) with the name and full postal address underneath of the author to whom communications, proofs, and reprints are to be sent; 3) references; 4) Tables with their headings; 5) legends to Figures.

Brief *Acknowledgements* of grants and other assistance, if any, will be printed at the end of the text.

FIGURES, TABLES, AND MATHEMATICAL SYMBOLS

All illustrations are to be considered as Figures. Each graph, drawing, or photograph should be numbered in sequence with arabic numerals, and should be identified on the back by the name of the journal, the author's name, and the Figure number. The top should be indicated. The Figures should be the original drawing. The columns of *Geophysica Norvegica* are 67 mm broad, and the size of the original drawings should be in proportion. Lines must be thick enough to allow for reduction. Letters and numbers should not be less than 2 mm high in the printed illustration. Photographs should be submitted as unmounted glossy enlargements showing good details.

Tables are to be numbered consecutively with roman numerals. Each Table should be typed on a separate sheet, with a descriptive heading that makes the Table self-explanatory.

All Figures and Tables should be referred to in the text by their number. Their approximate position should be indicated in the margin of the manuscript.

All numbered equations and all unnumbered but complicated equations should be typed on separate lines. Equations should be punctuated.

All text material will be set in roman type unless otherwise marked. Hence, all variables and other characters to be set in italic type should be underlined once with a straight line. Vectors and other characters in boldface type should be indicated by underlining with a single wavy line.

No footnotes should be used.

REFERENCES TO LITERATURE

In the text, Brown (1957, p. 9), Brown & White (1961). If more than two authors, Brown et al. (1963). Multiple references: 'As several authors have reported (Brown 1967, Brown & White 1961, Green et al. 1963)', i. e. chronological order, no commas between names and year.

Lists of References are to be unnumbered and in alphabetical order. The international alphabetical order of Scandinavian and German vowels, should be observed: Å = AA, Æ and Ä = AE, Ø and Ö = OE, Ü = UE. Indicate 1st, 2nd, 3rd, etc. works by the same author in the same year by a, b, c, etc. (White 1966a). No ditto marks should be used. Titles of journals should be abbreviated according to *World List of Scientific Periodicals.*

Examples:

Cadle, R. D. 1966. p. 83 in *Particles in the Atmosphere and Space.* Reinhold Publishing Corporation, New York.

Craig, R. A. 1965. p. 161 in *The Upper Atmosphere. Meteorology and Physics.* International Geophysics Series, Vol. 8. Academic Press, New York and London.

Eliassen, A. & Kleinschmidt, E. 1957. p. 66 in *Handbuch der Physik.* Vol. 48, Part 2, edited by S. Flügge. Springer-Verlag, Berlin.

Junge, C. 1972. *Quart. J. R. Met. Soc. 98,* 711.

PROOFS

Two copies of the first proof will be sent (page proofs). One copy, duly corrected, should be returned to the editor with the least possible delay. All technical parts of the article, including references, names, figures (numbers, formulae), illustrations, etc. are the responsibility of the authors. Authors will be required to pay for any major alterations they may make.

REPRINTS

Fifty reprints of each article will be supplied free. Additional reprints can be ordered at a charge.

International Journals

	Issues per year	Subscription price	Language
AMBIO A Journal of the Human Environment Research and Management	8		English
ARCTIC Journal of Arctic Biology	4		English
BLYTTIA Journal of the Norwegian Botanical Association	4		Norwegian
BOREAS An International Journal of Quaternary Geology	4		English
CETHACEA An International Journal of Paleontology and Stratigraphy	4		English
LITHOS An International Journal of Mineralogy, Petrology and Geochemistry	4		English
NORSK ENTOMOLOGISK TIDSSKRIFT Norwegian Journal of Entomology	4		English
NORSK GEOGRAFISK TIDSSKRIFT Norwegian Journal of Geography	4		English
NORSK GEOLOGISK TIDSSKRIFT Norwegian Journal of Geology	4		English
NORWEGIAN JOURNAL OF BOTANY	4		English
NORWEGIAN JOURNAL OF ZOOLOGY	4		English
ORNIS SCANDINAVICA	4		English

Periodicals

	Issues per year	Subscription price	Language
ACTA BOREALIA Journal of Aquatic Botany, Geology and Zoology	2		English
ASTROPHYSICA NORVEGICA Norwegian Journal of Physics Astrophysics	1		English
FOLIA LIMNOLOGICA SCANDINAVICA Scandinavian Journal of Limnology	1		English
GEOPHYSICA NORVEGICA Geofysiske Publikasjoner	1		English
PHYSICA NORVEGICA Norwegian Journal of General Physics	1		English
SARSIA Journal of Marine Biology	4		English

UNIVERSITETSFORLAGET